The Interaction between Water Vapor and Pure Silver Iodide in the Vicinity of Saturation

By
W.R. Barchet

Department of Atmospheric Science
Colorado State University
Fort Collins, Colorado

NSF Grant GA-11309

Colorado State University

Department of Atmospheric Science

Paper No. 168

THE INTERACTION BETWEEN WATER VAPOR AND PURE SILVER IODIDE IN THE VICINITY OF SATURATION

by

W. R. Barchet

This report was prepared with support from
the National Science Foundation
Grant No. GA-11309
Principal Investigator, Myron L. Corrin

Department of Atmospheric Science
Colorado State University
Fort Collins, Colorado

January 1971

Atmospheric Science Paper No. 168

ABSTRACT

The adsorptive interaction between water vapor and vacuum prepared, pure silver iodide leads to nucleation of a condensed phase at sufficiently low temperatures and high supersaturations. The purpose of this work is to determine: (1) if the patch model of adsorption of water vapor on pure silver iodide is valid at nucleation; (2) if the energetics of nucleation are comparable to the energetics of adsorption; (3) the mechanism of nucleation on pure silver iodide; and (4) how nucleation observed by adsorption methods compares to cloud chamber studies.

Previous adsorption studies were unable to answer these questions because of insufficient information near the onset of ice nucleation. Gravimetric adsorption measurements made with a Cahn electrobalance at pressures of water vapor between ice and water saturation in the absence of other gases demonstrated the ability of an adsorption technique to detect nucleation. Adsorption isotherms at -3.00C, -6.50C, and -10.00C led to isosteric heats of adsorption and $\underline{\Pi-\sigma}$ plots up to the onset of nucleation. Nucleation was detected as a rapid, continuous increase in the weight of the sample.

Peaks in the isosteric heat curves at coverages much below a statistical monolayer and coverages of one to three monolayers at the onset of nucleation at -10.00C and -6.50C demonstrated the patch model of adsorption is valid even at nucleation. At -3.00C nucleation did not occur even at water saturation. Kinks in the $\underline{\Pi-\sigma}$ plots for the -3.00C and -6.50C isotherms indicate a higher order phase transition in the film adsorbed on the patches of high energy sites.

Heats of adsorption and supersaturations at which nucleation of ice occurs are evidence for the formation of an increasingly duplex film as more water is adsorbed on the patch. The embryo does not acquire the bulk properties of ice until nucleation occurs.

The mechanism of nucleation on pure silver iodide involves primarily the high energy patches. At a sufficient coverage, ice is nucleated at the patch-embryo interface and propogates outward through the embryo. This adsorption technique detects the occurrence of nucleation on a single, most active site on the most active particle in the sample. From the three isotherms, a threshold temperature of -3.5C and ice supersaturation of 3.4% were estimated for nucleation on pure silver iodide. Cloud chamber studies, in contrast, require the number of nuclei activated to be several orders of magnitude larger to detect nucleation.

This work provides a much needed baseline against which future adsorption and nucleation studies on impure and doped silver iodide can be compared.

Wm. Richard Barchet
Atmospheric Science Department
Colorado State University
Fort Collins, Colorado 80521
March, 1971

TABLE OF CONTENTS

LIST OF TABLES

LIST OF FIGURES

CHAPTER I

INTRODUCTION

Adsorption of water vapor by silver iodide was long considered the first step in the interaction between silver iodide and water vapor that eventually led to the formation of ice. Demonstration of the ability of silver iodide to nucleate the ice phase was given by Schaefer [1] and Vonnegut [2] with laboratory studies in cold boxes. Numerous field studies sponsored by the Federal Government also showed the effectiveness of silver iodide powders and smokes in modifying supercooled clouds. [3,4]

Laboratory investigations of the isothermal adsorption of water vapor on silver iodide powders were first undertaken in the early 1950's. Since that time many studies were conducted with the purpose of describing this interaction and the surface characteristics of silver iodide using silver iodide powders made by various techniques. These adsorption measurements were made under isothermal conditions either volumetrically or gravimetrically.

Interpretation of these laboratory studies by the methods of adsorption thermodynamics gives information on the distribution of adsorbed molecules, the energies involved in adsorption, and the entropies of adsorption. These thermodynamic properties indicate the influence of the surface on adsorption. Correlation of these properties with the nucleation ability of the material leads to the patch and cluster models of adsorption which provide the foundations for nucleation.

1.1 Silver Iodide Used in Previous Studies

The majority of previous adsorption studies on silver iodide made use of powders obtained by precipitation from aqueous solution. Birstein, [5,6] Corrin and Storm, [7] Corrin, Edwards, and Nelson, [8] and Tcheurekdjian, Zettlemoyer, and Chessick [9] reported adsorption measurements on silver iodide powders they obtained by the reaction of silver nitrate with ammonium iodide in aqueous solution. Hall and Tompkins [10] and Tcheurekdjian, et al., [9] produced the silver iodide they used for adsorption studies by the reaction between silver nitrate and potassium iodide in aqueous solution. Powders obtained by precipitation were generally washed with distilled water to remove all traces of the counter ions in the wash water and then dried under vacuum. In some instances the dried powder was ground before use. Coulter and Candela [11] dissolved commercially prepared silver iodide in liquid ammonia and then recovered the silver iodide by pumping on the resulting complex. The powder obtained in this fashion had a larger surface area than the original.

Even though elaborate precautions were taken to wash precipitated silver iodide free of ionic impurities, the presence of these impurities was recognized. Coulter and Candela [11] corrected their isotherms for the hydration of impurities. Corrin and Storm [7] demonstrated the presence of both ammonium and nitrate ions by spot tests on sublimates obtained from precipitated silver iodide. Tcheurekdjian, et al., [9] also detected the presence of ammonium ions in their precipitates.

By the direct reaction of pure silver metal powder and pure iodine, Corrin, et al., [8] demonstrated the possibility of producing a silver iodide powder free from hygroscopic impurities. Further refinement of the technique by Corrin, Nelson, Cooley, and Rosenthal [12] resulted in powders of large surface area. The pure reactants, with an excess of silver metal, were sealed in a vessel which was then pumped on to remove volatile impurities while the iodine was kept at dry ice temperature. The vessel was placed in an oven and the reaction was allowed to proceed to completion. Unreacted iodine was removed from the reaction vessel by pumping at a temperature of 135C. Liquid ammonia was then distilled into the reaction vessel dissolving the silver iodide. This solution was transferred to another vessel by siphoning, leaving the excess silver metal in the reaction vessel. Finally, the liquid ammonia was removed by distillation producing a white ammonia-silver iodide complex. Decomposition of the complex occurred with continued pumping producing a finely divided, light insensitive, yellow silver iodide powder presumably free of ionic impurities. Corrin, et al., [8] made preliminary adsorption measurements on this material. Later, Nelson [13] and Corrin and Nelson [14] examined water vapor adsorption on this "pure" silver iodide at pressures much below saturation.

1.2 Adsorption Measurement Techniques Used in Previous Studies

Volumetric and gravimetric adsorption techniques are the two principal static means for measuring the isothermal adsorption of a vapor onto the surface of a solid. The isotherms measured by either

technique require the sample (adsorbent) to be maintained at a uniform temperature during the measurements. This is achieved by placing that portion of the adsorption system containing the sample into a constant temperature bath. The remaining parts of the adsorption system may be at any other (usually warmer) temperature.

In the volumetric technique, changes in the pressure of the adsorbate vapor within an adsorption system of known volume serve as a measure of the amount of vapor adsorbed. Initially, a specific quantity of the adsorbate is introduced into a portion of the system not containing the adsorbent. The pressure of the vapor in and the known volume of this portion of the system determine the amount of adsorbate present. Adsorption of the vapor by the sample occurs on exposing the adsorbent to the available adsorbate. The pressure in the system decreases to an equilibrium value. This pressure along with a new, known total volume gives the amount of adsorbate remaining as vapor in the system. The difference in the amount of adsorbate before and after exposure to the sample gives the amount of vapor adsorbed. Summing the increments in amount adsorbed gives the total quantity adsorbed at each equilibrium pressure.

The accuracy of the pressure gauge plays an important role in determining the accuracy of an isotherm. Each successive point on an isotherm is determined by summing the incremental amounts adsorbed. These increments are determined by differences in pressure-volume products. In effect, errors in pressure measurement at small coverages are carried into values at higher equilibrium pressures. As

shown in Appendix I, the error as well as the amount adsorbed is also accumulated.

Several different pressure measuring devices were used in volumetric adsorption studies of water vapor on silver iodide. Hall and Tompkins [10] used a Pirani gauge. Corrin, Moulik, and Cooley [15] used a capacitance manometer as a null meter and McLeod gauge to balance the system pressure. Mechanical gauges of several varieties were also employed: Coulter and Candela [11] used a Bodenstein quartz spiral; Tcheurekdjian, et al., [9] used a spoon gauge nulled by an oil manometer; Corrin, et al., [8] used a wide bore mercury manometer and cathetometer. Sensitivity of the pressure measuring devices, as reported by the authors, ranged from 0.005 torr [15] to 0.1 torr. [11] The accuracy to which the system volumes were determined was not mentioned.

Two difficulties are encountered in volumetric water adsorption measurements. Adsorption of water on the walls of the system must be taken into account by performing adsorption measurements without a sample in the system, i.e., a "blank" isotherm. Unless high surface area powders are used, the blank isotherm may be a substantial portion of the measured adsorption thereby compounding the errors introduced during the measurement of each isotherm. Also, at vapor pressures approaching saturation, the amount adsorbed rapidly increases on both the sample and walls requiring large doses of adsorbate to give detectable changes in the system pressure. In the case of water, this may lead to supersaturated conditions during dosing that may produce condensation in the system. Measurement of the pressure in this case would give an erroneous value for the amount of adsorbate

available. In the light of these problems, Corrin, et al., [7] considered equilibrium pressures equal to seventy percent of the saturation pressure to be the upper limit of volumetric measurements of water vapor adsorption.

Water adsorption isotherms are determined gravimetrically by measuring the change in weight of the sample and the equilibrium vapor pressure of the adsorbate. An essential difference from the volumetric method is that the change in weight of the sample gives the integral amount adsorbed at the measured equilibrium pressure. The accuracy of the balance weighing the sample as well as the accuracy of the pressure gauge determines the overall accuracy of the isotherm. Birstein [5,6] and Moskvitin, Dubinin, and Sarakhov [16] used quartz spiral springs with a cathetometer to measure the elongation of the spring as a function of the load. Nelson [13] and Corrin and Nelson [14] used a Cahn electrobalance to measure the change in weight of the sample. An advantage of the electrobalance over the quartz springs is that the electrobalance may be tared to maintain maximum sensitivity even under maximum load. Sensitivities from 0.2 to 10 micrograms were reported at the maximum rated load of one gram. A wide variety of pressure measuring and control techniques were employed: Birstein [5,6] used a Dubrovin gauge; Moskvitin, et al., [16] used a Pirani gauge; while Nelson [13] and Corrin and Nelson [14] maintained the equilibrium water vapor pressure by controlling the temperature of ice contained in their adsorption system.

Adsorption on the walls and balance is most pronounced on those portions of the adsorption and balance system which are the coldest.

In these studies this is the temperature of the sample. Unlike in the volumetric method, the adsorption on the walls of the gravimetric system does not interfere with the measurement of the change in weight of the sample. Also, the portion of the balance system at the same temperature as the sample generally has a surface area much smaller than the sample thereby reducing the blank isotherm contribution to the actual amount adsorbed by the powder sample.

1.3 Results of Previous Adsorption Studies

A comparison of adsorption isotherms measured on various samples of silver iodide points out the sensitivity of water adsorption on this material to impurities. The measurements of Nelson [13] on pure silver iodide yield Type II isotherms in the Brunauer classification with around one nanomole per square centimeter adsorbed at a vapor pressure eighty percent of the saturation pressure over the liquid. Tcheurekdjian, et al., [9] and Hall and Tompkins [10] found adsorption amounts several orders of magnitude greater at even lower pressures on carefully prepared samples of precipitated silver iodide. On material of more questionable purity, Moskvitin, et al., [16] measured still larger amounts and found essentially Type III isotherms with a knee at very low pressures. Coulter and Candela [11] and Birstein [5,6] obtained Type III isotherms with Birstein's amounts being the largest reported for water vapor adsorption on silver iodide. The measurements of Corrin, et al., [15] on pure silver iodide "doped" with hygroscopic impurities demonstrated the sensitivity of water adsorption on silver iodide to the presence of small amounts of impurities.

The wide variety of adsorption isotherms found for water adsorption on silver iodide produced a wide range of reported isosteric heats of adsorption computed directly from the isotherms. Very impure silver iodide gave isosteric heats much larger than the heat of condensation at low coverages. [5,6] Moskvitin, et al., [16] reported isosteric heats equal to the heat of condensation between 20C and 0C and a greater isosteric heat at temperatures between 0C and -20C. On carefully prepared, precipitated silver iodide, Tcheurekdjian, et al., [9] and Hall and Tompkins [10] found isosteric heats less than the heat of condensation at all coverages. In marked contrast, on pure silver iodide, Corrin and Nelson [14] reported isosteric heats greater than the heat of condensation at all coverages.

The diversity of adsorption information led to a considerable number of conflicting interpretations. However, as adsorption techniques improved and the role of impurities was recognized, the interpretations proposed rested on more subtle aspects of the observed adsorption.

1.4 Previous Interpretations Pertaining to Nucleation

Early adsorption studies by Coulter and Candela [11], Birstein, [5,6] and Moskvitin, et al., [16] were interpreted on the basis of the same epitaxy argument that led Vonnegut [2] to select silver iodide as a cloud seeding agent. With no direct or conclusive experimental evidence, the transition of the adsorbed water to ice was thought to occur because of an ice-like arrangement of water adsorbed on the underlying crystal structure. Further quantitative interpretation of

their works is difficult because the nature and amount of impurities present in their samples is unknown.

Zettlemoyer, Tcheurekdjian and Chessick [17] were the first to point out the deficiencies of the epitaxy argument in explaining the ability of silver iodide to nucleate ice. They contended the distribution of adsorbed water on the surface rather than the underlying crystal structure was the controlling factor in determining nucleation ability. Hall and Tompkins [10] interpreted their isosteric heats of adsorption as indicating the formation of clusters of adsorbed molecules on the surface. Clusters were more likely to form if the first molecules adsorbed were loosely bound to the surface and if the lattice spacing of adsorption sites was approximately the hydrogen bond length for water. There was no need to consider epitaxy other than to provide properly spaced adsorption sites.

Tcheurekdjian, et al., [9] confirmed Hall and Tompkins' findings. Comparing the B.E.T. area of their samples obtained from water adsorption to those found by argon adsorption led them to postulate the existance of isolated sites on which water adsorption occurs. These sites were thought to be hygroscopic impurities located at physical irregularities, steps, dislocations, etc. on the surface. Clusters formed at these sites then grew beyond the critical size and formed ice, the stable phase at subzero Celsius temperatures. Comparing several different nucleants with various ice nucleation efficiencies led them to postulate the water-argon site ratio was an important parameter determining the effectiveness of a given material as an ice nucleant.

Methanol vapor adsorption on pure silver iodide [12] by Edwards and Corrin [18] gave a different picture of the surface of pure silver iodide. The existence of a maximum and a minimum in the isosteric heat indicated both lateral cooperative interactions and a saturation of these interactions at higher coverages determined the heats of adsorption. This was interpreted as evidence for adsorption on patches of high energy sites on the surface. Patches rather than a uniform distribution of high energy sites were taken as the model because of the low coverage at which the minimum and maximum in the isosteric heat was observed. The use of methanol vapor as the adsorbate eliminated hydrogen bonding effects which could lead to the cluster formation model presented by Hall and Tompkins [10] and Tcheurekdjian, et al. [9] However, the water adsorption work of Corrin and Nelson [14] also found a maximum and minimum in the isosteric heats. This was also considered evidence that water adsorption occurred on high energy patches on the silver iodide surface with no three dimensional cluster formation occurring at the coverages studied.

The cluster model of adsorption, which appears to be valid for impure silver iodide powders, provides a convenient origin for a nucleation embryo. The three dimensional structure of the cluster grows by further adsorption until it exceeds the critical radius. Obviously ice must then form since at subzero Celsius temperatures ice is the stable phase. On pure silver iodide, however, no experimental evidence was found for cluster formation; adsorption occurred primarily on high energy patches. The studies which developed these models of adsorption on silver iodide covered a very limited

range of vapor pressures. Although interpretation of adsorption isotherms is most straight forward at low coverages where a thermodynamic approach is possible, it is at higher coverages, at pressures near saturation, that adsorption becomes the prelude to nucleation.

A few studies [6,11,16] extended their adsorption isotherms into the vicinity of saturation. Unfortunately, the material used in these studies appears, on hindsight, to be rather impure with little recognition of the amount or nature of the impurities by the authors. Birstein [5,6] assumed the adsorbed water at -20C was ice-like by an epitaxy argument. Coulter and Candela, [11] after correcting for a hydration effect ascribed to impurities, found a change in the slope of a Harkins-Jura plot of their data. This was interpreted as a change in phase of the adsorbed water although little significance was attached to this finding. Moskvitin, et al., [16] interpreted the change in slope of their isostere plots as a two-dimensional analog of a three dimensional phase change. Subsequent investigations did not indicate the occurrence of phase changes in adsorbed water on either pure or impure silver iodide powders at the coverages studied.

Evaluating adsorption measurements in the multilayer region led Zettlemoyer [19] to postulate the slope of the Frenkel-Halsey-Hill log vs log log plot of isotherm data is correlated to the nucleation ability of various materials. The slope of F-H-H isotherms is related, according to several authors, [20,21,22] to the propogation of surface effects through several molecular layers. Zettlemoyer's proposition was that good nucleants allow the effect of the surface

CHAPTER II

EXPERIMENTAL OBJECTIVES AND DESIGN

2.1 Objectives

The fundamental experimental objective of this work is to answer the following questions pertaining to the relationship between adsorption and nucleation on pure silver iodide:

1) Is the patch model of adsorption valid at the onset of nucleation?
2) What is the mechanism of nucleation on pure silver iodide?
3) Are the energetics of adsorption directly related to the energetics of nucleation?
4) How does the observed nucleation on pure silver iodide compare to cloud chamber studies?

These questions can be answered for pure silver iodide by measuring the adsorption of water vapor over a range of vapor pressures that leads to the nucleation of a condensed phase on the powder. In addition, future adsorption and nucleation studies on impure or doped silver iodide powders require a baseline for comparison to pure silver iodide.

2.2 Design

Adsorption studies emphasizing the region between ice and water saturation require a technique which is capable of measuring large amounts adsorbed on the powder with little interference to the measured amount by the adsorption system itself. A gravimetric approach using a Cahn electrobalance was chosen because of the relatively large capacity and accuracy of this type of balance.

Constant temperature baths, thermostats, provide thermally stable environments for the sample and a quantity of ice in the adsorption system. The temperature of the sample and ice specify the saturation pressures at the sample and the pressure of water vapor in the adsorption system, respectively.

An adsorption run consists of two parts: set up of the balance system, and measurement of the amount adsorbed. Initial set up consists in determining the zero offset and calibrating the balance while the system is evacuated. Adsorption measurements are made after admitting water vapor to the system. The amount adsorbed is detected as a change in weight of the sample. For each amount adsorbed, the equilibrium pressure of the vapor is specified by the ice reservoir temperature. This temperature is held constant until the weight of the sample becomes steady with time. Additional adsorption data points are determined by increasing the ice reservoir temperature in small increments. The pressure of the vapor in the system is thereby stepwise increased until the weight of the sample begins to increase without bound; the run is then terminated.

Adsorption data at -3.00C, -6.50C and -10.00C are adjusted for the zero offset and calibration for each run and the contribution of adsorption on the balance system itself. Interpretation of the data is by standard thermodynamic techniques for adsorption and nucleation.

CHAPTER III

THEORY

Physical adsorption of a gas by a solid implies the interactions between the gas and the solid are weak compared to chemical bonds. These interactions arise from short range van der Waals and London forces existing between molecules. Adsorbate molecules interact with adsorbent molecules and also with other adsorbate molecules. Physical adsorption occurs during the collision of a gas molecule with the surface of the adsorbent. Attractive van der Waals and London interactions cause gas molecules to linger in the vicinity of the surface. As long as a molecule remains bound to the surface under the influence of these weak interactions the molecule is physically adsorbed. Random fluctuations in the kinetic energy of an adsorbed molecule allow molecules to overcome the attractive forces holding it to the surface and return to the gas. Numerous collisions between molecules in the gas and the surface of the adsorbent permit physical adsorption to take place. The number of molecules adsorbed reaches an equilibrium condition when the rate at which molecules undergoing the adsorption process equals the rate at which molecules escape from the adsorbed state. This equilibrium can be statically detected by measuring the diminution of molecules in the gas phase as a change in gas pressure in the volumetric technique or by measuring the increase in mass of sample due to the adsorption of gas molecules in the gravimetric technique.

These measurements of physical adsorption are macroscopic averages over the entire surface of the adsorbent. The equivalence of these two techniques arises from the dynamic equilibrium established between the molecules in the vapor and adsorbed states.

3.1 Adsorption Isotherms

An adsorption isotherm relates the concentration of adsorbed molecules to the concentration of molecules in the vapor at a given temperature. The pressure of the vapor is a convenient measure of the concentration of molecules in the gas. The concentration of gas molecules adsorbed is frequently represented as the volume of gas adsorbed converted to STP conditions. A more direct measure of the concentration of gas molecules on the surface is moles of gas adsorbed per unit area of adsorbent surface.

In principle, the shape of an adsorption isotherm can be determined from the interactions between molecules and the dependence of these interactions on the nature of the adsorbent and adsorbate, the concentration and arrangement of adsorbed molecules, and the vapor pressure. However, the theoretical formulation of this dependence is not completely developed. Assumptions simplifying the nature of the adsorbent and the interactions between adsorbate and adsorbent lead to theoretical isotherms that empirically fit adsorption data over several ranges of amount adsorbed and pressure of the vapor but do not cover the entire isotherm. Usually, however, experimental isotherms are used to deduce the interactions that produced them.

3.2 Adsorption Thermodynamics

The thermodynamic system in which the adsorption process operates consists in an adsorbent, the adsorbate, and a vapor in equilibrium with the adsorbate. The adsorbent is usually a solid onto which molecules of the vapor are sorbed. These sorbed molecules are then referred to as the adsorbate. This system may be treated in several ways. Hill [23,24] treats adsorption as a special case of solution and develops thermodynamic functions specifically for the adsorbate. Everett [25,26] considers adsorption just as a modification of the solution process and uses solution thermodynamic functions to describe adsorption. Both approaches may use the method of surface excess introduced by Gibbs [27] and developed by Guggenheim [28] to conceptually separate the adsorbate from the vapor.

A basic assumption in the treatment of adsorption thermodynamics by both Hill's and Everett's methods is that the adsorbent is inert. That is, the thermodynamic properties of the adsorbent do not change even in the presence of the adsorbate. With this assumption, thermodynamic functions may be derived to pertain to the adsorbate alone. The difference between the thermodynamic properties of the vapor and of the adsorbate are attributed to the interaction of the adsorbate with the external potential field of the adsorbent. Perturbations of the structure and bond strengths of surface molecules in the adsorbent are included in the thermodynamic functions of the adsorbate and can not be treated separately. Hill [20,29] demonstrates that the asymmetrical adsorption thermodynamic approach he advocates and the symmetrical solution approach Everett advocates are equivalent

thermodynamically and differ only in the choice of parameters describing each system. The approach taken here is one of Gibbs' surface excess in which the assumption of an inert adsorbent produces an asymmetrical description of the adsorption process; i.e., only the chemical potential of the adsorbate is considered.

Consider a two component adsorption system of volume V containing n_1 and n_2 moles of the vapor and adsorbent, respectively, throughout which the temperature T, pressure P, and chemical potentials μ_1 and μ_2 of the components are uniform. This system may be subdivided by placing a boundary of surface area A in the vicinity of the vapor-adsorbent interface; the precise location of this boundary is later specified by assuming the adsorbent to be inert. The Gibbs free energy of the entire system is given by T, P, V, n_1, n_2, μ_1, μ_2, and the surface free energy of the arbitrary boundary ϕ:

$$dG = -SdT + VdP + \phi dA + \mu_1 dn_1 + \mu_2 dn_2. \tag{3.1}$$

Each portion of the total system can hypothetically be treated as being homogeneous up to the dividing surface with the same intensive variables as in the total system:

$$dG^V = -S^V dT + V^V dP + \mu_1 dn_1^V + \mu_2 dn_2^V \tag{3.2}$$

$$dG^S = -S^S dT + V^S dP + \mu_1 dn_1^S + \mu_2 dn_2^S \tag{3.3}$$

where the superscripts v and s indicate extensive quantities for the corresponding homogeneous subsystems. The contribution of the surface

region to the total Gibbs free energy is isolated by subtracting equations 3.2 and 3.3 from 3.1 leaving:

$$dG^{\sigma} = -S^{\sigma}dT + \phi dA + \mu_1 dn_1^{\sigma} + \mu_2 dn_2^{\sigma} \tag{3.4}$$

where the superscript σ refers to the extensive quantities of the surface region; i.e., surface excess quantities defined by:

$$\begin{aligned} G^{\sigma} &= G - G^{v} - G^{s} \\ S^{\sigma} &= S - S^{v} - S^{s} \\ n_{1,2}^{\sigma} &= n_{1,2} - n_{1,2}^{v} - n_{1,2}^{s}. \end{aligned} \tag{3.5}$$

The rigorous treatment of the volume of the surface region permitted by the Gibbs approach is shown by Hill [24,29] to exclude any treatment of perturbations of the adsorbent by the adsorbate.

Maintaining the intensive variables T, ϕ, μ_1, μ_2 constant, equation 3.4 can be integrated to give:

$$G^{\sigma} = \phi A + \mu_1 n_1^{\sigma} + \mu_2 n_2^{\sigma}. \tag{3.6}$$

Comparing the total differential of equation 3.6 to 3.4 leads to a Gibbs-Duhem expression for adsorption:

$$n_1^{\sigma} d\mu_1 + n_2^{\sigma} d\mu_2 = -S^{\sigma}dT + Ad\phi. \tag{3.7}$$

The precise location of the Gibbs dividing surface is now specified such that the surface excess of the adsorbent n_2 vanishes. This, in effect, places the dividing surface at the surface of an inert adsorbent such that the area A is just the surface area of the adsorbent [24]. With this assumption, equation 3.7 is reduced to:

$$d\mu_1 = -\tilde{S}^{\sigma}dT + (1/\Gamma)d\phi \tag{3.8}$$

where $\tilde{S}^{\sigma} = S^{\sigma}/n_1^{\sigma}$ is the molar entropy of the adsorbate and $\Gamma = n_1^{\sigma}/A$ is the surface excess of the adsorbate per unit area. For a one component system, Gibbs [27] defines the chemical potential such that for an ideal vapor:

$$d\mu_v = -\tilde{S}^{v}dT + RT\ d\ln p \tag{3.9}$$

where $\tilde{S}^{v}$ is the molar entropy of the vapor and p is the vapor pressure.

An analysis of the ratio of the fugacity to pressure for water vapor based on the second virial coefficient for water vapor given by Kauzmann and Eisenberg [30] and the relationship given by Lewis and Randall [31] indicates:

$$\frac{f}{p} = 1 - 5.2 \times 10^{-4}.$$

The approximation that water vapor behaves as an ideal gas in equation 3.9 is therefore justified.

For the vapor to be in equilibrium with the adsorbate the chemical potentials defined by equations 3.8 and 3.9 must be equal, therefore:

$$d\phi = \Gamma(\tilde{S}^{v} - \tilde{S}^{\sigma})dT - RT\Gamma d\ln p. \tag{3.10}$$

Under isothermal conditions, equation 3.10 can be integrated to yield the integrated form of the Gibbs equation:

$$\Pi_p = \phi_{(p=0)} - \phi_{(p)} = RT\int_{p'=0}^{p'=p} \Gamma d\ln p' \tag{3.11}$$

where Π_p is the change in surface free energy of the solid-vapor interface from $\phi_{(p=0)}$ without the adsorbate and $\phi_{(p)}$ in the presence

of the adsorbate at an equilibrium pressure p. Each adsorption isotherm giving Γ as a function of p allows Π_p to be computed. To completely determine Π_p, adsorption measurements must be made down to extremely low equilibrium vapor pressures and even then Γ must be extrapolated to zero pressure. This, of course, is necessary to compute the absolute magnitude of Π_p over the range of pressure indicated in equation 3.11. However, this range of pressure is completely arbitrary and depends only on the choice of reference state, in this case the bare adsorbent.

More information on the interaction between adsorbent and adsorbate can be obtained from isotherms measured on the same sample at different temperatures. These isotherms lead to the heats and entropies of adsorption. Several entropies and heats of adsorption can be defined in terms of the system conditions specified to obtain them. Hill [23,24,29] considers the entropy and heat defined by maintaining the intensive variables ϕ, T, and P constant to be most meaningful as they correspond to quantities derivable from statistical models. Everett [25,26], on the other hand, considers the heats and entropies obtained when Γ, T and A are held constant to be the most significant since they are more closely related to calorimetric measurements.

Hill's integral heat of adsorption [24,26] is readily found by setting $d\phi=0$ in equation 3.10 and rearranging the terms to give a Clausius-Clapeyron expression at constant ϕ:

$$\left(\frac{d\ \ln p}{dT}\right)_{\phi} = \frac{\tilde{S}^{v} - \tilde{S}^{\sigma}}{RT} \ . \qquad (3.12)$$

The integral heat of adsorption q_ϕ is defined by:

$$q_\phi = -R\left(\frac{d\ \ln p}{d(1/T)}\right)_\phi . \tag{3.13}$$

This integral heat of adsorption must be evaluated after the Gibbs equation is integrated over the entire range of adsorption amounts to obtain ϕ as a function of p. In the present experiment, such a large range of pressures is not investigated; the integral heat of adsorption will not be considered further.

A heat of adsorption easily obtained from adsorption studies is the isosteric heat of adsorption. This is the heat released per mole during the adsorption of an infinitesimally small amount of adsorbate at a given surface excess. Hill [24] and Everett [25] point out that this heat corresponds to heats obtained by calorimetry.

According to equation 3.4, the Gibbs free energy of the dividing surface is a function of the temperature, surface area, and composition. With the assumption that the adsorbent is inert and of constant area, equation 3.4 in partial differential form becomes:

$$dG^\sigma = \left(\frac{\partial G^\sigma}{\partial T}\right)_{n_1^\sigma} dT + \left(\frac{\partial G^\sigma}{\partial n_1^\sigma}\right)_T dn_1^\sigma . \tag{3.14}$$

Since dG^σ is an exact differential, the partial cross derivatives of the right hand terms must also be equal so that from equations 3.4 and 3.14:

$$-\left(\frac{\partial S^\sigma}{\partial n_1^\sigma}\right)_{T,A} = \frac{\partial}{\partial n_1^\sigma}\left(\frac{\partial G^\sigma}{\partial T}\right) = \frac{\partial}{\partial T}\left(\frac{\partial G^\sigma}{\partial n_1^\sigma}\right) = \left(\frac{\partial \mu_1}{\partial T}\right)_{n_1^\sigma,A} . \tag{3.15}$$

At equilibrium, the chemical potential of the adsorbate can be expressed as a function of $\underline{T}$ and $\underline{n_1^\sigma}$ for an adsorbent of constant area:

$$d\mu_1 = \left(\frac{\partial \mu_1}{\partial T}\right)_{n_1^\sigma, A} dT + \left(\frac{\partial \mu_1}{\partial n_1^\sigma}\right)_{T,A} dn_1^\sigma. \tag{3.16}$$

Equating the differentials of the chemical potentials given by equations 3.9 and 3.16 expresses the equilibrium between the vapor and adsorbate:

$$\left(\frac{\partial \mu_1}{\partial T}\right)_{n_1^\sigma, A} dT + \left(\frac{\partial \mu_1}{\partial n_1^\sigma}\right)_{T,A} dn_1^\sigma = - \tilde{S}^v dT + RT \, d\ln p. \tag{3.17}$$

From equation 3.15, the partial molar surface entropy is defined:

$$\bar{S}^\sigma = \left(\frac{\partial S^\sigma}{\partial n_1^\sigma}\right)_{T,A}. \tag{3.18}$$

At a constant surface excess, $dn_1^\sigma = 0$, equation 3.17 reduces to a Clausius - Clapeyron expression for the equilibrium pressure:

$$\left(\frac{d \ln p}{dT}\right)_\Gamma = \frac{\tilde{S}^v - \bar{S}^\sigma}{RT} \tag{3.19}$$

where $\underline{\Gamma}$ replaces $\underline{n_1^\sigma}$ to indicate constant surface excess. The isosteric heat of adsorption is defined from equation 3.19 as:

$$q_{st} = (\tilde{S}^v - \bar{S}^\sigma)T. \tag{3.20}$$

Rearranging the differential of temperature in equation 3.19 and using the definition in equation 3.20 yields:

$$q_{st} = -R \left(\frac{d \ln p}{d(1/T)}\right)_\Gamma. \tag{3.21}$$

The isosteric heat of adsorption can be computed from several isotherms measured on the same material but at different temperatures.

3.3 Nucleation Thermodynamics

Frenkel [32] viewed changes in phase as beginning with microscopic fluctuations in the density of a substance in the vicinity of the onset of a phase change. These heterophase fluctuations become more numerous and more stable as the conditions for a phase transition are approached. Volmer [33] first made use of this concept to describe the nucleation of a condensed phase from the vapor by a foreign substrate. Major contributions to the development of the theory of heterogeneous nucleation were made by Fletcher [34] during the last decade. The approach to heterogeneous nucleation taken here essentially follows Fletcher's treatment of the geometry of the embryo while incorporating some concepts from adsorption to make the symbolism of the two theories similar.

Most nucleation theories consider the direct transformation of a large number of molecules in the vapor via a heterophase fluctuation into a nucleation embryo. This embryo is assumed to contain a sufficient number of molecules to give the embryo the bulk properties of the condensed phase. The embryo then has a chemical potential and surface free energies similar to the bulk condensed phase in equilibrium with the substrate and vapor. The thermodynamic system includes only the embryo and vapor, with the remaining surface of the substrate included in the thermodynamics as a parameter. For

the transfer of dn moles of the vapor at constant temperature and pressure to an embryo containing n moles located on a plane substrate, the free energy change for the system can be written as:

$$dG = -(\mu_v - \mu_e)\, dn + \sum_i \phi_i\, dA_i \tag{3.22}$$

where μ_v and μ_e are the chemical potentials of the vapor and embryo and ϕ_i and A_i are the surface free energy and area of the i^{th} interface. In the simplest case three such surfaces exist: embryo-vapor, substrate-vapor, and substrate-embryo.

Spontaneous growth of the embryo occurs when the free energy change dG becomes negative. By dividing by dn, the critical size of the embryo can be determined by setting dG/dn = 0:

$$\frac{dG}{dn} = -(\mu_v - \mu_e) + \sum_i \phi_i \frac{dA_i}{dn} = 0$$

thus

$$\sum_i \phi_i \frac{dA_i}{dn} = \mu_v - \mu_e. \tag{3.23}$$

In order to evaluate the critical size, the dependence of the areas A_i on n must be established. All three areas are not independent. As the embryo grows laterally, the substrate-embryo interface enlarges causing a reduction in the substrate-vapor interface. Therefore, only two areas need to be defined to specify the summation in equation 3.23:

$$A_{ev} = \alpha\, n^{2/3}\ ,\ \frac{dA_{ev}}{dn} = \frac{2}{3}\,\alpha\, n^{-1/3}$$

$$A_{se} = \beta\, n^{2/3}\ ,\ \frac{dA_{se}}{dn} = \frac{2}{3}\,\beta\, n^{-1/3} \tag{3.24}$$

where α and β are arbitrary shape parameters. Equation 3.23 is simplified further by combining the surface free energy terms into a surface parameter [35] m:

$$m = \frac{\phi_{sv} - \phi_{se}}{\phi_{ev}} . \tag{3.25}$$

This surface parameter is dependent on the pressure of the vapor through ϕ_{sv}, for this interfacial free energy is dependent on the amount of vapor adsorbed on the surface surrounding the embryo through equation 3.11.

Equation 3.24 can now be rewritten incorporating equations 3.24 and 3.25:

$$n^{1/3} = \frac{\frac{2}{3}\phi_{ev}(\alpha - m\beta)}{\mu_v - \mu_e} . \tag{3.26}$$

For this equation to have physical significance $n^{1/3} > 0$, that is $\mu_v > \mu_e$ and $\alpha > m\beta$. Clearly $\alpha > \beta$ otherwise the volume of the embryo would be zero. Assuming the chemical potential of the embryo is similar but not quite equal to that for the bulk condensed phase:

$$\mu_v - \mu_e = RT \ln(p/p_o) - \mu' \tag{3.27}$$

where μ' accounts for the difference between the chemical potential of the embryo and of the bulk condensed phase and p_o is the equilibrium vapor pressure for the bulk phase. Now equation 3.26 becomes:

$$n^{1/3} = \frac{\frac{2}{3}\phi_{ev}(\alpha - m\beta)}{RT \ln(p/p_o) - \mu'} . \tag{3.28}$$

Above this size the embryo can grow spontaneously; nucleation occurs. Embellishments on this basic thermodynamic approach by Fletcher include consideration of nucleation: on curved substrates, [34] by spherical

cap shaped embryos, [34] by other embryo shapes, [35] on surface irregularities on the substrate, [36] on partially soluble particles, [37] etc. However, in each instance the same basic assumption is made: the embryo has the properties of the bulk phase.

Nucleation theory goes a step beyond thermodynamics to predict the rate of nucleation J. The kinetic basis for nucleation rate depends on the rate of collisions between molecules in the vapor and the surface of the embryo and the sticking or accommodation coefficient of the colliding molecules. A Boltzman distribution function based on the total free energy change required to form an embryo of critical size serves to properly weight the occurrence of any particular growth such that:

$$J = K \exp(\Delta G^*/RT) \tag{3.29}$$

where K is the kinetic coefficient giving rise to the growth and ΔG^* is the total free energy change of the embryo at its critical size as determined by equation 3.28 and the integration of equation 3.22.

CHAPTER IV

MATERIALS

The silver iodide used in this study of the interaction between water vapor and silver iodide was material prepared by the method of Corrin, et al., [12] at the University of Arizona in 1967. This material was stored during the intervening time in an evacuated, blackened pyrex ampule. All handling and transferring of this pure silver iodide powder was done in a closed, water vapor free glove box. After opening the ampule in the glove box, a portion of the powder was transferred to a red, glass-stoppered erlenmeyer flask.

The surface area of this powder was determined by krypton adsorption measurements to be 0.49 m^2/gm with a standard deviation of 5%. This surface area was determined from the combined data of measurements before the water adsorption measurements began and also after these measurements were completed. No change in the surface area was found over the time period of the water adsorption measurements, about nine months. Appendix I gives the results of the krypton adsorption measurements and an error analysis of this surface area computation technique.

The other component in the adsorption system investigated is the adsorbate, water vapor. During the adsorption measurements, water vapor is made available to the adsorbent from ice contained in the adsorption system. The water frozen to produce this ice is placed in its reservoir before any adsorption measurements are begun.

A small vessel containing water from a pyrex still was attached to the adsorption system through a small stopcock. The adsorption system was evacuated with the water at room temperature. As soon as the water began to boil the vessel was immersed in liquid nitrogen. Vacuum pumping continued to 10^{-6} torr. When this pressure was achieved the stopcock between the adsorption system and the water filled vessel was closed and the ice in the vessel was melted by placing a beaker of warm water around the vessel. Dissolved gases trapped in the ice rapidly escaped as the ice melted. Once completely melted, the stopcock was again opened and the freezing cycle repeated. Several freeze - thaw cycles effectively removed dissolved foreign gases from the water in the vessel. After the final freeze, the vacuum pump was turned off and a dewar of liquid nitrogen was placed around the ice reservoir on the adsorption system. The vessel was then immersed in an ice bath allowing water to be distilled by sublimation from the vessel to the ice reservoir until the reservoir was about half full. The stopcock to the water vessel was then closed leaving thoroughly degassed water in the ice reservoir of the adsorption system.

CHAPTER V

GRAVIMETRIC ADSORPTION SYSTEM

For the measurement of large adsorption amounts near saturation pressure, a gravimetric system based on a Cahn electrobalance was selected. Water vapor pressure regulation was obtained by thermostating a reservoir of ice attached to the system. Sample temperature was controlled by another thermostat. A diagram of the adsorption system is shown in Fig. 1.

5.1 Adsorption System

In the initial phase of an adsorption run the system is evacuated to insure the environment of the sample and the surface of the sample are free of volatile impurities. The silver iodide is not heated during degassing because of the ease with which this material sinters. Two stages of pumping are used to evacuate the system; a mechanical fore pump to reduce the system pressure below 10^{-3} torr and then an Ultek ion pump to bring the system pressure to about 10^{-6} torr. A 13X molecular sieve trap between the fore pump and adsorption system prevents the back-diffusion of pump oil vapors into the system. While the ion pump is in operation, the fore pump is isolated from the system by a bellows-sealed valve. The vacuum pumps are connected to the adsorption system through a large bore stopcock. A system pressure of less than 2×10^{-6} torr is maintained for twenty four hours prior to an adsorption run with the ion pump in operation.

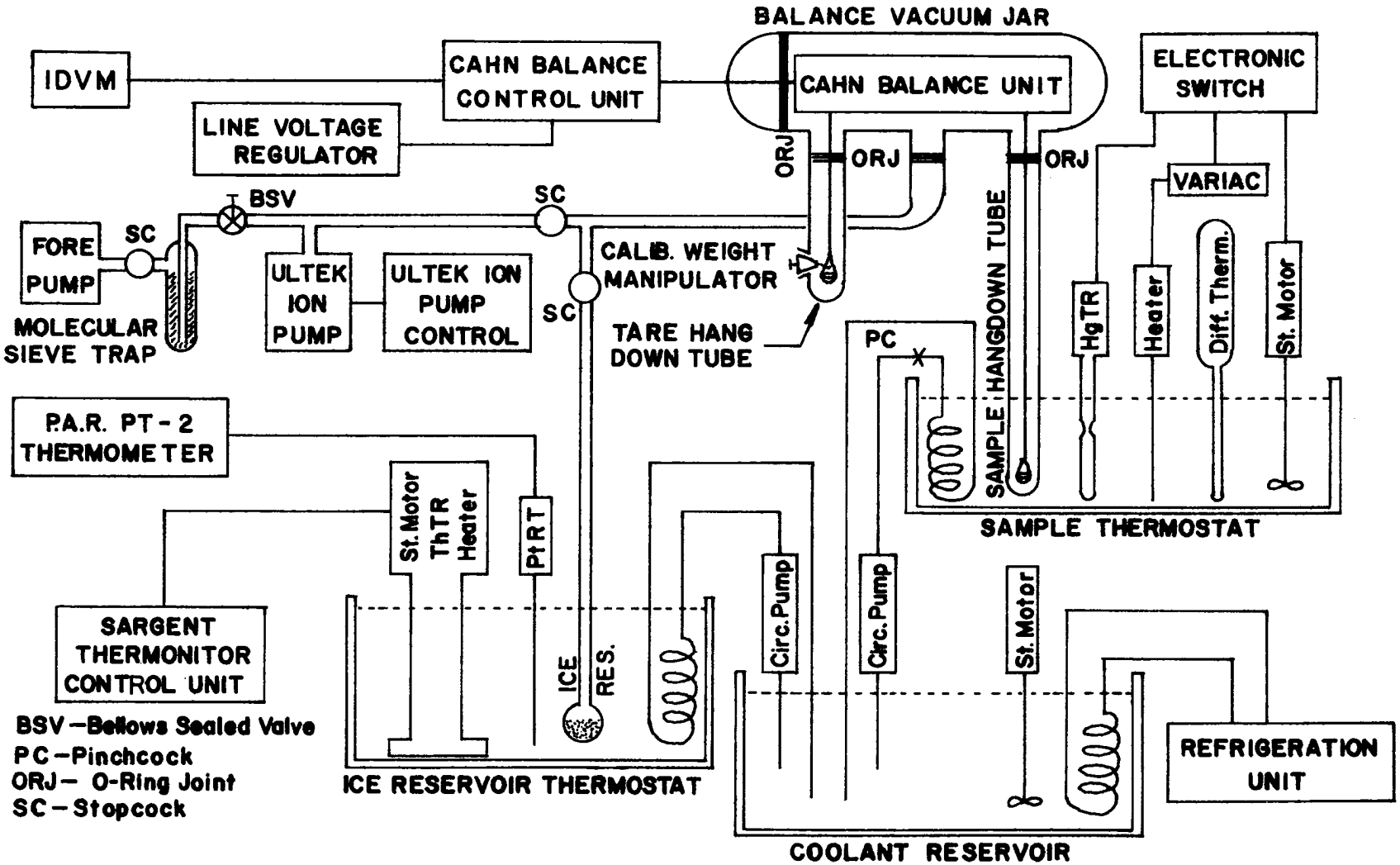

Figure 1: Diagram of gravimetric adsorption system.

A vacuum jar housing the Cahn electrobalance accounts for most of the system volume; approximately 3 liters. This cylindrical vessel has hemispherical end caps. One cap is removable for access to the balance and is sealed by an Apiezon-L greased Viton O-ring and doughnut-like ring clamps. Three greased, Viton O-ring sealed standard taper male joints on the underside of the balance jar allow the tare hangdown tube, sample hangdown tube and the remainder of the system to be attached to the jar. The sample hangdown tube extends a considerable distance below the balance. During a run this tube is immersed in a thermostat. The tare hangdown tube is much shorter. A small standard taper joint ground for a high vacuum seal with a male plug is attached near the bottom of the tare hangdown tube. Rotating the male plug allows a calibration weight to be raised and lowered while the system is evacuated. The third port is attached via 16 mm I.D. pyrex tubing to the stopcock from the vacuum line and to the stopcock from the ice reservoir.

The final portion of the adsorption system is the ice reservoir. A small stopcock connects this reservoir to the adsorption system. This spherical bulb contains approximately 6 ml of degassed, distilled water and is immersed in a thermostat.

5.2 Balance System

The Cahn model RG electrobalance determines the weight of a sample by measuring the current required to maintain the balance at a reference position. A flag on the balance arm intercepts a light beam falling on a phototube. The output current of the phototube is

proportional to the deflection of the balance arm. This current in turn activates a servoamplifier driving a torque motor to which the balance arm is attached. The feedback loop thus established maintains the arm at the reference position. The output signal from the balance is proportional to the torque motor current and thus also to the weight of the sample. Output sensitivity is rated at 50 millivolts/milligram.

Balance output voltage is measured with an integrating digital voltmeter (IDVM) that can be read to one microvolt. In order to reduce the noise on the balance signal induced by mechanical vibration (response of the electrobalance is very rapid) a 200 mfd capacitor is placed across the output terminals of the balance. In addition, the integrating feature of the voltmeter averages the signal over a period of one second. A Stabline voltage regulator isolates the balance from line voltage fluctuations minimizing electrical noise on the signal.

With a tared sample the minimum detectable weight change of the balance - voltmeter system in the mounting used is approximately 10 micrograms in a one gram sample. This value is larger than the rated sensitivity of the balance because of vibration noise on the balance output signal.

The sample pan and tare weight pan are suspended from opposite ends of the balance arm by quartz fibers. The pans are 16 mm diameter hemispherical shells of fused quartz weighing around 50 mg. Tare weights are of aluminum and tantalum along with a chromel wire support for a class M, 5 mg. rider used to calibrate the balance.

The balance jar and hangdown tubes are protected from ambient light by black paint and tape to prevent photodecay of the sample

and to provide the balance feedback network with a constant light level.

5.3 Sample Thermostat

Sample temperature is held constant during a run by a separate thermostat. A constant rate of cooling provided by a coolant circulated through a copper coil immersed in the bath is countered by on-off heating to maintain the control temperature. Temperature regulation is achieved with a mercurial thermoregulator. Cooling rate is controlled by a pinchcock throttling the coolant supply line. A variac in series with the heating element controls the heating rate. The temperature is kept uniform throughout the bath by a stirring motor. The sample hangdown tube is immersed some 20 cm. into the bath with the sample pan only a few centimeters from the bottom of the tube. Polyethylene foam insulation on the walls, bottom and top of the bath prevent diurnal room temperature fluctuations from disturbing the control temperature.

Temperature control over the duration of an isotherm measurement is possible to ±0.02C with the average deviation from the control temperature being even smaller. The period of the cyclic temperature fluctuations is approximately 3.5 minutes. Therefore, on the time scale of adsorption measurements made over several days, these fluctuations are effectively averaged out.

5.4 Ice Reservoir Thermostat

Temperature control in the ice reservoir is attained by countering a constant cooling rate with a proportional heat input. A Sargent

Thermonitor modified to control at subzero centigrade temperatures provides a heat input to the thermostat proportional to the temperature difference between the bath and control setting. The ice reservoir is immersed around 10 cm. into the bath. Polyethylene foam insulates the entire bath from room temperature fluctuations permitting long term temperature control to ±0.02C.

5.5 Coolant Supply

Both the sample thermostat and the ice reservoir thermostat are provided with coolant circulating through copper coils immersed in each bath. A large, well insulated vessel initially filled with a one to one solution of commercial ethylene glycol and tap water is cooled to -25C by a Blue M refrigeration unit. The bath is vigorously mixed. Two circulation pumps force the coolant through well insulated tubing, through the coils in the baths, and back into the coolant reservoir.

5.6 Platinum Resistance Thermometer

Both the sample temperature and ice reservoir temperature are measured by a platinum resistance thermometer. The resistance versus temperature response of a Rosemont Engineering probe was determined by the National Bureau of Standards and fitted to the Callendar-van Dusen equation:

$$\frac{R_s}{R_o} = 1 + \alpha T\left[1 + \frac{\delta}{100}\left(1 - \frac{T}{100}\right) + \frac{\beta T^2}{10^6}\left(1 - \frac{T}{100}\right)\right] \qquad (5.1)$$

where:

$$R_o = 25.5352 \text{ abs ohms},$$

$$\alpha = 3.926398 \times 10^{-3},$$

$$\beta = \begin{cases} 0.0 & , T > 0C, \\ 0.11011, & T < 0C, \end{cases}$$

$$\delta = 1.49166.$$

A Princeton Applied Research model PT-2 platinum resistance thermometer bridge unit serves to measure the sensor resistance. This unit is designed to follow the Callendar-van Dusen equation such that the temperature indicated by the front panel dials on the unit corresponds to the temperature of the sensor at temperatures above zero Celcius. At subzero temperatures the bridge resistance does not track the Callendar-van Dusen equation but simply follows a linear ramp function:

$$R_b = \frac{MR_o + ST}{M} \tag{5.2}$$

where M = 100 and S = 10 ohms/C. When the bridge is balanced, $R_s = R_b$, at subzero temperatures, the dial reading does not indicate the true sensor temperature.

To compensate for the discrepancy between the bridge resistance and temperature response of the platinum wire probe, a correction term must be added to the subzero temperature indicated by the PT-2 dials when the bridge is balanced. The first order correction for temperatures above -20C is:

$$\Delta = -T \; \frac{1 - \frac{1}{10\alpha R_o} + \frac{\delta}{100}\left(1 - \frac{T}{100}\right) + \frac{\beta T^2}{10^6}\left(1 - \frac{T}{100}\right)}{1 + \frac{S}{100}\left(1 - \frac{2T}{100}\right) + \frac{\beta T^2}{10^6}\left(3 - \frac{4T}{100}\right)} \tag{5.3}$$

where $\underline{T}$ is the dial temperature in degrees centigrade and $\underline{\Delta}$ is the correction term which must be added to the dial temperature to give the correct sensor temperature $\underline{T_s}$:

$$T_s = T + \Delta. \tag{5.4}$$

CHAPTER VI

PROCEDURE

The measurement of an adsorption isotherm with the gravimetric system described in Chapter V consists of several phases. Initially the sample is weighed out into a sample pan and then placed on the balance. Then the balance is tared and calibrated. Finally, isotherm points are obtained by measuring the weight change of the sample at constant ice reservoir temperatures.

6.1 Sample Preparation

A sample pan is partially filled with silver iodide in a closed, water vapor free glove box. The weight of the pan and a weighing bottle is determined beforehand. The sample pan containing silver iodide is placed into the weighing bottle while in the glove box, and the bottle is reweighed. By the change in weight of the bottle and pan the amount of sample in the pan is determined. The pan with sample is kept in the weighing bottle until the pan is placed on the balance.

6.2 Initial Sample Taring

Quartz suspension fibers are hung from loops at each end of the balance arm. On the tare hangdown fiber a tare pan is hung in which substitution weights are placed to approximately tare the sample pan plus sample. A 5 milligram, class M beam rider which serves as a calibration standard is also added to the tare pan. The tare hangdown tube is replaced with the O-ring joint lightly greased with Apiezon L.

Before the weighing bottle is opened, the sample hangdown tube is positioned beneath the suspension fiber. The weighing bottle is then opened and the sample pan is suspended on the quartz fiber. The hangdown tube is then carefully raised around the sample pan and afixed to the balance jar with the O-ring joint lightly greased. Clamps hold both the sample and tare hangdowns tubes in place.

With both the tare and sample hangdown tubes attached to the balance jar, the stopcock to the vacuum pump is very slowly opened, allowing a gradual decrease of system pressure. Static electricity which usually built up on the balance and adsorption system while placing a sample on the balance dissipated during the pump down; a polonium alpha particle source in the balance jar helped to dissipate the charge. The influence of the charges on the weight measured vanishes after several hours of pumping; the balance output signal on the IDVM becomes steady in time. This IDVM reading is noted and gives the zero offset in vacuum.

Dry nitrogen is then admitted to the balance jar through a small stopcock. The balance system is allowed to stabilize and the IDVM reading again noted; this gives the zero offset in air. The difference between the two zero offsets gives a buoyancy correction for taring the balance in air.

6.3 Final Taring

With the sample in a dry nitrogen atmosphere to prevent surface contamination of the sample, final taring is carried out by adjusting the contents of the tare pan to bring the IDVM reading to the buoyancy

correction. A slightly positive signal, i.e., sample heavier than tare, is desirable due to degassing of the sample during zero offset determination.

After the final adjustment of the tare weight, the 5 mg. rider is positioned on a small stirrup of chromel wire projecting out of the tare pan. The hangdown tube is positioned such that the wire arm of the vacuum manipulator engages the lifting loop of the rider. With this arrangement the rider may be removed from the tare pan and then replaced with the system closed and evacuated.

6.4 Zero Offset

The system is again slowly evacuated by the fore pump. After several hours the ion pump can be started and pumping continues with the fore pump isolated from the system. Pressure in the system drops rapidly to the pressure at which the pumping speed equals the degassing and low leak rate of the system. Zero offset observations begin after pressures below 4×10^{-6} torr are attained.

A zero offset value is determined by the average of 20 readings from the IDVM. The balance is set on the one milligram mass dial range with the recorder range set for 0.1 milligram full scale. With the IDVM sensitivity at 0.1 volts full scale, this allows the weight imbalance to be read from the IDVM to 0.1 micrograms. Readings are made at five second intervals and each reading is electronically averaged over one second. Zero offset averages are obtained at hourly intervals over a period of two days. Once the zero drift stabilizes, zero offset averages are taken at ten minute intervals to establish

the mean zero offset for the run; no consistent zero drift was found to take place once the zero offset is steady.

Zero offset is very sensitive to mechanical and electrical disturbances to the balance system. The balance jar is shielded from ambient light to help maintain a constant zero offset. The thermostats are mechanically isolated from the balance mounting grid by foam padding which adsorbs vibrations. The stirring motor for the sample thermostat is supported from the frame that carries the coolant circulating pumps and hoses. This frame is isolated from the balance mounting rack.

6.5 Balance Calibration

Removing the 5 mg. calibration weight from the tare pan produces an apparent increase in the sample weight. With the recorder span adjustment on the balance unit, the IDVM reading can be adjusted to correspond to 5 mg. As with the zero offset, the calibration value is also statistically determined. The calibration procedure is as follows:

The 5 mg. rider is removed from the tare pan by turning the vacuum manipulator after the zero offset has stabilized. After the system is again steady, calibration readings (20 values from the IDVM) are taken at ten minute intervals. Ten such averages usually suffice for an average calibration value. The rider is then replaced and a series of zero offset averages is again taken. The difference between the average calibration value and the average zero offset is the 5 mg. calibration weight. Dividing 5 mg. by this value gives a

multiplicative factor for adjusting all values to the 5 mg. calibration after subtracting the zero offset.

6.6 Sample Temperature Control

During the zero offset and calibration procedures the sample thermostat is installed around the sample hangdown tube; this thermostat must be removed to place a sample on the balance. Care is taken to prevent excess static electricity build up and mechanical shocks to the system. The bath is filled with an antifreeze solution. Coolant from the refrigeration unit is circulated through a cooling coil in the bath to begin lowering the bath temperature. The bath is stirred.

Bath temperature is monitored during the initial set up with the platinum resistance thermometer. A mercurial thermoregulator is adjusted to control at the desired sample temperature. Both the heating and cooling rates are varied to produce optimum temperature fluctuations about the mean consistant with long term thermal stability of the bath. The stability of the bath is monitored during the zero offset measurements with the PT-2 thermometer. During the isotherm measurements, sample bath temperature is monitored manually with a mercurial differential thermometer.

6.7 Isotherm Data Point

Each data point on an adsorption isotherm requires constancy of sample temperature and ice reservoir temperature. The sample temperature is kept constant throughout an isotherm measurement. Ice reservoir temperature is step wise increased to obtain new data points.

The temperature of the ice reservoir is adjusted via dials on the Thermonitor control unit and is monitored throughout a run with the platinum resistance thermometer. Adjustment of the Thermonitor control dials is done in gradual steps to prevent excessive overshoot of the desired bath temperature. The greater the temperature change desired the greater the overshoot; therefore, several small changes in temperature are made to reach the desired ice reservoir temperature, especially at pressures near saturation. The output of the PT-2 unit is graphically recorded for a permanent history of the ice reservoir temperature during a run.

With the ice reservoir maintained at constant temperature, adsorption of the vapor on the sample proceeds when the stopcock between the balance jar and ice reservoir is open. Twenty readings at five second intervals are read off the IDVM every half hour. When the weight ceases to continuously increase, readings are taken at ten minute intervals until a sufficient sample is collected to obtain an average value (usually ten). The average is recorded along with the ice reservoir temperature. Repeating this procedure, each time slightly increasing the ice reservoir temperature, produces an adsorption isotherm. A minimum of eight hours is given for the sample weight to reach equilibrium; as long as two days is allowed for equilibrium when large amounts are to be adsorbed.

6.8 Reversibility of Isotherm

After the equilibrium pressure exceeds saturation with respect to ice and before water saturation is attained, a desorption point is

obtained. The temperature of the ice reservoir is decreased to correspond to a vapor pressure just slightly below saturation with respect to ice. The sample weight decreases in the period of one or two days to an equilibrium value. The average weight is determined as above and is recorded along with the ice reservoir temperature. After the desorption point is obtained, the ice reservoir temperature is again increased and the isotherm continued.

6.9 Vapor Pressure Computation

Control of the sample and ice reservoir temperature effectively specifies the saturation vapor pressure at the sample and the equilibrium pressure of the vapor in the system, respectively. Analytical expressions for ice vapor pressure and the ratio of water to ice vapor pressures are used to compute the necessary pressures.

Washburn [38] derived the ratio of water to ice saturation pressure by an integration of a Clausius - Clapeyron expression using thermodynamic data. In the temperature range -16C to 0C the ratio of saturation pressures is:

$$\log_{10} \frac{p_w}{p_i} = - \frac{1.1489\ t}{T} - 1.33 \times 10^{-5}\ t^2 + 9.084 \times 10^{-8}\ t^3 - 1.08 \times 10^{-8}\ t^4 \qquad (6.1)$$

where $\underline{T}$ is the absolute temperature and $\underline{t}$ is the centigrade temperature and $\underline{w}$ and $\underline{i}$ correspond to water and ice saturation vapor pressures, respectively.

A recent experimental investigation of the vapor pressure of ice between 0.01C and -100C led Jancso, Papezin, and van Hook [39] to

the following expression for the saturation pressure of ice which fits their experimental values within measurement error:

$$\log_{10} p_i = -\frac{2481.604}{T} + 3.5712988 \log_{10} T + 1.901973 - 3.097203 \times 10^{-3} T - 1.7649 \times 10^{-7} T^2. \quad (6.2)$$

Equation 6.2 is used to obtain the equilibrium vapor pressure of water in the system from the ice reservoir temperature. Both equation 6.1 and 6.2 are needed to obtain the saturation pressure with respect to liquid supercooled water at the sample using the sample thermostat temperature. The relative pressure of water vapor at the sample is found by dividing the equilibrium vapor pressure by the saturation vapor pressure:

$$x = p_i/p_o \quad (6.3)$$

where x is the relative pressure and p_i the equilibrium pressure given by the ice reservoir temperature. The saturation pressure p_o may be either that over water or ice.

6.10 Corrections to Isotherms

After the isotherm is carried to as large a vapor pressure as possible, the values obtained must be adjusted for the zero offset. This gives the apparent amount adsorbed which is further corrected by multiplying that value by the calibration ratio to give the actual amount adsorbed at each data point.

The final correction accounts for adsorption on the balance system itself. To determine this correction, separate isotherms are measured at each sample temperature without having a sample of silver

iodide in the sample pan. Except for the tare weights, which are not all needed for the blank isotherm, all other factors and procedures are the same. The equilibrium relative pressure with respect to the liquid of the silver iodide adsorption isotherm determines the correction value taken from the blank isotherm that is to be subtracted from the previously corrected amount adsorbed. The totally corrected amount now corresponds to that adsorbed by the silver iodide powder alone.

Buoyancy corrections were calculated for the pressure range encountered and were found to be negligible in comparison to the estimated error of the weight change measurement.

THE INTERACTION BETWEEN WATER VAPOR AND PURE SILVER IODIDE IN THE VICINITY OF SATURATION

by

W. R. Barchet

This report was prepared with support from
the National Science Foundation
Grant No. GA-11309
Principal Investigator, Myron L. Corrin

Department of Atmospheric Science
Colorado State University
Fort Collins, Colorado

January 1971

Atmospheric Science Paper No. 168

ABSTRACT

The adsorptive interaction between water vapor and vacuum prepared, pure silver iodide leads to nucleation of a condensed phase at sufficiently low temperatures and high supersaturations. The purpose of this work is to determine: (1) if the patch model of adsorption of water vapor on pure silver iodide is valid at nucleation; (2) if the energetics of nucleation are comparable to the energetics of adsorption; (3) the mechanism of nucleation on pure silver iodide; and (4) how nucleation observed by adsorption methods compares to cloud chamber studies.

Previous adsorption studies were unable to answer these questions because of insufficient information near the onset of ice nucleation. Gravimetric adsorption measurements made with a Cahn electrobalance at pressures of water vapor between ice and water saturation in the absence of other gases demonstrated the ability of an adsorption technique to detect nucleation. Adsorption isotherms at -3.00C, -6.50C, and -10.00C led to isosteric heats of adsorption and $\underline{\Pi-\sigma}$ plots up to the onset of nucleation. Nucleation was detected as a rapid, continuous increase in the weight of the sample.

Peaks in the isosteric heat curves at coverages much below a statistical monolayer and coverages of one to three monolayers at the onset of nucleation at -10.00C and -6.50C demonstrated the patch model of adsorption is valid even at nucleation. At -3.00C nucleation did not occur even at water saturation. Kinks in the $\underline{\Pi-\sigma}$ plots for the -3.00C and -6.50C isotherms indicate a higher order phase transition in the film adsorbed on the patches of high energy sites.

Heats of adsorption and supersaturations at which nucleation of ice occurs are evidence for the formation of an increasingly duplex film as more water is adsorbed on the patch. The embryo does not acquire the bulk properties of ice until nucleation occurs.

The mechanism of nucleation on pure silver iodide involves primarily the high energy patches. At a sufficient coverage, ice is nucleated at the patch-embryo interface and propogates outward through the embryo. This adsorption technique detects the occurrence of nucleation on a single, most active site on the most active particle in the sample. From the three isotherms, a threshold temperature of -3.5C and ice supersaturation of 3.4% were estimated for nucleation on pure silver iodide. Cloud chamber studies, in contrast, require the number of nuclei activated to be several orders of magnitude larger to detect nucleation.

This work provides a much needed baseline against which future adsorption and nucleation studies on impure and doped silver iodide can be compared.

Wm. Richard Barchet
Atmospheric Science Department
Colorado State University
Fort Collins, Colorado 80521
March, 1971

ACKNOWLEDGMENTS

The encouragement and advice given by Dr. M. L. Corrin and the cooperation received from his doctoral committee is gratefully acknowledged by the author. A special word of thanks is extended to my wife, Doris, for her unbounded patience, understanding, and encouragement throughout the research for and writing of this manuscript. Miss Marji Allan is commended for typing the paper.

This work was funded by the Atmospheric Sciences Program, National Science Foundation, NSF Grant GA-11309.

The material presented in this report is taken from a dissertation by the author submitted as partial fulfillment of the degree of doctor of philosophy at Colorado State University.

TABLE OF CONTENTS

LIST OF TABLES

LIST OF FIGURES

CHAPTER I

INTRODUCTION

Adsorption of water vapor by silver iodide was long considered the first step in the interaction between silver iodide and water vapor that eventually led to the formation of ice. Demonstration of the ability of silver iodide to nucleate the ice phase was given by Schaefer [1] and Vonnegut [2] with laboratory studies in cold boxes. Numerous field studies sponsored by the Federal Government also showed the effectiveness of silver iodide powders and smokes in modifying supercooled clouds. [3,4]

Laboratory investigations of the isothermal adsorption of water vapor on silver iodide powders were first undertaken in the early 1950's. Since that time many studies were conducted with the purpose of describing this interaction and the surface characteristics of silver iodide using silver iodide powders made by various techniques. These adsorption measurements were made under isothermal conditions either volumetrically or gravimetrically.

Interpretation of these laboratory studies by the methods of adsorption thermodynamics gives information on the distribution of adsorbed molecules, the energies involved in adsorption, and the entropies of adsorption. These thermodynamic properties indicate the influence of the surface on adsorption. Correlation of these properties with the nucleation ability of the material leads to the patch and cluster models of adsorption which provide the foundations for nucleation.

1.1 Silver Iodide Used in Previous Studies

The majority of previous adsorption studies on silver iodide made use of powders obtained by precipitation from aqueous solution. Birstein, [5,6] Corrin and Storm, [7] Corrin, Edwards, and Nelson, [8] and Tcheurekdjian, Zettlemoyer, and Chessick [9] reported adsorption measurements on silver iodide powders they obtained by the reaction of silver nitrate with ammonium iodide in aqueous solution. Hall and Tompkins [10] and Tcheurekdjian, et al., [9] produced the silver iodide they used for adsorption studies by the reaction between silver nitrate and potassium iodide in aqueous solution. Powders obtained by precipitation were generally washed with distilled water to remove all traces of the counter ions in the wash water and then dried under vacuum. In some instances the dried powder was ground before use. Coulter and Candela [11] dissolved commercially prepared silver iodide in liquid ammonia and then recovered the silver iodide by pumping on the resulting complex. The powder obtained in this fashion had a larger surface area than the original.

Even though elaborate precautions were taken to wash precipitated silver iodide free of ionic impurities, the presence of these impurities was recognized. Coulter and Candela [11] corrected their isotherms for the hydration of impurities. Corrin and Storm [7] demonstrated the presence of both ammonium and nitrate ions by spot tests on sublimates obtained from precipitated silver iodide. Tcheurekdjian, et al., [9] also detected the presence of ammonium ions in their precipitates.

By the direct reaction of pure silver metal powder and pure iodine, Corrin, et al., [8] demonstrated the possibility of producing a silver iodide powder free from hygroscopic impurities. Further refinement of the technique by Corrin, Nelson, Cooley, and Rosenthal [12] resulted in powders of large surface area. The pure reactants, with an excess of silver metal, were sealed in a vessel which was then pumped on to remove volatile impurities while the iodine was kept at dry ice temperature. The vessel was placed in an oven and the reaction was allowed to proceed to completion. Unreacted iodine was removed from the reaction vessel by pumping at a temperature of 135C. Liquid ammonia was then distilled into the reaction vessel dissolving the silver iodide. This solution was transferred to another vessel by siphoning, leaving the excess silver metal in the reaction vessel. Finally, the liquid ammonia was removed by distillation producing a white ammonia-silver iodide complex. Decomposition of the complex occurred with continued pumping producing a finely divided, light insensitive, yellow silver iodide powder presumably free of ionic impurities. Corrin, et al., [8] made preliminary adsorption measurements on this material. Later, Nelson [13] and Corrin and Nelson [14] examined water vapor adsorption on this "pure" silver iodide at pressures much below saturation.

1.2 Adsorption Measurement Techniques Used in Previous Studies

Volumetric and gravimetric adsorption techniques are the two principal static means for measuring the isothermal adsorption of a vapor onto the surface of a solid. The isotherms measured by either

technique require the sample (adsorbent) to be maintained at a uniform temperature during the measurements. This is achieved by placing that portion of the adsorption system containing the sample into a constant temperature bath. The remaining parts of the adsorption system may be at any other (usually warmer) temperature.

In the volumetric technique, changes in the pressure of the adsorbate vapor within an adsorption system of known volume serve as a measure of the amount of vapor adsorbed. Initially, a specific quantity of the adsorbate is introduced into a portion of the system not containing the adsorbent. The pressure of the vapor in and the known volume of this portion of the system determine the amount of adsorbate present. Adsorption of the vapor by the sample occurs on exposing the adsorbent to the available adsorbate. The pressure in the system decreases to an equilibrium value. This pressure along with a new, known total volume gives the amount of adsorbate remaining as vapor in the system. The difference in the amount of adsorbate before and after exposure to the sample gives the amount of vapor adsorbed. Summing the increments in amount adsorbed gives the total quantity adsorbed at each equilibrium pressure.

The accuracy of the pressure gauge plays an important role in determining the accuracy of an isotherm. Each successive point on an isotherm is determined by summing the incremental amounts adsorbed. These increments are determined by differences in pressure-volume products. In effect, errors in pressure measurement at small coverages are carried into values at higher equilibrium pressures. As

shown in Appendix I, the error as well as the amount adsorbed is also accumulated.

Several different pressure measuring devices were used in volumetric adsorption studies of water vapor on silver iodide. Hall and Tompkins [10] used a Pirani gauge. Corrin, Moulik, and Cooley [15] used a capacitance manometer as a null meter and McLeod gauge to balance the system pressure. Mechanical gauges of several varieties were also employed: Coulter and Candela [11] used a Bodenstein quartz spiral; Tcheurekdjian, et al., [9] used a spoon gauge nulled by an oil manometer; Corrin, et al., [8] used a wide bore mercury manometer and cathetometer. Sensitivity of the pressure measuring devices, as reported by the authors, ranged from 0.005 torr [15] to 0.1 torr. [11] The accuracy to which the system volumes were determined was not mentioned.

Two difficulties are encountered in volumetric water adsorption measurements. Adsorption of water on the walls of the system must be taken into account by performing adsorption measurements without a sample in the system, i.e., a "blank" isotherm. Unless high surface area powders are used, the blank isotherm may be a substantial portion of the measured adsorption thereby compounding the errors introduced during the measurement of each isotherm. Also, at vapor pressures approaching saturation, the amount adsorbed rapidly increases on both the sample and walls requiring large doses of adsorbate to give detectable changes in the system pressure. In the case of water, this may lead to supersaturated conditions during dosing that may produce condensation in the system. Measurement of the pressure in this case would give an erroneous value for the amount of adsorbate

available. In the light of these problems, Corrin, et al., [7] considered equilibrium pressures equal to seventy percent of the saturation pressure to be the upper limit of volumetric measurements of water vapor adsorption.

Water adsorption isotherms are determined gravimetrically by measuring the change in weight of the sample and the equilibrium vapor pressure of the adsorbate. An essential difference from the volumetric method is that the change in weight of the sample gives the integral amount adsorbed at the measured equilibrium pressure. The accuracy of the balance weighing the sample as well as the accuracy of the pressure gauge determines the overall accuracy of the isotherm. Birstein [5,6] and Moskvitin, Dubinin, and Sarakhov [16] used quartz spiral springs with a cathetometer to measure the elongation of the spring as a function of the load. Nelson [13] and Corrin and Nelson [14] used a Cahn electrobalance to measure the change in weight of the sample. An advantage of the electrobalance over the quartz springs is that the electrobalance may be tared to maintain maximum sensitivity even under maximum load. Sensitivities from 0.2 to 10 micrograms were reported at the maximum rated load of one gram. A wide variety of pressure measuring and control techniques were employed: Birstein [5,6] used a Dubrovin gauge; Moskvitin, et al., [16] used a Pirani gauge; while Nelson [13] and Corrin and Nelson [14] maintained the equilibrium water vapor pressure by controlling the temperature of ice contained in their adsorption system.

Adsorption on the walls and balance is most pronounced on those portions of the adsorption and balance system which are the coldest.

In these studies this is the temperature of the sample. Unlike in the volumetric method, the adsorption on the walls of the gravimetric system does not interfere with the measurement of the change in weight of the sample. Also, the portion of the balance system at the same temperature as the sample generally has a surface area much smaller than the sample thereby reducing the blank isotherm contribution to the actual amount adsorbed by the powder sample.

1.3 Results of Previous Adsorption Studies

A comparison of adsorption isotherms measured on various samples of silver iodide points out the sensitivity of water adsorption on this material to impurities. The measurements of Nelson [13] on pure silver iodide yield Type II isotherms in the Brunauer classification with around one nanomole per square centimeter adsorbed at a vapor pressure eighty percent of the saturation pressure over the liquid. Tcheurekdjian, et al., [9] and Hall and Tompkins [10] found adsorption amounts several orders of magnitude greater at even lower pressures on carefully prepared samples of precipitated silver iodide. On material of more questionable purity, Moskvitin, et al., [16] measured still larger amounts and found essentially Type III isotherms with a knee at very low pressures. Coulter and Candela [11] and Birstein [5,6] obtained Type III isotherms with Birstein's amounts being the largest reported for water vapor adsorption on silver iodide. The measurements of Corrin, et al., [15] on pure silver iodide "doped" with hygroscopic impurities demonstrated the sensitivity of water adsorption on silver iodide to the presence of small amounts of impurities.

The wide variety of adsorption isotherms found for water adsorption on silver iodide produced a wide range of reported isosteric heats of adsorption computed directly from the isotherms. Very impure silver iodide gave isosteric heats much larger than the heat of condensation at low coverages. [5,6] Moskvitin, et al., [16] reported isosteric heats equal to the heat of condensation between 20C and 0C and a greater isosteric heat at temperatures between 0C and -20C. On carefully prepared, precipitated silver iodide, Tcheurekdjian, et al., [9] and Hall and Tompkins [10] found isosteric heats less than the heat of condensation at all coverages. In marked contrast, on pure silver iodide, Corrin and Nelson [14] reported isosteric heats greater than the heat of condensation at all coverages.

The diversity of adsorption information led to a considerable number of conflicting interpretations. However, as adsorption techniques improved and the role of impurities was recognized, the interpretations proposed rested on more subtle aspects of the observed adsorption.

1.4 Previous Interpretations Pertaining to Nucleation

Early adsorption studies by Coulter and Candela [11], Birstein, [5,6] and Moskvitin, et al., [16] were interpreted on the basis of the same epitaxy argument that led Vonnegut [2] to select silver iodide as a cloud seeding agent. With no direct or conclusive experimental evidence, the transition of the adsorbed water to ice was thought to occur because of an ice-like arrangement of water adsorbed on the underlying crystal structure. Further quantitative interpretation of

their works is difficult because the nature and amount of impurities present in their samples is unknown.

Zettlemoyer, Tcheurekdjian and Chessick [17] were the first to point out the deficiencies of the epitaxy argument in explaining the ability of silver iodide to nucleate ice. They contended the distribution of adsorbed water on the surface rather than the underlying crystal structure was the controlling factor in determining nucleation ability. Hall and Tompkins [10] interpreted their isosteric heats of adsorption as indicating the formation of clusters of adsorbed molecules on the surface. Clusters were more likely to form if the first molecules adsorbed were loosely bound to the surface and if the lattice spacing of adsorption sites was approximately the hydrogen bond length for water. There was no need to consider epitaxy other than to provide properly spaced adsorption sites.

Tcheurekdjian, et al., [9] confirmed Hall and Tompkins' findings. Comparing the B.E.T. area of their samples obtained from water adsorption to those found by argon adsorption led them to postulate the existance of isolated sites on which water adsorption occurs. These sites were thought to be hygroscopic impurities located at physical irregularities, steps, dislocations, etc. on the surface. Clusters formed at these sites then grew beyond the critical size and formed ice, the stable phase at subzero Celsius temperatures. Comparing several different nucleants with various ice nucleation efficiencies led them to postulate the water-argon site ratio was an important parameter determining the effectiveness of a given material as an ice nucleant.

Methanol vapor adsorption on pure silver iodide [12] by Edwards and Corrin [18] gave a different picture of the surface of pure silver iodide. The existence of a maximum and a minimum in the isosteric heat indicated both lateral cooperative interactions and a saturation of these interactions at higher coverages determined the heats of adsorption. This was interpreted as evidence for adsorption on patches of high energy sites on the surface. Patches rather than a uniform distribution of high energy sites were taken as the model because of the low coverage at which the minimum and maximum in the isosteric heat was observed. The use of methanol vapor as the adsorbate eliminated hydrogen bonding effects which could lead to the cluster formation model presented by Hall and Tompkins [10] and Tcheurekdjian, et al. [9] However, the water adsorption work of Corrin and Nelson [14] also found a maximum and minimum in the isosteric heats. This was also considered evidence that water adsorption occurred on high energy patches on the silver iodide surface with no three dimensional cluster formation occurring at the coverages studied.

The cluster model of adsorption, which appears to be valid for impure silver iodide powders, provides a convenient origin for a nucleation embryo. The three dimensional structure of the cluster grows by further adsorption until it exceeds the critical radius. Obviously ice must then form since at subzero Celsius temperatures ice is the stable phase. On pure silver iodide, however, no experimental evidence was found for cluster formation; adsorption occurred primarily on high energy patches. The studies which developed these models of adsorption on silver iodide covered a very limited

range of vapor pressures. Although interpretation of adsorption isotherms is most straight forward at low coverages where a thermodynamic approach is possible, it is at higher coverages, at pressures near saturation, that adsorption becomes the prelude to nucleation.

A few studies [6,11,16] extended their adsorption isotherms into the vicinity of saturation. Unfortunately, the material used in these studies appears, on hindsight, to be rather impure with little recognition of the amount or nature of the impurities by the authors. Birstein [5,6] assumed the adsorbed water at -20C was ice-like by an epitaxy argument. Coulter and Candela, [11] after correcting for a hydration effect ascribed to impurities, found a change in the slope of a Harkins-Jura plot of their data. This was interpreted as a change in phase of the adsorbed water although little significance was attached to this finding. Moskvitin, et al., [16] interpreted the change in slope of their isostere plots as a two-dimensional analog of a three dimensional phase change. Subsequent investigations did not indicate the occurrence of phase changes in adsorbed water on either pure or impure silver iodide powders at the coverages studied.

Evaluating adsorption measurements in the multilayer region led Zettlemoyer [19] to postulate the slope of the Frenkel-Halsey-Hill log vs log log plot of isotherm data is correlated to the nucleation ability of various materials. The slope of F-H-H isotherms is related, according to several authors, [20,21,22] to the propogation of surface effects through several molecular layers. Zettlemoyer's proposition was that good nucleants allow the effect of the surface

to be felt through several layers while the initially adsorbed molecules were loosely bound to the surface. Materials that gave slopes around -0.53 were found to be good nucleants; silver iodide was one of them.

It is clear that many previous adsorption studies on both pure and impure silver iodide failed to extend their measurements into the region of coverages and vapor pressures at which adsorption has a direct bearing on nucleation. The cluster models [10,16] consider a continuous growth of the cluster leads to nucleation with no experimental evidence to verify this assumption. The patch model [14,18] does not indicate how adsorption on the patch leads to a three dimensional water structure which may then serve as a nucleation embryo. These points can be resolved by measurements in the vicinity of the occurrence of nucleation, i.e., above ice saturation vapor pressure.

CHAPTER II

EXPERIMENTAL OBJECTIVES AND DESIGN

2.1 Objectives

The fundamental experimental objective of this work is to answer the following questions pertaining to the relationship between adsorption and nucleation on pure silver iodide:

1) Is the patch model of adsorption valid at the onset of nucleation?
2) What is the mechanism of nucleation on pure silver iodide?
3) Are the energetics of adsorption directly related to the energetics of nucleation?
4) How does the observed nucleation on pure silver iodide compare to cloud chamber studies?

These questions can be answered for pure silver iodide by measuring the adsorption of water vapor over a range of vapor pressures that leads to the nucleation of a condensed phase on the powder. In addition, future adsorption and nucleation studies on impure or doped silver iodide powders require a baseline for comparison to pure silver iodide.

2.2 Design

Adsorption studies emphasizing the region between ice and water saturation require a technique which is capable of measuring large amounts adsorbed on the powder with little interference to the measured amount by the adsorption system itself. A gravimetric approach using a Cahn electrobalance was chosen because of the relatively large capacity and accuracy of this type of balance.

Constant temperature baths, thermostats, provide thermally stable environments for the sample and a quantity of ice in the adsorption system. The temperature of the sample and ice specify the saturation pressures at the sample and the pressure of water vapor in the adsorption system, respectively.

An adsorption run consists of two parts: set up of the balance system, and measurement of the amount adsorbed. Initial set up consists in determining the zero offset and calibrating the balance while the system is evacuated. Adsorption measurements are made after admitting water vapor to the system. The amount adsorbed is detected as a change in weight of the sample. For each amount adsorbed, the equilibrium pressure of the vapor is specified by the ice reservoir temperature. This temperature is held constant until the weight of the sample becomes steady with time. Additional adsorption data points are determined by increasing the ice reservoir temperature in small increments. The pressure of the vapor in the system is thereby stepwise increased until the weight of the sample begins to increase without bound; the run is then terminated.

Adsorption data at -3.00C, -6.50C and -10.00C are adjusted for the zero offset and calibration for each run and the contribution of adsorption on the balance system itself. Interpretation of the data is by standard thermodynamic techniques for adsorption and nucleation.

CHAPTER III

THEORY

Physical adsorption of a gas by a solid implies the interactions between the gas and the solid are weak compared to chemical bonds. These interactions arise from short range van der Waals and London forces existing between molecules. Adsorbate molecules interact with adsorbent molecules and also with other adsorbate molecules. Physical adsorption occurs during the collision of a gas molecule with the surface of the adsorbent. Attractive van der Waals and London interactions cause gas molecules to linger in the vicinity of the surface. As long as a molecule remains bound to the surface under the influence of these weak interactions the molecule is physically adsorbed. Random fluctuations in the kinetic energy of an adsorbed molecule allow molecules to overcome the attractive forces holding it to the surface and return to the gas. Numerous collisions between molecules in the gas and the surface of the adsorbent permit physical adsorption to take place. The number of molecules adsorbed reaches an equilibrium condition when the rate at which molecules undergoing the adsorption process equals the rate at which molecules escape from the adsorbed state. This equilibrium can be statically detected by measuring the diminution of molecules in the gas phase as a change in gas pressure in the volumetric technique or by measuring the increase in mass of sample due to the adsorption of gas molecules in the gravimetric technique.

These measurements of physical adsorption are macroscopic averages over the entire surface of the adsorbent. The equivalence of these two techniques arises from the dynamic equilibrium established between the molecules in the vapor and adsorbed states.

3.1 Adsorption Isotherms

An adsorption isotherm relates the concentration of adsorbed molecules to the concentration of molecules in the vapor at a given temperature. The pressure of the vapor is a convenient measure of the concentration of molecules in the gas. The concentration of gas molecules adsorbed is frequently represented as the volume of gas adsorbed converted to STP conditions. A more direct measure of the concentration of gas molecules on the surface is moles of gas adsorbed per unit area of adsorbent surface.

In principle, the shape of an adsorption isotherm can be determined from the interactions between molecules and the dependence of these interactions on the nature of the adsorbent and adsorbate, the concentration and arrangement of adsorbed molecules, and the vapor pressure. However, the theoretical formulation of this dependence is not completely developed. Assumptions simplifying the nature of the adsorbent and the interactions between adsorbate and adsorbent lead to theoretical isotherms that empirically fit adsorption data over several ranges of amount adsorbed and pressure of the vapor but do not cover the entire isotherm. Usually, however, experimental isotherms are used to deduce the interactions that produced them.

3.2 Adsorption Thermodynamics

The thermodynamic system in which the adsorption process operates consists in an adsorbent, the adsorbate, and a vapor in equilibrium with the adsorbate. The adsorbent is usually a solid onto which molecules of the vapor are sorbed. These sorbed molecules are then referred to as the adsorbate. This system may be treated in several ways. Hill [23,24] treats adsorption as a special case of solution and develops thermodynamic functions specifically for the adsorbate. Everett [25,26] considers adsorption just as a modification of the solution process and uses solution thermodynamic functions to describe adsorption. Both approaches may use the method of surface excess introduced by Gibbs [27] and developed by Guggenheim [28] to conceptually separate the adsorbate from the vapor.

A basic assumption in the treatment of adsorption thermodynamics by both Hill's and Everett's methods is that the adsorbent is inert. That is, the thermodynamic properties of the adsorbent do not change even in the presence of the adsorbate. With this assumption, thermodynamic functions may be derived to pertain to the adsorbate alone. The difference between the thermodynamic properties of the vapor and of the adsorbate are attributed to the interaction of the adsorbate with the external potential field of the adsorbent. Perturbations of the structure and bond strengths of surface molecules in the adsorbent are included in the thermodynamic functions of the adsorbate and can not be treated separately. Hill [20,29] demonstrates that the asymmetrical adsorption thermodynamic approach he advocates and the symmetrical solution approach Everett advocates are equivalent

thermodynamically and differ only in the choice of parameters describing each system. The approach taken here is one of Gibbs' surface excess in which the assumption of an inert adsorbent produces an asymmetrical description of the adsorption process; i.e., only the chemical potential of the adsorbate is considered.

Consider a two component adsorption system of volume V containing n_1 and n_2 moles of the vapor and adsorbent, respectively, throughout which the temperature T, pressure P, and chemical potentials μ_1 and μ_2 of the components are uniform. This system may be subdivided by placing a boundary of surface area A in the vicinity of the vapor-adsorbent interface; the precise location of this boundary is later specified by assuming the adsorbent to be inert. The Gibbs free energy of the entire system is given by T, P, V, n_1, n_2, μ_1, μ_2, and the surface free energy of the arbitrary boundary ϕ:

$$dG = -SdT + VdP + \phi dA + \mu_1 dn_1 + \mu_2 dn_2. \tag{3.1}$$

Each portion of the total system can hypothetically be treated as being homogeneous up to the dividing surface with the same intensive variables as in the total system:

$$dG^V = -S^V dT + V^V dP + \mu_1 dn_1^V + \mu_2 dn_2^V \tag{3.2}$$

$$dG^S = -S^S dT + V^S dP + \mu_1 dn_1^S + \mu_2 dn_2^S \tag{3.3}$$

where the superscripts v and s indicate extensive quantities for the corresponding homogeneous subsystems. The contribution of the surface

region to the total Gibbs free energy is isolated by subtracting equations 3.2 and 3.3 from 3.1 leaving:

$$dG^{\sigma} = -S^{\sigma}dT + \phi dA + \mu_1 dn_1^{\sigma} + \mu_2 dn_2^{\sigma} \tag{3.4}$$

where the superscript $\underline{\sigma}$ refers to the extensive quantities of the surface region; i.e., surface excess quantities defined by:

$$\begin{aligned} G^{\sigma} &= G - G^{v} - G^{s} \\ S^{\sigma} &= S - S^{v} - S^{s} \\ n_{1,2}^{\sigma} &= n_{1,2} - n_{1,2}^{v} - n_{1,2}^{s}. \end{aligned} \tag{3.5}$$

The rigorous treatment of the volume of the surface region permitted by the Gibbs approach is shown by Hill [24,29] to exclude any treatment of perturbations of the adsorbent by the adsorbate.

Maintaining the intensive variables $\underline{T}$, $\underline{\phi}$, $\underline{\mu_1}$, $\underline{\mu_2}$ constant, equation 3.4 can be integrated to give:

$$G^{\sigma} = \phi A + \mu_1 n_1^{\sigma} + \mu_2 n_2^{\sigma}. \tag{3.6}$$

Comparing the total differential of equation 3.6 to 3.4 leads to a Gibbs-Duhem expression for adsorption:

$$n_1^{\sigma}d\mu_1 + n_2^{\sigma}d\mu_2 = -S^{\sigma}dT + Ad\phi. \tag{3.7}$$

The precise location of the Gibbs dividing surface is now specified such that the surface excess of the adsorbent $\underline{n_2}$ vanishes. This, in effect, places the dividing surface at the surface of an inert adsorbent such that the area $\underline{A}$ is just the surface area of the adsorbent [24]. With this assumption, equation 3.7 is reduced to:

$$d\mu_1 = -\tilde{S}^{\sigma}dT + (1/\Gamma)d\phi \tag{3.8}$$

where $\tilde{S}^{\sigma} = S^{\sigma}/n_1^{\sigma}$ is the molar entropy of the adsorbate and $\Gamma = n_1^{\sigma}/A$ is the surface excess of the adsorbate per unit area. For a one component system, Gibbs [27] defines the chemical potential such that for an ideal vapor:

$$d\mu_v = -\tilde{S}^{v}dT + RT\ d\ln p \tag{3.9}$$

where $\tilde{S}^{v}$ is the molar entropy of the vapor and p is the vapor pressure.

An analysis of the ratio of the fugacity to pressure for water vapor based on the second virial coefficient for water vapor given by Kauzmann and Eisenberg [30] and the relationship given by Lewis and Randall [31] indicates:

$$\frac{f}{p} = 1 - 5.2 \times 10^{-4}.$$

The approximation that water vapor behaves as an ideal gas in equation 3.9 is therefore justified.

For the vapor to be in equilibrium with the adsorbate the chemical potentials defined by equations 3.8 and 3.9 must be equal, therefore:

$$d\phi = \Gamma(\tilde{S}^{v} - \tilde{S}^{\sigma})dT - RT\Gamma d\ln p. \tag{3.10}$$

Under isothermal conditions, equation 3.10 can be integrated to yield the integrated form of the Gibbs equation:

$$\Pi_p = \phi_{(p=0)} - \phi_{(p)} = RT\int_{p'=0}^{p'=p} \Gamma d\ln p' \tag{3.11}$$

where Π_p is the change in surface free energy of the solid-vapor interface from $\phi_{(p=0)}$ without the adsorbate and $\phi_{(p)}$ in the presence

of the adsorbate at an equilibrium pressure p. Each adsorption isotherm giving Γ as a function of p allows Π_p to be computed. To completely determine Π_p, adsorption measurements must be made down to extremely low equilibrium vapor pressures and even then Γ must be extrapolated to zero pressure. This, of course, is necessary to compute the absolute magnitude of Π_p over the range of pressure indicated in equation 3.11. However, this range of pressure is completely arbitrary and depends only on the choice of reference state, in this case the bare adsorbent.

More information on the interaction between adsorbent and adsorbate can be obtained from isotherms measured on the same sample at different temperatures. These isotherms lead to the heats and entropies of adsorption. Several entropies and heats of adsorption can be defined in terms of the system conditions specified to obtain them. Hill [23,24,29] considers the entropy and heat defined by maintaining the intensive variables ϕ, T, and P constant to be most meaningful as they correspond to quantities derivable from statistical models. Everett [25,26], on the other hand, considers the heats and entropies obtained when Γ, T and A are held constant to be the most significant since they are more closely related to calorimetric measurements.

Hill's integral heat of adsorption [24,26] is readily found by setting $d\phi=0$ in equation 3.10 and rearranging the terms to give a Clausius-Clapeyron expression at constant ϕ:

$$\left(\frac{d\ \ln p}{dT}\right)_{\phi} = \frac{\tilde{S}^{v} - \tilde{S}^{\sigma}}{RT} . \qquad (3.12)$$

The integral heat of adsorption q_ϕ is defined by:

$$q_\phi = -R\left(\frac{d\ \ln p}{d(1/T)}\right)_\phi . \tag{3.13}$$

This integral heat of adsorption must be evaluated after the Gibbs equation is integrated over the entire range of adsorption amounts to obtain ϕ as a function of p. In the present experiment, such a large range of pressures is not investigated; the integral heat of adsorption will not be considered further.

A heat of adsorption easily obtained from adsorption studies is the isosteric heat of adsorption. This is the heat released per mole during the adsorption of an infinitesimally small amount of adsorbate at a given surface excess. Hill [24] and Everett [25] point out that this heat corresponds to heats obtained by calorimetry.

According to equation 3.4, the Gibbs free energy of the dividing surface is a function of the temperature, surface area, and composition. With the assumption that the adsorbent is inert and of constant area, equation 3.4 in partial differential form becomes:

$$dG^\sigma = \left(\frac{\partial G^\sigma}{\partial T}\right)_{n_1^\sigma} dT + \left(\frac{\partial G^\sigma}{\partial n_1^\sigma}\right)_T dn_1^\sigma . \tag{3.14}$$

Since dG^σ is an exact differential, the partial cross derivatives of the right hand terms must also be equal so that from equations 3.4 and 3.14:

$$-\left(\frac{\partial S^\sigma}{\partial n_1^\sigma}\right)_{T,A} = \frac{\partial}{\partial n_1^\sigma}\left(\frac{\partial G^\sigma}{\partial T}\right) = \frac{\partial}{\partial T}\left(\frac{\partial G^\sigma}{\partial n_1^\sigma}\right) = \left(\frac{\partial \mu_1}{\partial T}\right)_{n_1^\sigma, A} . \tag{3.15}$$

At equilibrium, the chemical potential of the adsorbate can be expressed as a function of $\underline{T}$ and $\underline{n_1^\sigma}$ for an adsorbent of constant area:

$$d\mu_1 = \left(\frac{\partial \mu_1}{\partial T}\right)_{n_1^\sigma, A} dT + \left(\frac{\partial \mu_1}{\partial n_1^\sigma}\right)_{T,A} dn_1^\sigma. \tag{3.16}$$

Equating the differentials of the chemical potentials given by equations 3.9 and 3.16 expresses the equilibrium between the vapor and adsorbate:

$$\left(\frac{\partial \mu_1}{\partial T}\right)_{n_1^\sigma, A} dT + \left(\frac{\partial \mu_1}{\partial n_1^\sigma}\right)_{T,A} dn_1^\sigma = -\tilde{S}^v dT + RT\, d\ln p. \tag{3.17}$$

From equation 3.15, the partial molar surface entropy is defined:

$$\bar{S}^\sigma = \left(\frac{\partial S^\sigma}{\partial n_1^\sigma}\right)_{T,A}. \tag{3.18}$$

At a constant surface excess, $dn_1^\sigma = 0$, equation 3.17 reduces to a Clausius - Clapeyron expression for the equilibrium pressure:

$$\left(\frac{d\ \ln p}{dT}\right)_\Gamma = \frac{\tilde{S}^v - \bar{S}^\sigma}{RT} \tag{3.19}$$

where $\underline{\Gamma}$ replaces $\underline{n_1^\sigma}$ to indicate constant surface excess. The isosteric heat of adsorption is defined from equation 3.19 as:

$$q_{st} = (\tilde{S}^v - \bar{S}^\sigma)T. \tag{3.20}$$

Rearranging the differential of temperature in equation 3.19 and using the definition in equation 3.20 yields:

$$q_{st} = -R\left(\frac{d\ \ln\ p}{d(1/T)}\right)_\Gamma. \tag{3.21}$$

The isosteric heat of adsorption can be computed from several isotherms measured on the same material but at different temperatures.

3.3 Nucleation Thermodynamics

Frenkel [32] viewed changes in phase as beginning with microscopic fluctuations in the density of a substance in the vicinity of the onset of a phase change. These heterophase fluctuations become more numerous and more stable as the conditions for a phase transition are approached. Volmer [33] first made use of this concept to describe the nucleation of a condensed phase from the vapor by a foreign substrate. Major contributions to the development of the theory of heterogeneous nucleation were made by Fletcher [34] during the last decade. The approach to heterogeneous nucleation taken here essentially follows Fletcher's treatment of the geometry of the embryo while incorporating some concepts from adsorption to make the symbolism of the two theories similar.

Most nucleation theories consider the direct transformation of a large number of molecules in the vapor via a heterophase fluctuation into a nucleation embryo. This embryo is assumed to contain a sufficient number of molecules to give the embryo the bulk properties of the condensed phase. The embryo then has a chemical potential and surface free energies similar to the bulk condensed phase in equilibrium with the substrate and vapor. The thermodynamic system includes only the embryo and vapor, with the remaining surface of the substrate included in the thermodynamics as a parameter. For

the transfer of dn moles of the vapor at constant temperature and pressure to an embryo containing n moles located on a plane substrate, the free energy change for the system can be written as:

$$dG = -(\mu_v - \mu_e)\, dn + \sum_i \phi_i\, dA_i \tag{3.22}$$

where μ_v and μ_e are the chemical potentials of the vapor and embryo and ϕ_i and A_i are the surface free energy and area of the i^{th} interface. In the simplest case three such surfaces exist: embryo-vapor, substrate-vapor, and substrate-embryo.

Spontaneous growth of the embryo occurs when the free energy change dG becomes negative. By dividing by dn, the critical size of the embryo can be determined by setting dG/dn = 0:

$$\frac{dG}{dn} = -(\mu_v - \mu_e) + \sum_i \phi_i \frac{dA_i}{dn} = 0$$

thus

$$\sum_i \phi_i \frac{dA_i}{dn} = \mu_v - \mu_e. \tag{3.23}$$

In order to evaluate the critical size, the dependence of the areas A_i on n must be established. All three areas are not independent. As the embryo grows laterally, the substrate-embryo interface enlarges causing a reduction in the substrate-vapor interface. Therefore, only two areas need to be defined to specify the summation in equation 3.23:

$$A_{ev} = \alpha\, n^{2/3}\ ,\ \frac{dA_{ev}}{dn} = \frac{2}{3}\,\alpha\, n^{-1/3}$$

$$A_{se} = \beta\, n^{2/3}\ ,\ \frac{dA_{se}}{dn} = \frac{2}{3}\,\beta\, n^{-1/3} \tag{3.24}$$

where α and β are arbitrary shape parameters. Equation 3.23 is simplified further by combining the surface free energy terms into a surface parameter [35] m:

$$m = \frac{\phi_{sv} - \phi_{se}}{\phi_{ev}} . \tag{3.25}$$

This surface parameter is dependent on the pressure of the vapor through ϕ_{sv}, for this interfacial free energy is dependent on the amount of vapor adsorbed on the surface surrounding the embryo through equation 3.11.

Equation 3.24 can now be rewritten incorporating equations 3.24 and 3.25:

$$n^{1/3} = \frac{\frac{2}{3}\phi_{ev}(\alpha - m\beta)}{\mu_v - \mu_e} . \tag{3.26}$$

For this equation to have physical significance $n^{1/3} > 0$, that is $\mu_v > \mu_e$ and $\alpha > m\beta$. Clearly $\alpha > \beta$ otherwise the volume of the embryo would be zero. Assuming the chemical potential of the embryo is similar but not quite equal to that for the bulk condensed phase:

$$\mu_v - \mu_e = RT \ln(p/p_o) - \mu' \tag{3.27}$$

where μ' accounts for the difference between the chemical potential of the embryo and of the bulk condensed phase and p_o is the equilibrium vapor pressure for the bulk phase. Now equation 3.26 becomes:

$$n^{1/3} = \frac{\frac{2}{3}\phi_{ev}(\alpha - m\beta)}{RT \ln(p/p_o) - \mu'} . \tag{3.28}$$

Above this size the embryo can grow spontaneously; nucleation occurs. Embellishments on this basic thermodynamic approach by Fletcher include consideration of nucleation: on curved substrates, [34] by spherical

cap shaped embryos, [34] by other embryo shapes, [35] on surface irregularities on the substrate, [36] on partially soluble particles, [37] etc. However, in each instance the same basic assumption is made: the embryo has the properties of the bulk phase.

Nucleation theory goes a step beyond thermodynamics to predict the rate of nucleation J. The kinetic basis for nucleation rate depends on the rate of collisions between molecules in the vapor and the surface of the embryo and the sticking or accommodation coefficient of the colliding molecules. A Boltzman distribution function based on the total free energy change required to form an embryo of critical size serves to properly weight the occurrence of any particular growth such that:

$$J = K \exp(\Delta G^*/RT) \tag{3.29}$$

where K is the kinetic coefficient giving rise to the growth and ΔG^* is the total free energy change of the embryo at its critical size as determined by equation 3.28 and the integration of equation 3.22.

CHAPTER IV

MATERIALS

The silver iodide used in this study of the interaction between water vapor and silver iodide was material prepared by the method of Corrin, et al., [12] at the University of Arizona in 1967. This material was stored during the intervening time in an evacuated, blackened pyrex ampule. All handling and transferring of this pure silver iodide powder was done in a closed, water vapor free glove box. After opening the ampule in the glove box, a portion of the powder was transferred to a red, glass-stoppered erlenmeyer flask.

The surface area of this powder was determined by krypton adsorption measurements to be 0.49 m^2/gm with a standard deviation of 5%. This surface area was determined from the combined data of measurements before the water adsorption measurements began and also after these measurements were completed. No change in the surface area was found over the time period of the water adsorption measurements, about nine months. Appendix I gives the results of the krypton adsorption measurements and an error analysis of this surface area computation technique.

The other component in the adsorption system investigated is the adsorbate, water vapor. During the adsorption measurements, water vapor is made available to the adsorbent from ice contained in the adsorption system. The water frozen to produce this ice is placed in its reservoir before any adsorption measurements are begun.

A small vessel containing water from a pyrex still was attached to the adsorption system through a small stopcock. The adsorption system was evacuated with the water at room temperature. As soon as the water began to boil the vessel was immersed in liquid nitrogen. Vacuum pumping continued to 10^{-6} torr. When this pressure was achieved the stopcock between the adsorption system and the water filled vessel was closed and the ice in the vessel was melted by placing a beaker of warm water around the vessel. Dissolved gases trapped in the ice rapidly escaped as the ice melted. Once completely melted, the stopcock was again opened and the freezing cycle repeated. Several freeze - thaw cycles effectively removed dissolved foreign gases from the water in the vessel. After the final freeze, the vacuum pump was turned off and a dewar of liquid nitrogen was placed around the ice reservoir on the adsorption system. The vessel was then immersed in an ice bath allowing water to be distilled by sublimation from the vessel to the ice reservoir until the reservoir was about half full. The stopcock to the water vessel was then closed leaving thoroughly degassed water in the ice reservoir of the adsorption system.

CHAPTER V

GRAVIMETRIC ADSORPTION SYSTEM

For the measurement of large adsorption amounts near saturation pressure, a gravimetric system based on a Cahn electrobalance was selected. Water vapor pressure regulation was obtained by thermostating a reservoir of ice attached to the system. Sample temperature was controlled by another thermostat. A diagram of the adsorption system is shown in Fig. 1.

5.1 Adsorption System

In the initial phase of an adsorption run the system is evacuated to insure the environment of the sample and the surface of the sample are free of volatile impurities. The silver iodide is not heated during degassing because of the ease with which this material sinters. Two stages of pumping are used to evacuate the system; a mechanical fore pump to reduce the system pressure below 10^{-3} torr and then an Ultek ion pump to bring the system pressure to about 10^{-6} torr. A 13X molecular sieve trap between the fore pump and adsorption system prevents the back-diffusion of pump oil vapors into the system. While the ion pump is in operation, the fore pump is isolated from the system by a bellows-sealed valve. The vacuum pumps are connected to the adsorption system through a large bore stopcock. A system pressure of less than 2×10^{-6} torr is maintained for twenty four hours prior to an adsorption run with the ion pump in operation.

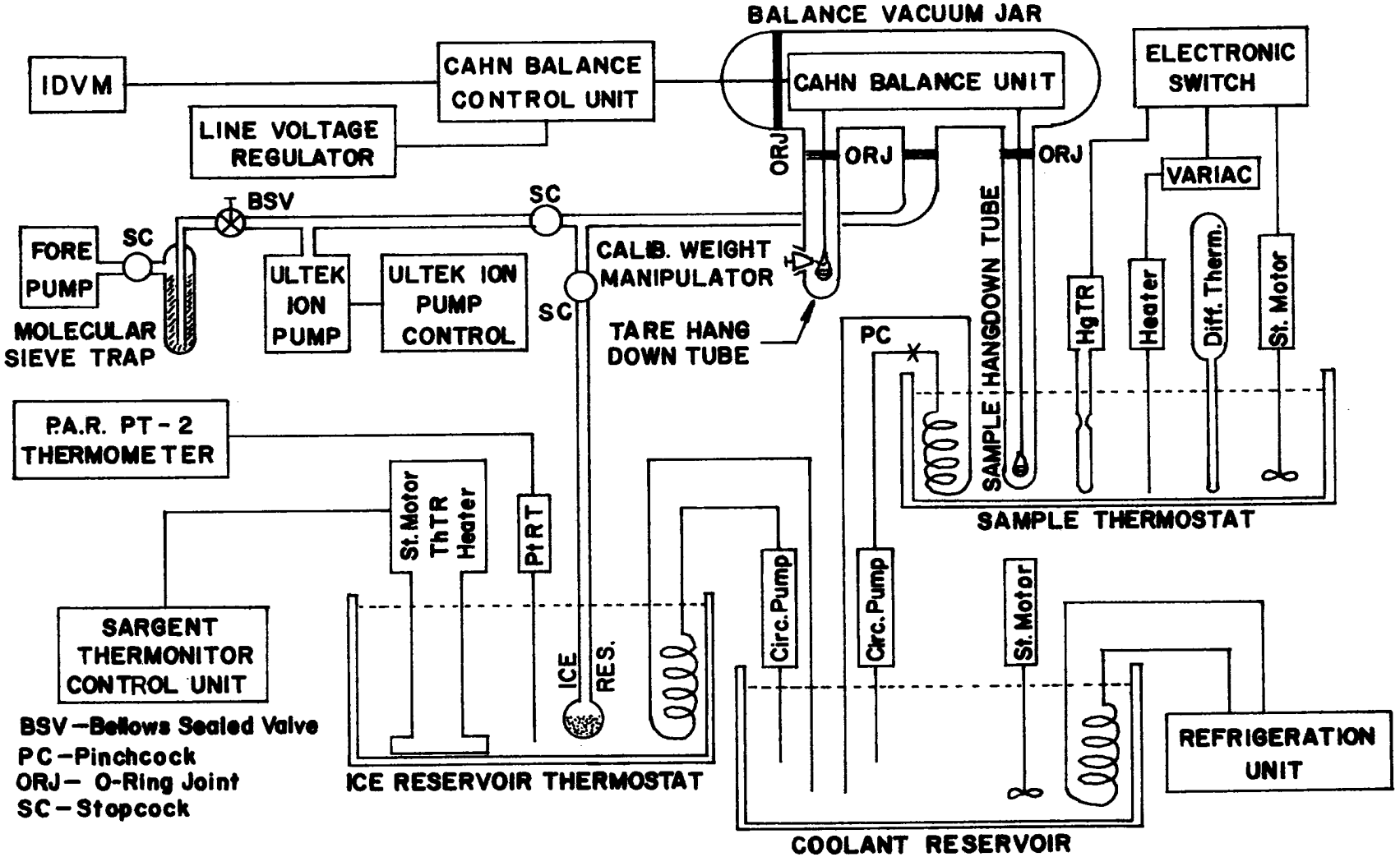

Figure 1: Diagram of gravimetric adsorption system.

A vacuum jar housing the Cahn electrobalance accounts for most of the system volume; approximately 3 liters. This cylindrical vessel has hemispherical end caps. One cap is removable for access to the balance and is sealed by an Apiezon-L greased Viton O-ring and doughnut-like ring clamps. Three greased, Viton O-ring sealed standard taper male joints on the underside of the balance jar allow the tare hangdown tube, sample hangdown tube and the remainder of the system to be attached to the jar. The sample hangdown tube extends a considerable distance below the balance. During a run this tube is immersed in a thermostat. The tare hangdown tube is much shorter. A small standard taper joint ground for a high vacuum seal with a male plug is attached near the bottom of the tare hangdown tube. Rotating the male plug allows a calibration weight to be raised and lowered while the system is evacuated. The third port is attached via 16 mm I.D. pyrex tubing to the stopcock from the vacuum line and to the stopcock from the ice reservoir.

The final portion of the adsorption system is the ice reservoir. A small stopcock connects this reservoir to the adsorption system. This spherical bulb contains approximately 6 ml of degassed, distilled water and is immersed in a thermostat.

5.2 Balance System

The Cahn model RG electrobalance determines the weight of a sample by measuring the current required to maintain the balance at a reference position. A flag on the balance arm intercepts a light beam falling on a phototube. The output current of the phototube is

proportional to the deflection of the balance arm. This current in turn activates a servoamplifier driving a torque motor to which the balance arm is attached. The feedback loop thus established maintains the arm at the reference position. The output signal from the balance is proportional to the torque motor current and thus also to the weight of the sample. Output sensitivity is rated at 50 millivolts/milligram.

Balance output voltage is measured with an integrating digital voltmeter (IDVM) that can be read to one microvolt. In order to reduce the noise on the balance signal induced by mechanical vibration (response of the electrobalance is very rapid) a 200 mfd capacitor is placed across the output terminals of the balance. In addition, the integrating feature of the voltmeter averages the signal over a period of one second. A Stabline voltage regulator isolates the balance from line voltage fluctuations minimizing electrical noise on the signal.

With a tared sample the minimum detectable weight change of the balance - voltmeter system in the mounting used is approximately 10 micrograms in a one gram sample. This value is larger than the rated sensitivity of the balance because of vibration noise on the balance output signal.

The sample pan and tare weight pan are suspended from opposite ends of the balance arm by quartz fibers. The pans are 16 mm diameter hemispherical shells of fused quartz weighing around 50 mg. Tare weights are of aluminum and tantalum along with a chromel wire support for a class M, 5 mg. rider used to calibrate the balance.

The balance jar and hangdown tubes are protected from ambient light by black paint and tape to prevent photodecay of the sample

and to provide the balance feedback network with a constant light level.

5.3 Sample Thermostat

Sample temperature is held constant during a run by a separate thermostat. A constant rate of cooling provided by a coolant circulated through a copper coil immersed in the bath is countered by on-off heating to maintain the control temperature. Temperature regulation is achieved with a mercurial thermoregulator. Cooling rate is controlled by a pinchcock throttling the coolant supply line. A variac in series with the heating element controls the heating rate. The temperature is kept uniform throughout the bath by a stirring motor. The sample hangdown tube is immersed some 20 cm. into the bath with the sample pan only a few centimeters from the bottom of the tube. Polyethylene foam insulation on the walls, bottom and top of the bath prevent diurnal room temperature fluctuations from disturbing the control temperature.

Temperature control over the duration of an isotherm measurement is possible to ±0.02C with the average deviation from the control temperature being even smaller. The period of the cyclic temperature fluctuations is approximately 3.5 minutes. Therefore, on the time scale of adsorption measurements made over several days, these fluctuations are effectively averaged out.

5.4 Ice Reservoir Thermostat

Temperature control in the ice reservoir is attained by countering a constant cooling rate with a proportional heat input. A Sargent

Thermonitor modified to control at subzero centigrade temperatures provides a heat input to the thermostat proportional to the temperature difference between the bath and control setting. The ice reservoir is immersed around 10 cm. into the bath. Polyethylene foam insulates the entire bath from room temperature fluctuations permitting long term temperature control to ±0.02C.

5.5 Coolant Supply

Both the sample thermostat and the ice reservoir thermostat are provided with coolant circulating through copper coils immersed in each bath. A large, well insulated vessel initially filled with a one to one solution of commercial ethylene glycol and tap water is cooled to -25C by a Blue M refrigeration unit. The bath is vigorously mixed. Two circulation pumps force the coolant through well insulated tubing, through the coils in the baths, and back into the coolant reservoir.

5.6 Platinum Resistance Thermometer

Both the sample temperature and ice reservoir temperature are measured by a platinum resistance thermometer. The resistance versus temperature response of a Rosemont Engineering probe was determined by the National Bureau of Standards and fitted to the Callendar-van Dusen equation:

$$\frac{R_s}{R_o} = 1 + \alpha T\left[1 + \frac{\delta}{100}\left(1 - \frac{T}{100}\right) + \frac{\beta T^2}{10^6}\left(1 - \frac{T}{100}\right)\right] \qquad (5.1)$$

where:

$$R_o = 25.5352 \text{ abs ohms},$$

$$\alpha = 3.926398 \times 10^{-3},$$

$$\beta = \begin{cases} 0.0 & , T > 0C, \\ 0.11011, & T < 0C, \end{cases}$$

$$\delta = 1.49166.$$

A Princeton Applied Research model PT-2 platinum resistance thermometer bridge unit serves to measure the sensor resistance. This unit is designed to follow the Callendar-van Dusen equation such that the temperature indicated by the front panel dials on the unit corresponds to the temperature of the sensor at temperatures above zero Celcius. At subzero temperatures the bridge resistance does not track the Callendar-van Dusen equation but simply follows a linear ramp function:

$$R_b = \frac{MR_o + ST}{M} \tag{5.2}$$

where M = 100 and S = 10 ohms/C. When the bridge is balanced, $R_s = R_b$, at subzero temperatures, the dial reading does not indicate the true sensor temperature.

To compensate for the discrepancy between the bridge resistance and temperature response of the platinum wire probe, a correction term must be added to the subzero temperature indicated by the PT-2 dials when the bridge is balanced. The first order correction for temperatures above -20C is:

$$\Delta = -T \; \frac{1 - \frac{1}{10\alpha R_o} + \frac{\delta}{100}\left(1 - \frac{T}{100}\right) + \frac{\beta T^2}{10^6}\left(1 - \frac{T}{100}\right)}{1 + \frac{S}{100}\left(1 - \frac{2\,T}{100}\right) + \frac{\beta T^2}{10^6}\left(3 - \frac{4\,T}{100}\right)} \tag{5.3}$$

where $\underline{T}$ is the dial temperature in degrees centigrade and $\underline{\Delta}$ is the correction term which must be added to the dial temperature to give the correct sensor temperature $\underline{T_s}$:

$$T_s = T + \Delta. \tag{5.4}$$

CHAPTER VI

PROCEDURE

The measurement of an adsorption isotherm with the gravimetric system described in Chapter V consists of several phases. Initially the sample is weighed out into a sample pan and then placed on the balance. Then the balance is tared and calibrated. Finally, isotherm points are obtained by measuring the weight change of the sample at constant ice reservoir temperatures.

6.1 Sample Preparation

A sample pan is partially filled with silver iodide in a closed, water vapor free glove box. The weight of the pan and a weighing bottle is determined beforehand. The sample pan containing silver iodide is placed into the weighing bottle while in the glove box, and the bottle is reweighed. By the change in weight of the bottle and pan the amount of sample in the pan is determined. The pan with sample is kept in the weighing bottle until the pan is placed on the balance.

6.2 Initial Sample Taring

Quartz suspension fibers are hung from loops at each end of the balance arm. On the tare hangdown fiber a tare pan is hung in which substitution weights are placed to approximately tare the sample pan plus sample. A 5 milligram, class M beam rider which serves as a calibration standard is also added to the tare pan. The tare hangdown tube is replaced with the O-ring joint lightly greased with Apiezon L.

Before the weighing bottle is opened, the sample hangdown tube is positioned beneath the suspension fiber. The weighing bottle is then opened and the sample pan is suspended on the quartz fiber. The hangdown tube is then carefully raised around the sample pan and afixed to the balance jar with the O-ring joint lightly greased. Clamps hold both the sample and tare hangdowns tubes in place.

With both the tare and sample hangdown tubes attached to the balance jar, the stopcock to the vacuum pump is very slowly opened, allowing a gradual decrease of system pressure. Static electricity which usually built up on the balance and adsorption system while placing a sample on the balance dissipated during the pump down; a polonium alpha particle source in the balance jar helped to dissipate the charge. The influence of the charges on the weight measured vanishes after several hours of pumping; the balance output signal on the IDVM becomes steady in time. This IDVM reading is noted and gives the zero offset in vacuum.

Dry nitrogen is then admitted to the balance jar through a small stopcock. The balance system is allowed to stabilize and the IDVM reading again noted; this gives the zero offset in air. The difference between the two zero offsets gives a buoyancy correction for taring the balance in air.

6.3 Final Taring

With the sample in a dry nitrogen atmosphere to prevent surface contamination of the sample, final taring is carried out by adjusting the contents of the tare pan to bring the IDVM reading to the buoyancy

correction. A slightly positive signal, i.e., sample heavier than tare, is desirable due to degassing of the sample during zero offset determination.

After the final adjustment of the tare weight, the 5 mg. rider is positioned on a small stirrup of chromel wire projecting out of the tare pan. The hangdown tube is positioned such that the wire arm of the vacuum manipulator engages the lifting loop of the rider. With this arrangement the rider may be removed from the tare pan and then replaced with the system closed and evacuated.

6.4 Zero Offset

The system is again slowly evacuated by the fore pump. After several hours the ion pump can be started and pumping continues with the fore pump isolated from the system. Pressure in the system drops rapidly to the pressure at which the pumping speed equals the degassing and low leak rate of the system. Zero offset observations begin after pressures below 4×10^{-6} torr are attained.

A zero offset value is determined by the average of 20 readings from the IDVM. The balance is set on the one milligram mass dial range with the recorder range set for 0.1 milligram full scale. With the IDVM sensitivity at 0.1 volts full scale, this allows the weight imbalance to be read from the IDVM to 0.1 micrograms. Readings are made at five second intervals and each reading is electronically averaged over one second. Zero offset averages are obtained at hourly intervals over a period of two days. Once the zero drift stabilizes, zero offset averages are taken at ten minute intervals to establish

the mean zero offset for the run; no consistent zero drift was found to take place once the zero offset is steady.

Zero offset is very sensitive to mechanical and electrical disturbances to the balance system. The balance jar is shielded from ambient light to help maintain a constant zero offset. The thermostats are mechanically isolated from the balance mounting grid by foam padding which adsorbs vibrations. The stirring motor for the sample thermostat is supported from the frame that carries the coolant circulating pumps and hoses. This frame is isolated from the balance mounting rack.

6.5 Balance Calibration

Removing the 5 mg. calibration weight from the tare pan produces an apparent increase in the sample weight. With the recorder span adjustment on the balance unit, the IDVM reading can be adjusted to correspond to 5 mg. As with the zero offset, the calibration value is also statistically determined. The calibration procedure is as follows:

The 5 mg. rider is removed from the tare pan by turning the vacuum manipulator after the zero offset has stabilized. After the system is again steady, calibration readings (20 values from the IDVM) are taken at ten minute intervals. Ten such averages usually suffice for an average calibration value. The rider is then replaced and a series of zero offset averages is again taken. The difference between the average calibration value and the average zero offset is the 5 mg. calibration weight. Dividing 5 mg. by this value gives a

multiplicative factor for adjusting all values to the 5 mg. calibration after subtracting the zero offset.

6.6 Sample Temperature Control

During the zero offset and calibration procedures the sample thermostat is installed around the sample hangdown tube; this thermostat must be removed to place a sample on the balance. Care is taken to prevent excess static electricity build up and mechanical shocks to the system. The bath is filled with an antifreeze solution. Coolant from the refrigeration unit is circulated through a cooling coil in the bath to begin lowering the bath temperature. The bath is stirred.

Bath temperature is monitored during the initial set up with the platinum resistance thermometer. A mercurial thermoregulator is adjusted to control at the desired sample temperature. Both the heating and cooling rates are varied to produce optimum temperature fluctuations about the mean consistant with long term thermal stability of the bath. The stability of the bath is monitored during the zero offset measurements with the PT-2 thermometer. During the isotherm measurements, sample bath temperature is monitored manually with a mercurial differential thermometer.

6.7 Isotherm Data Point

Each data point on an adsorption isotherm requires constancy of sample temperature and ice reservoir temperature. The sample temperature is kept constant throughout an isotherm measurement. Ice reservoir temperature is step wise increased to obtain new data points.

The temperature of the ice reservoir is adjusted via dials on the Thermonitor control unit and is monitored throughout a run with the platinum resistance thermometer. Adjustment of the Thermonitor control dials is done in gradual steps to prevent excessive overshoot of the desired bath temperature. The greater the temperature change desired the greater the overshoot; therefore, several small changes in temperature are made to reach the desired ice reservoir temperature, especially at pressures near saturation. The output of the PT-2 unit is graphically recorded for a permanent history of the ice reservoir temperature during a run.

With the ice reservoir maintained at constant temperature, adsorption of the vapor on the sample proceeds when the stopcock between the balance jar and ice reservoir is open. Twenty readings at five second intervals are read off the IDVM every half hour. When the weight ceases to continuously increase, readings are taken at ten minute intervals until a sufficient sample is collected to obtain an average value (usually ten). The average is recorded along with the ice reservoir temperature. Repeating this procedure, each time slightly increasing the ice reservoir temperature, produces an adsorption isotherm. A minimum of eight hours is given for the sample weight to reach equilibrium; as long as two days is allowed for equilibrium when large amounts are to be adsorbed.

6.8 Reversibility of Isotherm

After the equilibrium pressure exceeds saturation with respect to ice and before water saturation is attained, a desorption point is

obtained. The temperature of the ice reservoir is decreased to correspond to a vapor pressure just slightly below saturation with respect to ice. The sample weight decreases in the period of one or two days to an equilibrium value. The average weight is determined as above and is recorded along with the ice reservoir temperature. After the desorption point is obtained, the ice reservoir temperature is again increased and the isotherm continued.

6.9 Vapor Pressure Computation

Control of the sample and ice reservoir temperature effectively specifies the saturation vapor pressure at the sample and the equilibrium pressure of the vapor in the system, respectively. Analytical expressions for ice vapor pressure and the ratio of water to ice vapor pressures are used to compute the necessary pressures.

Washburn [38] derived the ratio of water to ice saturation pressure by an integration of a Clausius - Clapeyron expression using thermodynamic data. In the temperature range -16C to 0C the ratio of saturation pressures is:

$$\log_{10} \frac{p_w}{p_i} = - \frac{1.1489\ t}{T} - 1.33 \times 10^{-5}\ t^2 + 9.084 \times 10^{-8}\ t^3 - 1.08 \times 10^{-8}\ t^4 \qquad (6.1)$$

where $\underline{T}$ is the absolute temperature and $\underline{t}$ is the centigrade temperature and $\underline{w}$ and $\underline{i}$ correspond to water and ice saturation vapor pressures, respectively.

A recent experimental investigation of the vapor pressure of ice between 0.01C and -100C led Jancso, Papezin, and van Hook [39] to

the following expression for the saturation pressure of ice which fits their experimental values within measurement error:

$$\log_{10} p_i = -\frac{2481.604}{T} + 3.5712988 \log_{10} T + 1.901973 - 3.097203 \times 10^{-3} T - 1.7649 \times 10^{-7} T^2. \quad (6.2)$$

Equation 6.2 is used to obtain the equilibrium vapor pressure of water in the system from the ice reservoir temperature. Both equation 6.1 and 6.2 are needed to obtain the saturation pressure with respect to liquid supercooled water at the sample using the sample thermostat temperature. The relative pressure of water vapor at the sample is found by dividing the equilibrium vapor pressure by the saturation vapor pressure:

$$x = p_i/p_o \quad (6.3)$$

where x is the relative pressure and p_i the equilibrium pressure given by the ice reservoir temperature. The saturation pressure p_o may be either that over water or ice.

6.10 Corrections to Isotherms

After the isotherm is carried to as large a vapor pressure as possible, the values obtained must be adjusted for the zero offset. This gives the apparent amount adsorbed which is further corrected by multiplying that value by the calibration ratio to give the actual amount adsorbed at each data point.

The final correction accounts for adsorption on the balance system itself. To determine this correction, separate isotherms are measured at each sample temperature without having a sample of silver

iodide in the sample pan. Except for the tare weights, which are not all needed for the blank isotherm, all other factors and procedures are the same. The equilibrium relative pressure with respect to the liquid of the silver iodide adsorption isotherm determines the correction value taken from the blank isotherm that is to be subtracted from the previously corrected amount adsorbed. The totally corrected amount now corresponds to that adsorbed by the silver iodide powder alone.

Buoyancy corrections were calculated for the pressure range encountered and were found to be negligible in comparison to the estimated error of the weight change measurement.

CHAPTER VII

ANALYSIS OF ERROR

Errors arise in any experimental work from the inaccuracy of the measurements used to obtain the experimental data. In this gravimetric adsorption study a major source of these errors lies in the measurement of the change in weight of the sample of silver iodide during adsorption of water vapor. In addition to the errors in the weight of adsorbed water, the surface area of the silver iodide powder also has an error associated with it. An error analysis of the surface area measurement technique is presented in Appendix I.

The following error analysis of the gravimetric technique used in this work to obtain the surface excess of adsorbed water is based on material taken from a text on statistics by Volk [40] and essentially treats an analysis of the variance. Basic to this approach is the variance of a function of several variables. If $y=f(x_1, x_2, x_3,...)$ then the variance $s^2(y)$ is given by:

$$s^2(y) = \left(\frac{\partial f}{\partial x_1}\right)^2 s^2(x_1) + \left(\frac{\partial f}{\partial x_2}\right)^2 s^2(x_2) + \left(\frac{\partial f}{\partial x_3}\right)^2 s^2(x_3) + \ldots \quad (7.1)$$

where $s^2(x_1)$, etc., are the variances of each independent variable. Unbiased variances are computed from a sample of n data points by:

$$s^2(x) = \frac{\Sigma x^2 - (\Sigma x)^2/n}{n-1} \quad (7.2)$$

whenever such data is available.

Confidence limits can be placed on the various parameters by using the student's t or normal distribution and the standard deviation of the parameter. All data reported in this work will be with only the standard deviation given unless otherwise specified.

7.1 Adsorption Data Error Analysis

Each adsorption data point is determined by the average of many readings from the IDVM. This large data sample permits the variance of each data point to be estimated statistically using equation 7.2. Before adsorption measurements are made, preliminary measurements of the zero offset z and calibration weight w_c establish a baseline variance for the adsorption measurements which follow. Also, since the adsorption measured must be corrected for the blank isotherm, the variance associated with the blank also contributes to the variance of the amount adsorbed.

The weight of water vapor adsorbed by the silver iodide powder may be expressed as a function of the zero offset, calibration ratio C, apparent weight change w and the blank isotherm correction b:

$$w_a = C(w - z) - b \tag{7.3}$$

and the variance of w_a can be found by equation 7.1 to be:

$$s^2(w_a) = (w - z)^2 \, s^2(C) + C^2[\, s^2(w) + s^2(z) \,] + s^2(b). \tag{7.4}$$

The calibration ratio C is found from the zero offset and the 5 mg. calibration weight w_c:

$$C = 50/(w_c - z) \tag{7.5}$$

for the weight in millivolts (0.1 milligram = 1 millivolt) as it is throughout this work. The variance $s^2(C)$ is found to be:

$$s^2(C) = C^2\left[\frac{s^2(w_c) + s^2(z)}{(w_c - z)^2}\right] . \tag{7.6}$$

Measuring the blank isotherm b follows the same procedure as measuring w_a so that:

$$b = C_b(w_b - z_b) \tag{7.7}$$

and the variance of the blank isotherm is given by:

$$s^2(b) = (w_b - z_b)^2\, s^2(C_b) + C_b^2\,[\, s^2(w_b) + s^2(z_b)\,]. \tag{7.8}$$

As in equation 7.5, the blank calibration ratio C_b is given as:

$$C_b = 50/(w_{cb} - z_b) \tag{7.9}$$

and its variance is found to be:

$$s^2(C_b) = C_b^2\left[\frac{s^2(w_{cb}) + s^2(z_b)}{(w_{cb} - z_b)^2}\right] . \tag{7.10}$$

Rearranging equation 7.4 and including the variances for w, C, and b leads to the following expression for the variance of w_a:

$$s^2(w_a) = C^2\left[s^2(w) + \left(1 + \frac{(w - z)^2}{(w_c - z)^2}\right)s^2(z) + \left(\frac{w - z}{w_c - z}\right)^2 s^2(w_c)\right]$$

$$+ C_b^2\left[s^2(w_b) + \left(1 + \frac{(w_b - z_b)^2}{(w_{cb} - z_b)^2}\right)s^2(z_b) + \left(\frac{w_b - z_b}{w_{cb} - z_b}\right)^2 s^2(w_{cb})\right] \tag{7.11}$$

This expression clearly shows the role each measured variance plays in determining the overall variance. Of interest is the role of $s^2(z)$. Notice that the relative contribution of the zero offset variance to the total variance may vary from a minimum of one to greater than two depending on the net amount adsorbed.

Still another factor affects the computation of w_a. The blank correction is measured independently of the adsorption amount. The equilibrium relative pressure for the amount adsorbed is used to determine the blank correction that must be applied to the measured isotherm. This procedure involves considerable estimation since, in this case, the blanks are determined at only three or four points on the isotherms. Interpolation between these points (and in some cases, extrapolation) gives at best only an estimate of b and $s^2(b)$.

From the amount adsorbed, the surface excess Γ is found to be:

$$\Gamma = w_a/MAW \tag{7.12}$$

where M is the molecular weight of the adsorbate (water), A is the specific surface area of the sample, and W is the weight of silver iodide sample. From equation 7.1, the variance of Γ is shown to be:

$$s^2(\Gamma) = \Gamma^2\left(\frac{s^2(w_a)}{w_a^2} + \frac{s^2(A)}{A^2} + \frac{s^2(W)}{W^2} \right) . \tag{7.13}$$

The variance of the weight of sample is estimated to be 10^{-8} gm^2. Confidence limits of Γ can be estimated using the normal distribution since the degrees of freedom for each Γ is large and moreover difficult

to define:

$$\tilde{\Gamma} = \Gamma \pm t_{\alpha} s(\Gamma) \tag{7.14}$$

where t_{α} is the number of standard deviations about the mean required to enclose α percent of the normally distributed fluctuation about Γ.

7.2 Relative Pressure Computation

An analysis of the variance of the formulas given in section 6.9 permits an estimation of the variance and standard deviation of the vapor pressure of water in the system and the relative vapor pressure with respect to the liquid or solid. From equation 6.2, the variance of the vapor pressure of ice is determined using equation 7.1:

$$s^2(p_i) = \left(\frac{p_i}{\ln 10}\right)^2 \left(\frac{2481.604}{T^2} + \frac{3.5712988}{T} \log_{10} e - 3.097203 \times 10^{-3} \right.$$
$$\left. -3.5298 \times 10^{-7}\, T \right) s^2(T) \tag{7.15}$$

where T is the absolute Kelvin temperature of the ice and p_i is in mm Hg. A similar expression is obtained for the variance of the vapor pressure of water from equation 6.1:

$$s^2(p_w) = \left(\frac{p_w}{\ln 10}\right)^2 \left(\frac{2481.604}{T^2} + \frac{3.5712988}{T} \log_{10} e - 3.097203 \times 10^{-3} \right.$$
$$-3.5298 \times 10^{-7}\, T - 2.66 \times 10^{-5}\, t$$
$$\left. +2.7252 \times 10^{-8}\, t^2 - 4.32 \times 10^{-9}\, t^3 \right) s^2(T) \tag{7.16}$$

where $t = T - 273.16$, T is the absolute Kelvin temperature of the water with p_w in mm Hg.

Equations 7.15 and 7.16 are used to determine the variance of the saturation pressure p_o at the sample for ice and water respectively. Only equation 7.15 is needed to determine the variance of the equilibrium vapor pressure in the system. The variance of the relative pressure is given by:

$$s^2(x) = x^2 \left(\frac{s^2(p_i)}{p_i^2} + \frac{s^2(p_o)}{p_o^2} \right) \qquad (7.17)$$

where p_o is chosen to be either for ice or water and $x = p_i/p_o$.

With the thermostats used in this work, temperature control to ± 0.02C allows the vapor pressures and relative pressures to be determined to 0.03% and 0.04%, respectively. The vapor pressures and relative pressures reported herein, therefore, are given without reference to their standard deviations.

7.3 Isosteric Heats of Adsorption

Operationally, isosteric heats of adsorption q_{st} are determined by reading pressures p from isotherms at different temperatures T that corresponds to a given surface excess. These pressures are plotted natural logarithm of p versus the inverse absolute temperature. The slope of the best fit straight line through those points corresponding to the same Γ gives the isosteric heat of adsorption at that surface excess.

Smooth isotherms are required to determine the pressure. Isotherms based on the data points one standard deviation above and below the mean data points define a one standard deviation envelope about the mean isotherm. These envelope isotherms serve to give an estimate of the accuracy with which the pressure can be determined

at a given surface excess. The mean pressure and the pressures specified by the error envelope give an error band on an isostere plot.

The slope of the isostere through the mean $\underline{\ln p}$ data points gives the average isosteric heat. Maximum and minimum slopes determined by the deviation pressures give an estimate of the error associated with the isosteric heat computation.

7.4 Integrated Gibbs Equation

The integrated form of the Gibbs equation given in equation 3.11 can be rewritten for pressures not close to zero as:

$$\Pi_{\Delta p} = RT \int_{p'=p_1}^{p'=p_2} \frac{\Gamma}{p'} \, dp' \, . \tag{7.18}$$

Following equation 7.1, the variance of $\underline{\Pi_{\Delta p}}$ is found to be [41] :

$$s^2(\Pi_{\Delta p}) = \left(RT \int_{p'=p_1}^{p'=p_2} \frac{s(\Gamma)}{p'} \, dp' \right)^2 \, . \tag{7.19}$$

The $\underline{\Delta p}$ indicates the integration need not start at zero pressure as given in equation 3.11, but can be computed over any range of pressures desired. The reference point for the computation of $\underline{\Pi_{\Delta p}}$ then becomes the starting point of the integration.

CHAPTER VIII

EXPERIMENTAL RESULTS

Adsorption isotherms were measured on samples of pure silver iodide at -3.00C, -6.50C and -10.00C using the adsorption system and technique described in Chapters V and VI and the data were analyzed using the techniques of Chapter VII. At each temperature an isotherm was determined on two different samples. The data points at each temperature were used to obtain smooth isotherms from which isosteric heats of adsorption were computed. In addition, the Gibbs integration was carried out over the available range of data.

8.1 Adsorption Isotherms

The adsorption data at -3.00C presented in Fig. 2 were obtained by two different methods. Before the IDVM was used to indicate the balance output signal, this signal was recorded on a strip chart recorder. The data points of the first run were obtained in this manner; the procedure was essentially as written in Chapter VI except a recorder was used in place of the IDVM. The vertical bars on the data points extend one standard deviation above and below the average value. For the first run, the mean variance for all the adsorption measurements made with the IDVM was used to compute the error band.

Several features of the -3.00C isotherm bear further comment. The steep rise of the isotherm shown in Fig. 2 occurs only after ice saturation pressure, 3.752 mm Hg, is exceeded. The amount

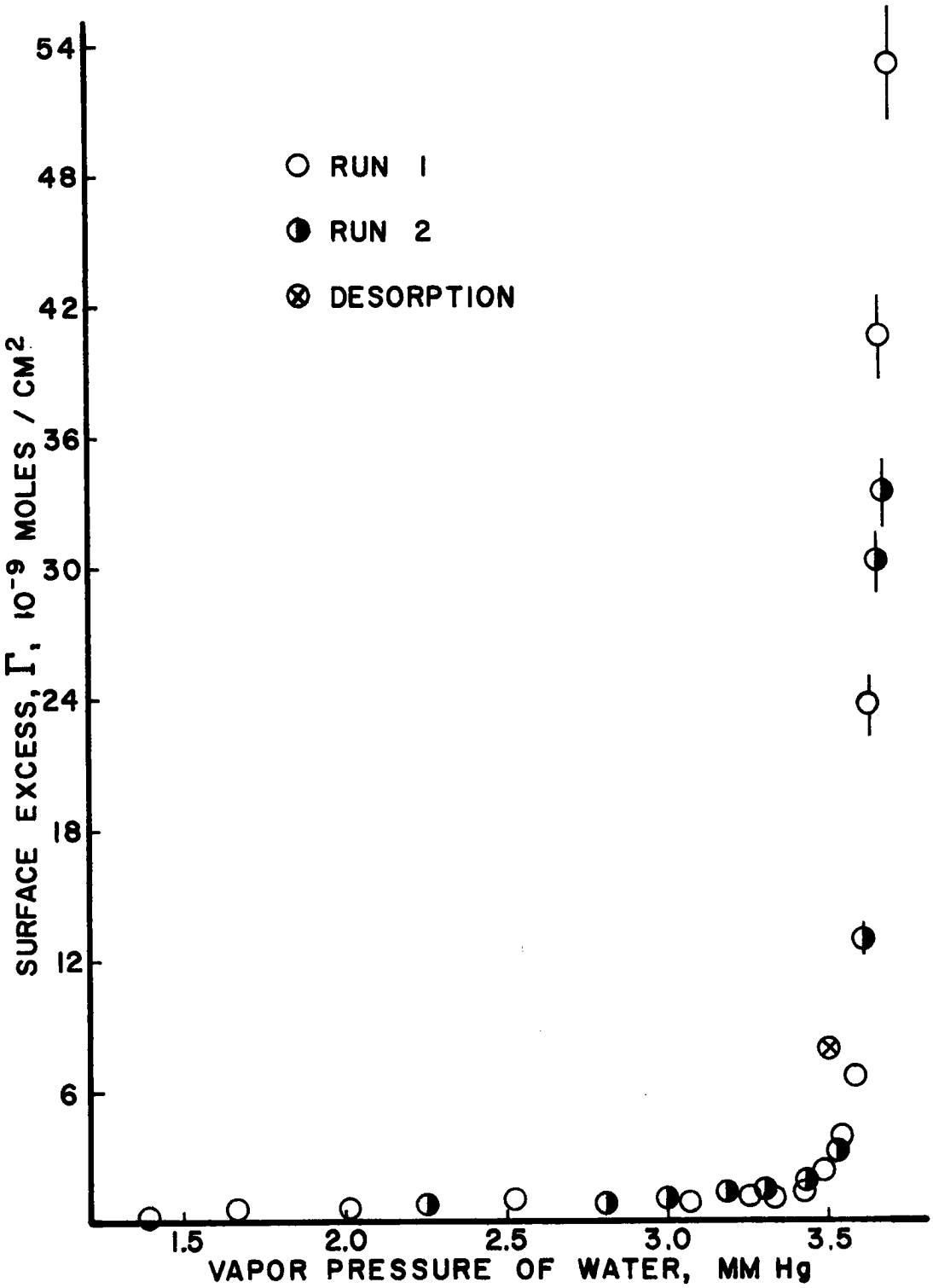

Figure 2: The complete water adsorption isotherm at -3.00C on pure silver iodide. Adsorption is finite at water saturation, 3.677 mm Hg.

adsorbed remains finite even as water saturation, 3.677 mm Hg, is approached. An amount equivalent to slightly more than 33 statistical monolayers of water is adsorbed at water saturation. An attempt to measure adsorption amounts at pressures above water saturation failed because water began to condense in the sample hangdown tube. Before making the second run at -3.00C, the hangdown tube was treated with a Sylil-8 solution to replace water active hydroxyl groups on the walls of the hangdown tube with less active methyl groups. However, the second isotherm also could not be extended beyond water saturation. It is important that the observed condensation occurred on the walls of the hangdown tube and not on the pure silver iodide sample. These isotherms at -3.00C attained an ice supersaturation of 3.0% at water saturation pressure.

Following the isotherms at -3.00C, three isotherms were measured at -10.00C. Figure 3 presents the data for -10.00C. Unlike the -3.00C isotherms, adsorption amounts at -10.00C could not be measured above a vapor pressure of 2.00 mm Hg. which corresponds to a supersaturation of 2.5% with respect to ice. The amount adsorbed, a maximum of 1.8 nanomoles/cm^2, was in equilibrium with the vapor at pressures below 2.00 mm Hg. Above this pressure, the weight of the sample began to increase rapidly and seemingly without bound in comparison to the amounts adsorbed at -3.00C near saturation. When this occurred, the run was terminated. Run 2 was made on the same sample as run one after the system was evacuated for several days at 4×10^{-6} torr. Run 3, on a different sample, was made because of the apparent difference between runs one and two.

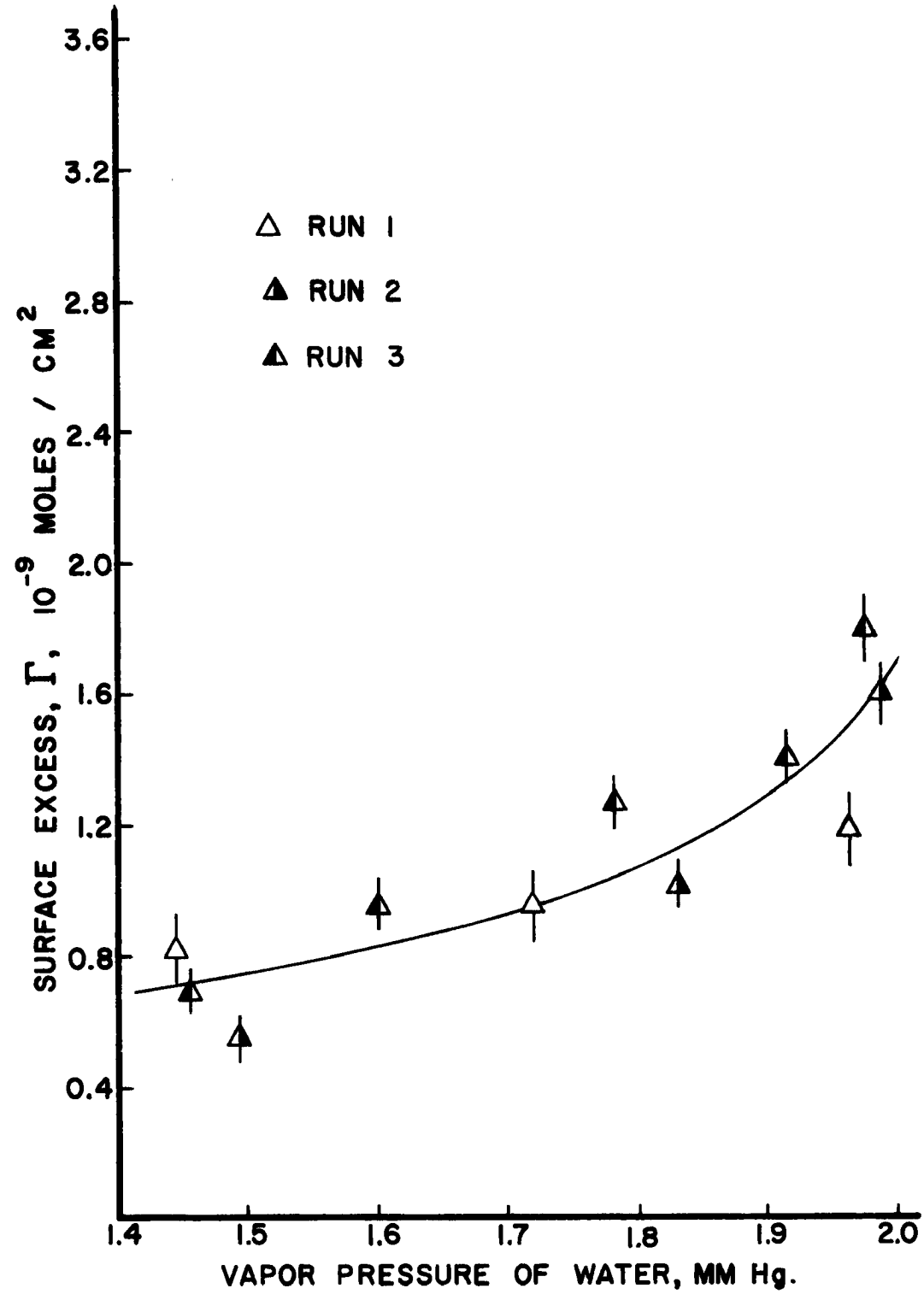

Figure 3: The water adsorption isotherm at -10.00C on pure silver iodide. Nucleation occurs at pressures greater than 2.00 mm Hg.

The experiment was concluded after two isotherms at -6.50C shown in Fig. 4 were measured. These isotherms could not be carried above a vapor pressure of 2.73 mm Hg. which corresponds to a supersaturation of 3.0% with respect to ice. The maximum amount adsorbed was 3.7 nanomoles/cm^2.

Combining or comparing the three sets of isotherms is difficult because of the great difference in amounts adsorbed. Therefore, Fig. 5 presents an expanded view of the low coverage portion of the -3.00C isotherm. The vertical scale is the same as in Figures 3 and 4. Tables I, II, and III present the adsorption data, including the blank isotherms, for the isotherms shown in Figures 2 through 5.

Another obvious feature of the adsorption isotherms is the scatter of the data points for different runs for the same isotherm. This scatter influences the ability to select isosteres and evaluate the Gibbs equation. Because of the scatter, the isotherms had to be treated with an objective smoothing technique. The smooth isotherms were then used to evaluate isosteres, isosteric heats of adsorption, and integrate the Gibbs equation.

Vibration noise contributed significantly to the standard deviation computed for each data point and also enters into the scatter observed from one run to another. Mechanical or electrical disturbances to the balance system produce changes in the zero offset. At the start of each run, the adsorption system must be pressurized with the adsorbate. Opening the stopcock to the ice reservoir admits water vapor to the balance jar. Even when done cautiously, the streaming of vapor into the balance jar and hangdown

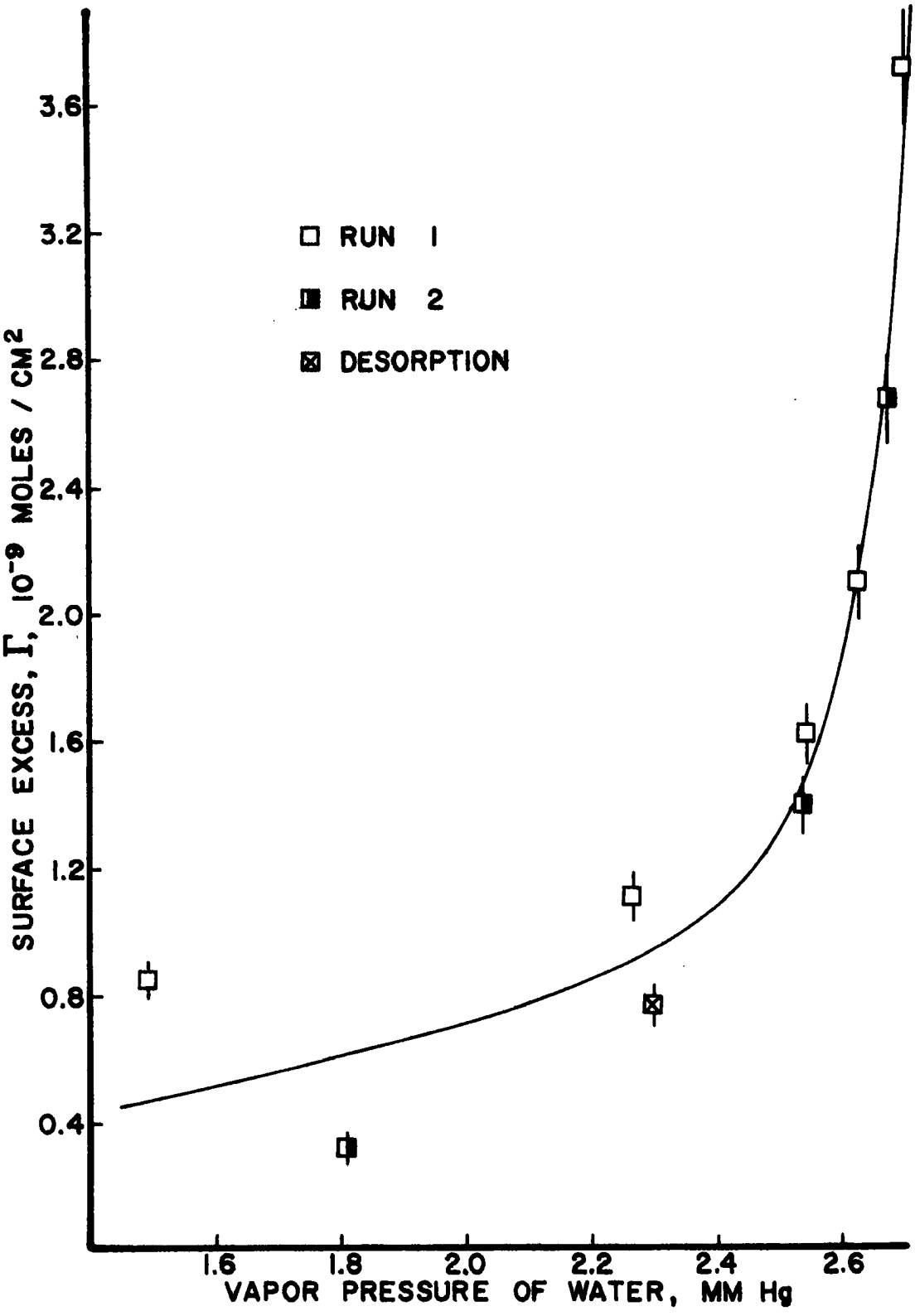

Figure 4: The water adsorption isotehrm at -6.50C on pure silver iodide. Nucleation occurs at pressures greater than 2.73 mm Hg.

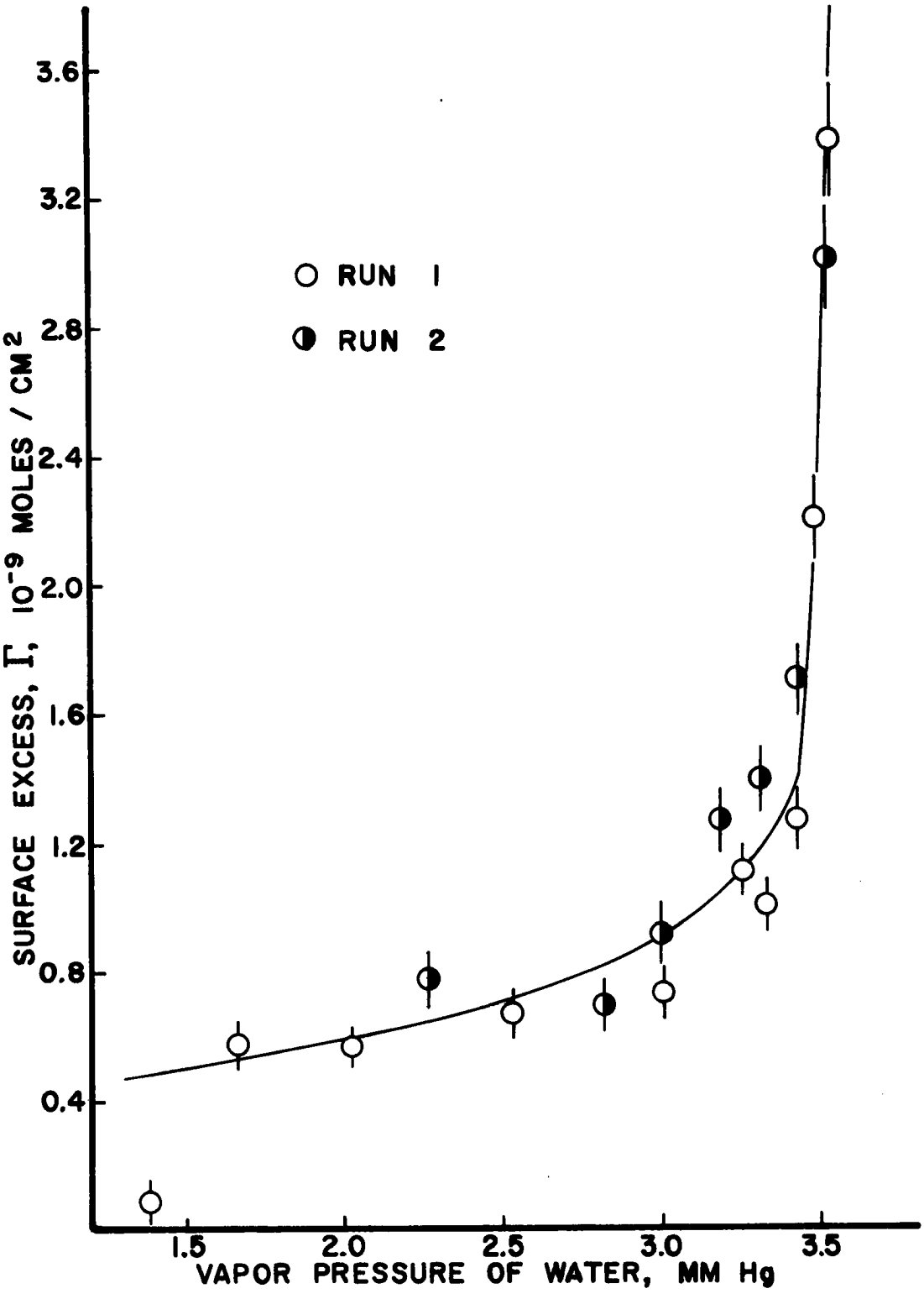

Figure 5: An expanded view of the low coverage portion of the -3.00C isotherm with the same vertical scale as in Figures 3 and 4.

tubes creates a considerable disturbance on the balance output signal. This mechanical disturbance to the balance may produce a change in zero offset. Such a change can not be detected or taken into account in evaluating the isotherms. A very slow pressurization of the adsorption system would be necessary to avoid this possible cause of a change in zero offset. Once an adsorption run is underway, further changes in zero offset can also contribute to the scatter and remain undetected.

Another source of scatter between runs lies in the selection of the silver iodide powder sample. Once the powder is removed from the sealed ampule and is placed in the red erlenmeyer flask, further mixing does not occur except on removing samples. Sample pans are filled by removing with a spatula small portions of the powder in the flask selected at random. However, only two or three such portions are needed to fill the sample pan. If variations in the surface area and other surface properties of the powder exist from one portion of the powder to another, the samples selected may differ appreciably from one another in terms of the adsorption isotherms measured. Differences in surface area from one sample to another can explain a displacement of congruent isotherms. Differences in the surface properties affecting the relationship between the pressure of the vapor and the amount adsorbed can produce changes in the shape of the isotherms. Numerical values can not be assigned to either effect, only a statistical treatment is possible.

8.2 Isosteric Heats of Adsorption

Computation of the isosteric heats of adsorption using equation 3.21 requires smooth isotherms from which pressures corresponding to constant coverages can be read. However, the isotherms presented in Figures 3 through 5 are far from smooth. The scatter of the data is large enough to make smoothing by eye overly subjective. Therefore, an objective smoothing technique based on an empirical equation resembling the Frenkel-Halsey-Hill isotherm [19,20,21] is used. The empirical equation to which the isotherm data is fitted is given by a straight line when the logarithm of the surface excess Γ is plotted against the logarithm of the logarithm of the inverse of the relative pressure, i.e.:

$$\ln \Gamma = a + b \ln \ln \frac{p_o}{p} \qquad (8.1)$$

where a and b are the intercept and slope of the straight line $y = a + bx$ in which $y = \ln \Gamma$ and $x = \ln \ln(p_o/p)$.

To determine if this isotherm represents a reasonable analytic expression for the adsorption isotherms measured, the data are plotted $\log \Gamma$ versus $\log(-\ln x)$ as shown in Fig. 6. Note that the $\log(-\ln x)$ axis is shifted for each isotherm in order to show all three isotherms clearly. Only the -10.00C isotherm appears to follow approximately a straight line over the complete range of data. The -3.00C and -6.50C isotherms have more than one straight line section. In order to fit the data to the empirical isotherm, the data for each straight line segment are treated separately and the appropriate straight line parameters are computed using a least squares fitting technique. The straight line parameters for the mean isotherms and the envelope

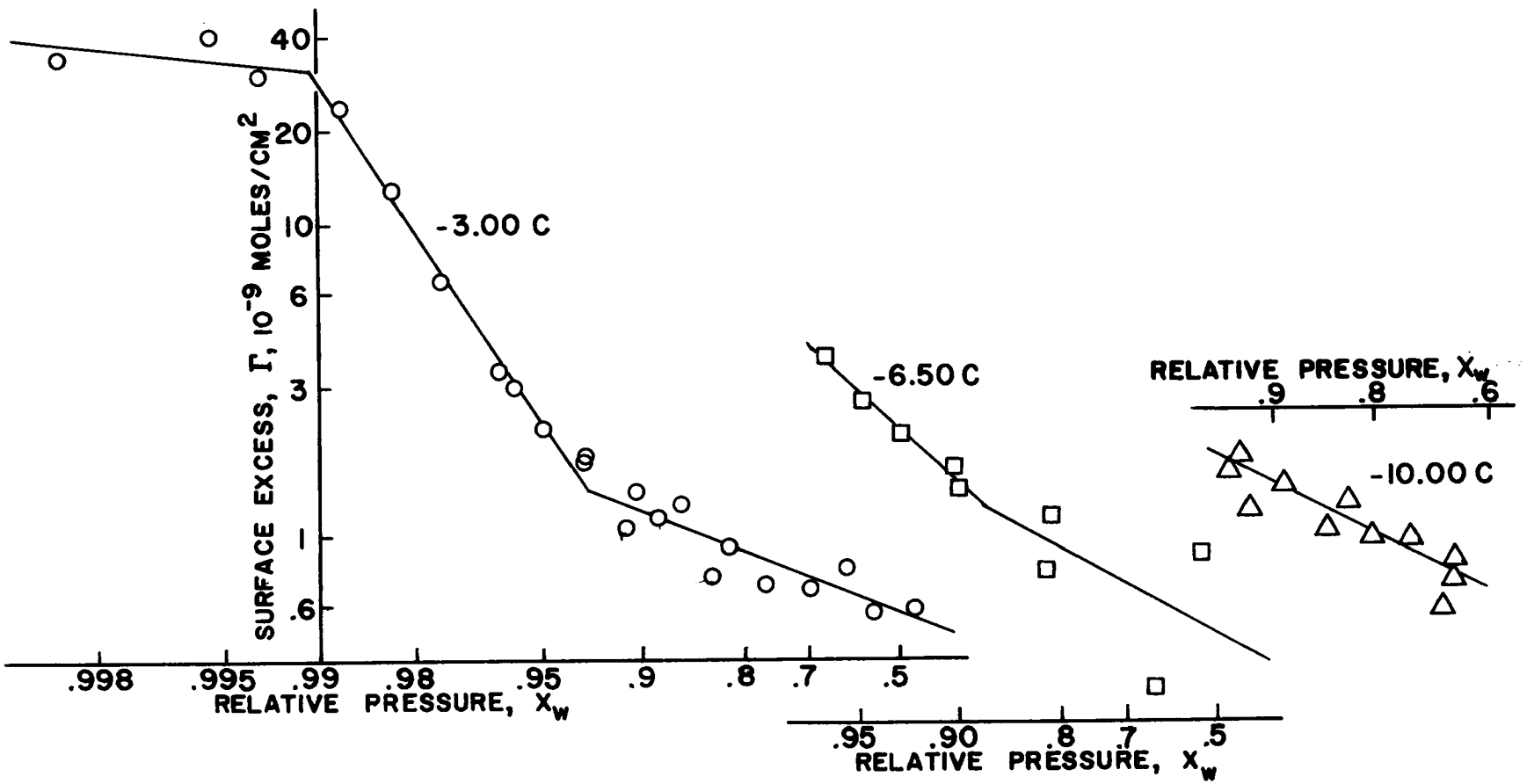

Figure 6: The -3.00C, -6.50C and -10.00C isotherm data plotted log Γ versus log(-ln x). The relative pressure scales are offset for each isotherm for clarity; individual scales are given. Solid line represents the least squares best fit straight line of the data to the empirical isotherm equation.

isotherms based on a one standard deviation about the mean are given in Table IV. The vapor pressure, relative pressure and coverage intervals over which each straight line segment is valid are also given in the table. The solid lines in Figures 3 through 5 give the smooth empirical isotherms based on the mean data points.

The isosteres shown in Fig. 7 are computed from these parameters by modifying the empirical isotherm equation:

$$\ln p = \ln p_o - \exp\left[\frac{\ln \Gamma - a}{b}\right] . \qquad (8.2)$$

The vertical bars through the data points are determined from the one standard deviation isotherms. Only a few isosteres are shown in Fig. 7 for clarity.

Isosteric heats of adsorption are computed from the isosteres determined from the smoothed isotherms. Three isosteric heats are computed at coverages less than 1.8 nanomoles/cm^2. Above this coverage, only the -3.00C and -6.50C isotherms are available for isostere data. The solid line in Fig. 8 gives the isosteric heat of adsorption determined by a least squares fit to isostere points from all three isotherms; the error band associated with this computation is given by the vertical bars through the data points. Heats determined by pairs of isotherms are also computed. The dashed line in Fig. 8 gives the isosteric heat computed from the -6.50C and -10.00C isosteres. The dash-dot line gives the heats from the -3.00C and -6.50C isosteres; the computation is made up to a coverage of 4.0 nanomoles/cm^2. Tabulated data for the isosteres and isosteric heats are found in Table V.

Figure 7: Adsorption isosteres from the smoothed isotherms. Numerals on curves give the coverage in nanomoles/cm^2.

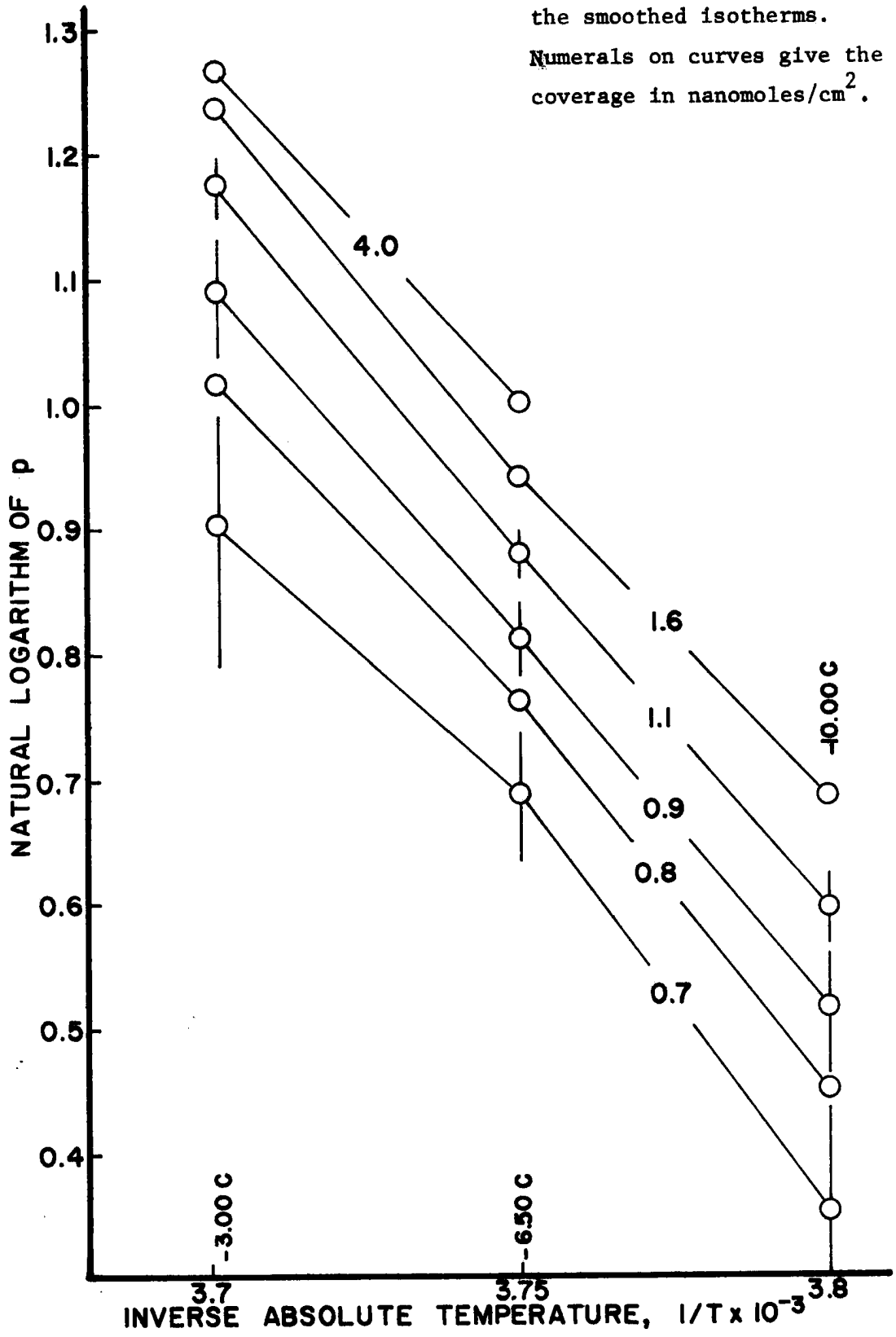

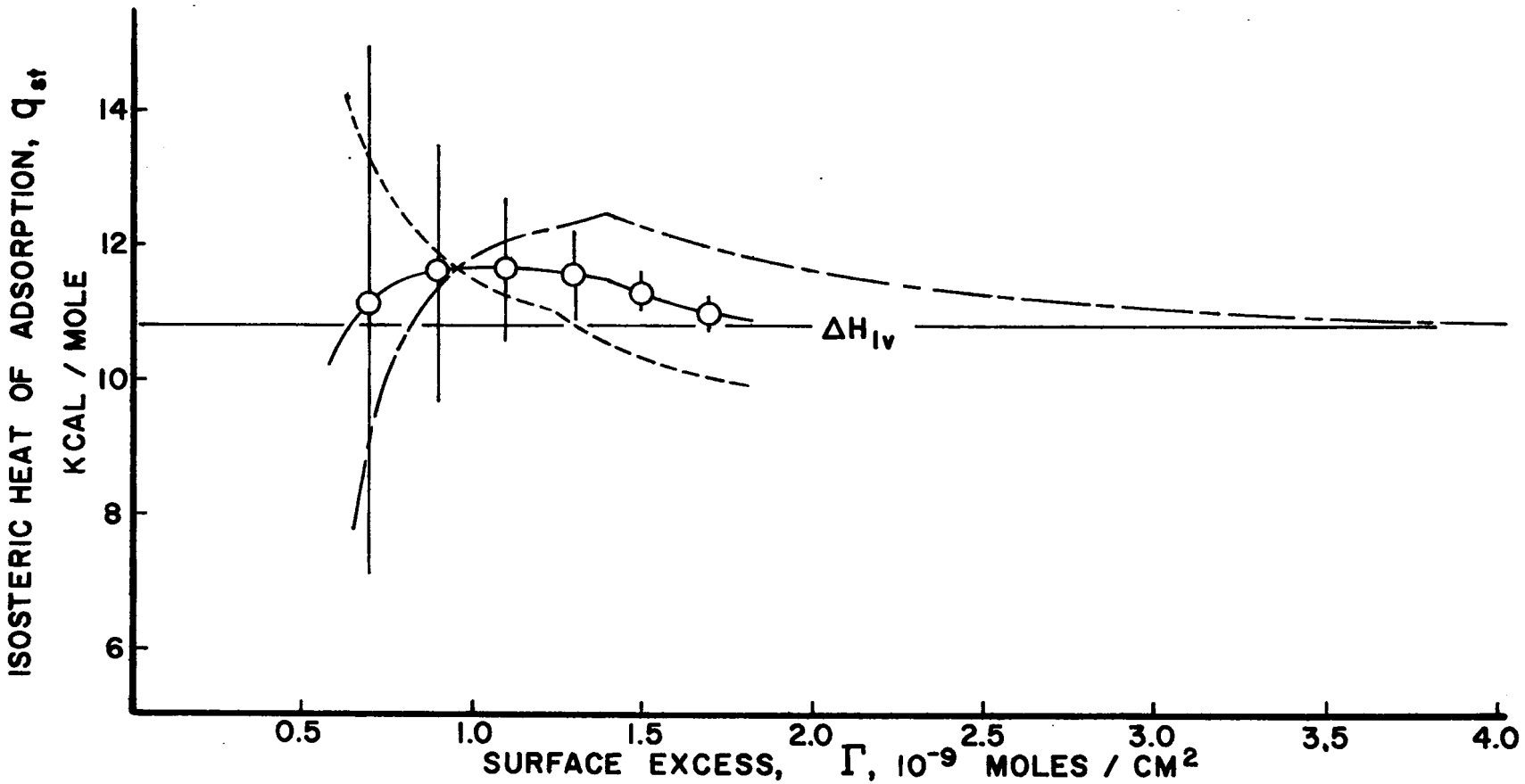

Figure 8: The isosteric heats of adsorption obtained from the smoothed isotherms. Solid line through open circles is the least squares isosteric heat from all three isotherms. Dashed line gives heats from the -6.50C and -10.00C isotherms. Dash-dot curve gives heats from the -3.00C and -6.50C isotherms.

A discontinuity in the slope of the isosteric heat occurs at a coverage of 1.4 nanomoles/cm^2, which corresponds to the transition of the -3.00C isotherm from the shallow to steep slope region in Fig. 6. A similar transition in the isosteric heat curve computed from the -6.50C and -10.00C isotherms occurs at a coverage of 1.25 nanomoles/cm^2, which corresponds to the transition of the -6.50C isotherm to a steeper slope. The sharp change in slope of the isosteric heat curves is due, in part, to the artificial separation of the isotherms into the straight line portions shown in Fig. 6; an actual isosteric heat curve would show a continuous transition through the peak. Heats of adsorption obtained from adsorption isotherms are averages over the entire adsorbing surface.

8.3 Gibbs Equation Integration

Integration of the Gibbs equation is carried out analytically using the smoothed isotherms. Substituting the expression for the empirical isotherm into the Gibbs equation and integrating yields:

$$\Pi_{\Delta x} = - \frac{RTe^a}{b + 1} \left[(-\ln x_2)^{b+1} - (-\ln x_1)^{b+1} \right] \qquad (8.5)$$

where x_1 and x_2 are the relative pressure with respect to water at the limits of the integration and a and b are the empirical parameters of the isotherm. For convenience, the relative pressure with respect to water that corresponds to saturation with respect to ice is chosen as the starting point for all the Gibbs integrations. The surface free energy ϕ of the adsorbent-vapor interface at ice saturation is taken to be the reference state. This means that $\Pi_{\Delta x}$ is zero at the water

relative pressure that corresponds to ice saturation and measures the departure of ϕ from that at ice saturation.

Figure 9 shows the variation of Π with relative pressure. A large increase in adsorption above ice saturation at -3.00C gives rise to the sharp increase in Π for this isotherm. The -6.50C and -10.00C isotherms are terminated before large adsorption amounts are attained. Table VI gives the data used to form Fig. 9. From the empirical isotherm equation the surface area occupied per molecule, $\sigma = 1/\Gamma$, is easily found and a Π versus σ plot can be drawn. The Π-σ plot shown in Fig. 10 indicates a distinct kink in the -3.00C and -6.50C curves. The surface area occupied per nanomole decreases much more rapidly than Π increases above the transition. This indicates the contribution to Π per molecule adsorbed decreases at the transition and that this decrease is also associated with the peak or kink in the isosteric heat curves. Computation of Π from isotherms yields an average for the entire surface.

Computation of the integral heats of adsorption from this Π data is not possible since an arbitrary reference pressure and reference value for Π are chosen. Only if the integration is carried out from very low pressures where ϕ is that for the bare surface of the adsorbent can such a computation be made.

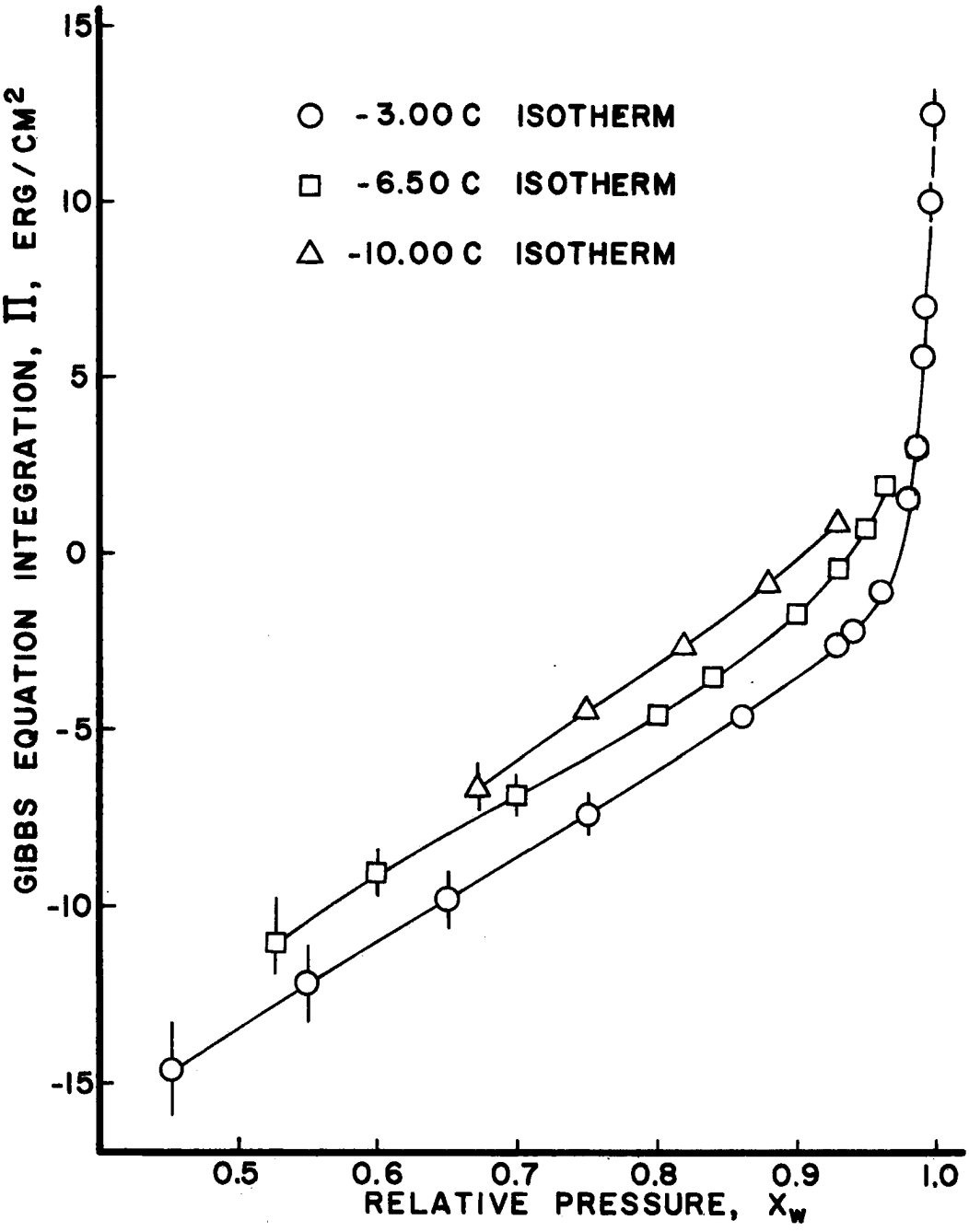

Figure 9: The variation of the Gibbs equation integration with relative pressure computed analytically from the smoothed isotherms. Arbitrary zero reference point chosen to be saturation with respect to ice.

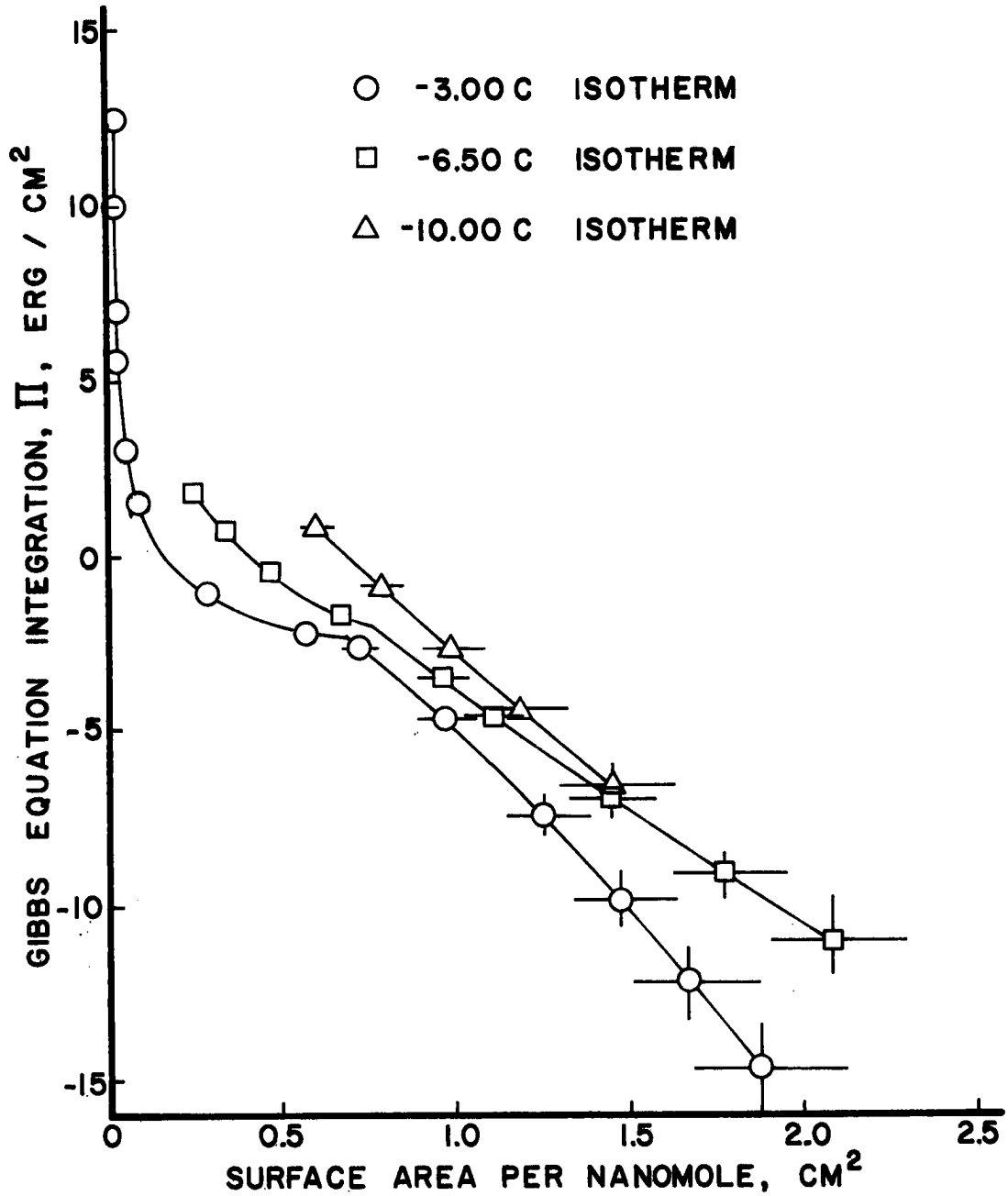

Figure 10: A Π-σ plot showing the abrupt transition from shallow to steep slope of the isotherms in Fig. 6 corresponds to a phase transition in the adsorpbed water. Horizontal and vertical bars give a one standard deviation error estimate.

CHAPTER IX

INTERPRETATION

The isosteric heat of adsorption gives the heat released per mole during the adsorption of an infinitesimal amount of vapor at a specific surface excess. This heat, therefore, can be interpreted as the energy of interaction between the vapor and adsorbed film. In Fig. 8, the isosteric heat based on all three isotherms and on the -3.00C and -6.50C isotherms shows a maximum. The increase in the heat of adsorption at coverages smaller than at the maximum are due to lateral cooperative interactions between molecules adsorbed on high energy sites. These lateral interactions give rise to an energy of adsorption that is larger than that on the bare surface of the adsorbent. Although high energy sites on the surface also could cause an increase in the heat of adsorption, these sites are completely occupied even at the lowest coverages studied in this work. It is between the water molecules adsorbed on high energy sites that the lateral interactions occur.

As the number of adsorbed molecules increases, the number of lateral interactions which can occur decreases. Lateral interactions permit the effect of high energy sites on the surface to be extended to several molecular layers. The peak in the isosteric heat curves occurs when the number of possible lateral interactions rapidly begins to decrease. Once the lateral interactions are saturated, the heat of adsorption is produced by the interaction between loosely adsorbed molecules and molecules in the vapor. Very little interaction energy is due to the surface since its effects are masked by

the large number of molecular layers. As the amount adsorbed increases, the heat of adsorption decreases to the heat of condensation.

The occurrence of lateral interactions is, in itself, not significant. However, the disappearance of the effects of lateral interactions at coverages less than 1.4 nanomoles/cm^2 is important. Based on 10.2 A^2 as the surface area occupied by a single adsorbed water molecule [7], statistical monolayer coverage occurs at 1.63 nanomoles/cm^2. The peaks in the isosteric heat curves occur at coverages significantly smaller than this value. For lateral interactions to be dominated by interactions between loosely adsorbed molecules and the vapor means that a considerable portion of the surface must be covered by a multilayer film of water. Comparing the coverages at the maximum isosteric heat to the statistical monolayer coverage leads to the same patch-like adsorption picture presented by Edwards and Corrin [18] and Corrin and Nelson [14] also on pure silver iodide.

According to Jura and Harkins [42] the distinct break seen in the Π-σ curves of Fig. 10 indicates a two-dimensional change in phase of the adsorbate. A transformation of the empirical equation used to smooth the data leads to a modified Harkins-Jura condensed phase expression:

$$\Pi = k\sigma^n + k' \qquad (9.1)$$

where $\underline{n}$ and $\underline{k}$ are related to the slope $\underline{b}$ and intercept $\underline{a}$ of the empirical isotherm equation by:

$$n = -\frac{(b+1)}{b} \text{ and } k = \frac{RTe^{-a/b}}{b+1} . \qquad (9.2)$$

The value of $\underline{n}$ corresponding to the various smoothed isotherms is given in Table IV. The transition from $\underline{n}$ approximately equal to unity, a range from 0.76 to 1.53, for the low coverage portion of the isotherms indicates the existence of a condensed surface phase as envisioned by Jura and Harkins.[42] Pierce[21,22] interprets the change in slope of isotherms plotted as in Fig. 6 as indicating a transition from a localized to mobile adsorbed film. Clearly a similar transition occurs here.

Both the change in the trend of the isosteric heat curves and the kink in the $\underline{\Pi-\sigma}$ plots indicate a change to a denser packed, though more loosely bound, mobile structure of the adsorbed film. This transition is observed in the -3.00C and -6.50C isotherms only. Estimated from Figures 10 and 9, a transition at -10.00C should occur at a surface excess of 1.1 nanomoles/cm^2 and a vapor pressure of 1.82 mm Hg; however, insufficient data exists above this coverage to conclusively indicate the occurrence of a phase transition in the adsorbed water at this temperature.

At a silver iodide temperature of -6.50C and -10.00C adsorption runs are terminated above 2.73 mm Hg and 2.00 mm Hg, respectively, because the weight of the samples continuously increases at vapor pressures above these values. This sudden, unbounded increase in the weight of the sample is interpreted as the onset of nucleation

of a bulk condensed phase on the powder. The relative pressure at which this onset of nucleation occurred is well below water saturation in both cases. Table VII gives some of the adsorption parameters at the onset of nucleation. The condensed phase must clearly be ice since, by a free energy argument, ice is the stable phase at temperatures below 0C and at pressures below water saturation. The nucleation of ice observed in this experiment must proceed directly from the vapor. Furthermore, unlike cloud chamber studies which consider the onset of nucleation in terms of orders of magnitude of ice particles nucleated, this method of observing nucleation detects the onset of nucleation on the most active site on the most active particle in the entire sample. In some respects this may be a disadvantage in studying the nucleation mechanism with adsorption techniques for once nucleation occurs, little can be gained from continued observation of the change in weight of the sample.

The amount adsorbed at nucleation gives direct evidence that the patch model of adsorption is valid up to the onset of nucleation. At -10.00C nucleation occurs with little more than statistical monolayer coverage, at -6.50C slightly more than two monolayers are adsorbed. These patches must then grow by adsorption both vertically and laterally until they exceed the critical mass of an ice embryo. High energy patches on the silver iodide surface provide the foundation for that growth.

Of considerable interest is the observation that nucleation did not occur at -3.00C even as water saturation is approached. An explanation is that water saturation does not provide a sufficient

supersaturation with respect to ice to initiate nucleation. Considering the relationship between ice and water saturation vapor pressures, given by equation 6.1, unless the sample temperature is below -3.5C the vapor pressure must always exceed water saturation to achieve sufficient ice supersaturation. Under these conditions, nucleation of supercooled water is favored from both free energy and entropy considerations; ice can then form by a freezing mechanism. The threshold temperature for the most active site is significantly warmer than the frequently quoted -4C determined from cloud chamber studies. Many more experiments designed to detect nucleation at different sample temperatures are needed to precisely define the threshold temperature and supersaturations required to nucleate ice on pure silver iodide. The threshold temperature of -3.5C and supersaturation of 3.4% obtained in this experiment are based on a linear extrapolation of the supersaturations with respect to ice that led to ice nucleation at -6.50C and -10.00C.

As seen in Chapter III, nucleation thermodynamics approaches the growth of an embryo from a distinctly different point of view than adsorption thermodynamics. The fundamental difference is that nucleation theory considers the embryo to be a duplex film; the embryo-vapor interface being independent of the adsorbent-embryo interface. Classical adsorption thermodynamics, however, deals with a nonduplex film at all coverages although changes in phase of this film can occur. The quantity $\underline{\Pi}$ computed from the Gibbs equation is explicitly for

nonduplex films. In this experiment, however, a transition from a nonduplex to a duplex film on the patch must occur if nucleation is to take place. Figure 8 and Table VII show that at the onset of nucleation, the isosteric heat of adsorption has decreased to the heat of condensation. Energetically, at least, just prior to nucleation, the interface between water adsorbed on a patch and the vapor resembles the liquid. If, according to nucleation theory, the embryo is already a duplex film, then the surface free energy of this interface must lie between that for a liquid water - vapor and ice - vapor interface.

Continuing with this interpretation, the transition of the adsorbed nonduplex film into a duplex film occurs prior to nucleation. Based on the Π-σ plots of Fig. 10, the isosteric heat curves of Fig. 8, and also on the isotherms plotted as in Fig. 6, only one transition in adsorbed phase occurs before nucleation. Treated with classical adsorption thermodynamics that can not recognize the existence of surface heterogeneities, this phase change does not seem unusual, yet nucleation thermodynamics depends on its existence.

Comparing the conditions at the onset of nucleation at -10.00C and those at -3.00C, which do not lead to nucleation, to the requirements for obtaining a critical embryo as given by equation 3.28, points out several inconsistencies which can be resolved in only one way. At -3.00C, both the temperature T and saturation ratio p/p_o is larger than at -10.00C. Also, the bulk interfacial free energy of the ice-vapor surface is larger than the liquid-vapor value.[34] Provided that α and β are temperature independent, variations in m, dependent

on the Gibbs equation, would make $\underline{m}$ larger at -3.00C than at -10.00C. All these effects would lead to a smaller critical size of the embryo at -3.00C than at -10.00C. However, 30 times as much water is adsorbed at -3.00C than at -10.00C indicating that the embryos present at -3.00C are larger than those at -10.00C which lead to nucleation. The only term in equation 3.28 which can possibly lead to a larger critical embryo is $\underline{\mu'}$, the deviation of the chemical potential of the embryo from that of the bulk condensed phase. Therefore, at -10.00C, the small amount adsorbed indicates small critical embryos and a small $\underline{\mu'}$. A low supersaturation overcomes the volume-surface area effects and leads to nucleation. At -3.00C, large embryos are present but nucleation does not occur, therefore, $\underline{\mu'}$ must be larger than at -10.00C. This behavior means that at -10.00C the adsorbed water is more ice-like than that adsorbed at -3.00C on similar high energy patches. A more liquid-like adsorbed film in terms of its chemical potential at -3.00C is further evidence of the increasingly duplex nature of the adsorbed film as the amount adsorbed increases.

The ice-like chemical potential of the adsorbed film at small coverages on the patch and the increasingly liquid-like chemical potential as more water is adsorbed indicates that epitaxy still plays a role in nucleation. The transition of the ice-like structure bridging the high energy sites on the patch to an ice structure is undoubtedly enhanced by the underlying crystal structure and is the final step leading to ice nucleation on pure silver iodide.

CHAPTER X

CONCLUSIONS

The surface of pure silver iodide consists of patches of sites which interact strongly with water vapor and are surrounded by a surface which plays only a minor role in the adsorption process. As the amount adsorbed increases, a change in phase of adsorbed water occurs producing a more mobile adsorbed film on the patch and allowing the film to act as a duplex film. Small adsorption amounts at the onset of nucleation indicate the adsorbed water is still patch-wise distributed over the surface of the powder; the patch model of adsorption remains valid up to the onset of nucleation.

These patches enter the nucleation mechanism in the following way. Adsorption occurs preferentially on the patches because of the high energy of interaction between adsorption sites in the patch and water vapor. The spacing between these sites is such that the first adsorbed molecules can still interact strongly with molecules in the vapor forming a strongly bound but loosely packed structure of water molecules bridging the high energy sites. This process continues until the patch is completely bridged over. Molecules adsorbed on this structure are bound more loosely and can move around on the open structure of water molecules bound to the high energy sites. Migration of molecules over and filling of this open structure leads to a denser packing and the idea that a phase change in the adsorbed film has occurred. The vapor and silver iodide

interfaces of the water adsorbed on the patch become sufficiently separated so that the film adsorbed on the patch acquires characteristics of a duplex film, becoming more duplex as additional molecules are adsorbed. Nucleation occurs when the decrease in free energy of the embryo due to adsorption of additional molecules overcomes the free energy penalty accompanying the increase in surface area of the embryo.

On pure silver iodide, the threshold temperature and supersaturation with respect to ice required to nucleate ice are estimated to be -3.5C and 3.4%, respectively. Under these conditions, nucleation of ice directly from the vapor, as in the Bergeron process, on the most active site on the most active particle in the sample is detected by this adsorption measurement technique; since the number of particles in the sample is not known, an estimate of the efficiency of nucleation can not be made. In contrast, nucleation efficiencies of pure silver iodide aerosols determined by cloud chamber methods generally include the contribution to nucleation by a freezing mechanism since liquid water droplets are present in the cloud. Furthermore, the number of nuclei activated must be several orders of magnitude larger than in this study to be confidently detected by present cloud chamber techniques. Only one crystal need be nucleated to be detected by the adsorption method. The rapid increase in the number of nuclei activated as the temperature decreases below the -4C threshold determined from cloud chamber studies indicates the nucleation activity of the high energy patches is strongly temperature dependent. Another important difference between the

nucleation reported here and that studied in cloud chambers involves the purity of the silver iodide. Dispersal of silver iodide by acetone - silver iodide - potassium (or sodium) iodide solution burners, pyrotechnics, or even liquid ammonia - silver iodide solution sprayers does not yield pure, uncontaminated silver iodide aerosols. Yet these are the aerosols that produce nucleation, both in the laboratory cloud chambers and in the free atmosphere. The silver iodide powder used in this study is, in contrast, the purest now obtainable.

Information on the energetics of adsorption is, of necessity, based on averages over the surface. Isosteric heats of adsorption which consider the effect of adding to the total amount adsorbed gives an insight into the energies involved, on the average, in adsorption onto the outer most layers of the adsorbed film. Above the transition to a duplex film on the patch, a clear cut interpretation of $\underline{\Pi}$ is impossible; only on the nonduplex film surrounding the patch or on the patch itself will $\underline{\Pi}$ have an unambiguous meaning. Even at coverages below the transition, the heteroenergetic nature of the silver iodide surface does not permit $\underline{\Pi}$ to represent anything but a gross average change in the interfacial free energy.

At the onset of nucleation, the heat of adsorption is very close to the heat of condensation indicating a liquid-like interface between the embryo patch and vapor. A sharp discontinuity in the heat of adsorption must occur on nucleation; the heat increasing to the heat of deposition. This increase in the heat of adsorption

is accompanied by an internal rearrangement of the molecules into an ice structure propogating outward from the silver iodide surface through the embryo. Adsorptions studies are unable to detect this increase in isosteric heat because the nucleation process and subsequent adsorption are time dependent while gravimetric and volumetric adsorption techniques give a static measure of the amount adsorbed.

Aside from the difference in the treatment of the embryo film, nucleation theory must account for time dependent effects. Adsorption theory does not and, as it stands on classical thermodynamic grounds alone, can not account for these temporal effects. Furthermore, adsorption energetics imply an average over the entire surface while nucleation deals with a microscopically small portion of the surface. Reconciliation of the nonduplex-duplex nature of the film adsorbed and embryo formed on the high energy patches in a heteroenergetic surface is necessary before a complete theory of nucleation energetics is possible.

This work provides a starting point from which future studies can develop. Previous studies on impure silver iodide indicated considerably larger amounts adsorbed with significantly different heats of adsorption. These differences are attributed to impurities and the effect of these impurities completely overwhelms the contribution of the uncontaminated portion of the surface to adsorption and heats of adsorption. The results reported here, therefore, may serve as a baseline against which future studies with the intent to detect nucleation on impure silver iodide can be compared.

LIST OF REFERENCES

1. Schaefer, V. J., Science, 104, 457 (1946).
2. Vonnegut, B., J. Applied Phys., 18, 593 (1947).
3. MacCready, P. B., Bull. Amer. Met. Soc., 33, 48 (1952).
4. Beaumont, R. T., Bull. Amer. Met. Soc., 34, 298 (1953).
5. Birstein, S. J., Geophys. Res. Paper #32, AFCRC-TR-54-200, 37 pp. (1954).
6. Birstein, S. J., J. Met., 12, 324 (1955).
7. Corrin, M. L. and N. S. Storm, J. Phys. Chem., 67, 1509 (1963).
8. Corrin, M. L., H. W. Edwards, and J. A. Nelson, J. Atmos. Sci., 21, 555 (1964).
9. Tcheurekdjian, N., A. C. Zettlemoyer, and J. J. Chessick, J. Phys. Chem., 68, 773 (1964).
10. Hall, P. G. and F. C. Tompkins, Trans. Faraday Soc., 58, 1734 (1962).
11. Coulter, M. L. and G. A. Candela, Z. Electrochem., 56, 449 (1952).
12. Corrin, M. L., J. A. Nelson, B. Cooley, and B. Rosenthal, J. Atmos. Sci., 24, 594 (1967).
13. Nelson, J. A., Ph.D. Dissertation, University of Arizona, 96 pp (1967).
14. Corrin, M. L. and J. A. Nelson, J. Phys. Chem., 73, 643 (1968).
15. Corrin, M. L., S. P. Moulik, and B. Cooley, J. Atmos. Sci., 24, 530 (1967).
16. Moskvitin, N. N., M. M. Dubinin, and A. I. Sarakhov, Izvest. Akad. Nauk SSSR, Otdel. Khim. Nauk, 12, 2080 (1959).

17. Zettlemoyer, A. C., N. Tcheurekdjian, and J. J. Chessick, Nature, 192, 653 (1961).

18. Edwards, H. W. and M. L. Corrin, J. Phys. Chem., 71, 3373 (1967).

19. Zettlemoyer, A. C., J. Colloid Interfac. Sci., 28, 343 (1968).

20. Hill, T. L., Advances in Catalysis, IV, Academic Press, Inc., New York, 211 (1952).

21. Pierce, C., J. Phys. Chem., 64, 1184 (1960).

22. Pierce, C. and B. Ewing, J. Amer. Chem. Soc., 84, 4070 (1962).

23. Hill, T. L., J. Chem. Phys., 17, 520 (1949).

24. Hill, T. L., J. Chem. Phys., 18, 246 (1950).

25. Everett, D. H., Trans. Faraday Soc., 46, 453 (1950).

26. Everett, D. H., Trans. Faraday Soc., 46, 942 (1950).

27. Gibbs, J. W., The Scientific Papers of J. Willard Gibbs, Vol. I, Dover Publications, Inc., New York (1961).

28. Guggenheim, E. A., Trans. Faraday Soc., 36, 397 (1940).

29. Hill, T. L., Trans. Faraday Soc., 47, 376 (1950).

30. Eisenberg, D. and W. Kauzmann, The Structure and Properties of Water, Oxford University Press, New York, 48 (1969).

31. Lewis, G. N. and M. Randall, revised by K. S. Pitzer and L. Brewer, Thermodynamics, 2nd ed., McGraw-Hill Book Co., New York, 186 (1961).

32. Frenkel, J., J. Chem. Phys., 7, 538 (1939).

33. Volmer, M., Kinetik der Phasenbildung, Steinkopff, Dresden and Leipzig, 100 (1939).

34. Fletcher, N. H., The Physics of Rainclouds, Cambridge University Press, London, Ch. II (1962).

35. Fletcher, N. H., J. Chem. Phys., 38, 237 (1963).

36. Fletcher, N. H., J. Atmos. Sci., 26, 1266 (1969).

37. Fletcher, N. H., J. Atmos. Sci., 25, 1058 (1968).

38. Washburn, E. W., Mon. Weather Rev., 52, 488 (1924).

39. Jancso, G., J. Pupezin, and W. A. van Hook, J. Phys. Chem., 74, 2984 (1970).

40. Volk, W., Applied Statistics for Engineers, McGraw-Hill Book Co., Inc., New York, 136 (1958).

41. Widder, D. V., Advanced Calculus, Prentice-Hall, Inc., New York, 351 (1947).

42. Jura, G. and W. D. Harkins, J. Amer. Chem. Soc., 68, 1941 (1946).

43. Freeman, M. P. and G. D. Halsey, Jr., J. Phys. Chem., 60, 1119 (1956).

44. Farkas, A. and H. W. Melville, Experiments in Gas Reactions, Macmillan and Co., London, 203 (1939).

45. Parshall, M., Bulletin 509-S, Agricultural Experiment Station, Fort Collins, Colorado, 17 (1961).

APPENDIX I

SURFACE AREA MEASUREMENT AND ERROR ANALYSIS

The surface area of the pure silver iodide powder used in this work was determined by applying the B.E.T. relation to krypton adsorption measurements made on a Numinco-Orr Pore Size and Surface Area Analyzer; a volumetric krypton adsorption system. Krypton adsorption isotherms were obtained at liquid nitrogen boiling point on samples of pure silver iodide taken from the same ampule which provided samples for the water adsorption measurements. The discussion presented here treats primarily an analysis of the variance, as in Chapter VII, of this B.E.T. method for determining surface areas.

Volumetric krypton adsorption isotherms used in the B.E.T. surface area computation involve the measurement of several variables. Two helium pressure measurements $\underline{p_1}$ and $\underline{p_2}$ serve to determine the system volumes; the manifold volume $\underline{V_m}$ is assumed to be a known constant. Variance of the helium pressure measurements was approximated from the precision with which an aneroid manometer on the Numinco unit could be read; $\underline{s^2(P)=0.01mm^2}$. From these variances, the variance of the total system volume and residual sample bulb volume was computed from equation 7.1:

$$V_f = \frac{P_1}{P_2} V_m \text{ and } V_r = V_f - V_m \tag{I.1}$$

$$s^2(V_f) = s^2(V_r) = \left(\frac{P_1}{P_2} V_m\right)^2 \left(\frac{s^2(P_1)}{P_1^2} + \frac{s^2(P_2)}{P_2^2}\right) . \tag{I.2}$$

Determination of the adsorption isotherm requires measurement of two krypton pressures and the manifold temperature $\underline{T}$. The later is assumed to remain constant during the measurement; a variance for the temperature is taken to be $\underline{s^2(T)=0.01K^2}$. System krypton pressure is determined from calibration curves relating Pirani gauge bridge potentiometer setting to the krypton pressure. The variance of the krypton pressure measurement was assumed to be dependent on the slope of the calibration curve, i.e.:

$$s^2(p_{Kr}) = \left(\frac{p_{Kr}}{100}\right)^2 \qquad (I.3)$$

with $\underline{p_{Kr}}$ in mm Hg. This however does not imply the Pirani gauge is more accurate at the lowest pressure measured. It simply implies that the pressure indicated by the gauge can be read with more precision at lower pressures. At higher pressures, the steepness of the calibration curve makes interpolation difficult and subject to greater error; hence the choice of this expression for the variance of the krypton pressure measurement.

Adsorption amounts are determined by the system volumes and krypton pressure measurements. Each set of initial and final krypton pressures, $\underline{p_i}$ and $\underline{p_f}$, permits the incremental amount absorbed $\underline{n}$ to be computed:

$$n = \frac{p_i V_m}{wRT} + \frac{p_{f-1} V_r}{wRT} - \frac{p_f V_f}{wRT} \quad . \qquad (I.4)$$

From equation 7.1, the variance of the incremental amount adsorbed is

found to be:

$$s^2(n) = \left(\frac{p_i V_m}{wRT}\right)^2 \left(\frac{s^2(p_i)}{p_i^2} + \frac{s^2(T)}{T^2} + \frac{s^2(w)}{w^2}\right)$$

$$+\left(\frac{p_{f-1} V_r}{wRT}\right)^2 \left(\frac{s^2(V_r)}{V_r^2} + \frac{s^2(p_{f-1})}{p_{f-1}^2} + \frac{s^2(T)}{T^2} + \frac{s^2(w)}{w^2}\right)$$

$$+\left(\frac{p_f V_f}{wRT}\right)^2 \left(\frac{s^2(V_f)}{V_f^2} + \frac{s^2(p_f)}{p_f^2} + \frac{s^2(T)}{T^2} + \frac{s^2(w)}{w^2}\right) \tag{I.5}$$

where p_{f-1} is the final pressure of the previous set of measurements and equals zero for the first set, R is the ideal gas constant, and w is the weight of sample. The total amount adsorbed per gram for each set of krypton pressure measurements is given by the sum of the n's given by equation I.4:

$$n_a = \sum n \tag{I.6}$$

and the variance of n_a, the total amount adsorbed, is given by:

$$s^2(n_a) = \sum s^2(n). \tag{I.7}$$

Along with the quantity n_a the equilibrium relative pressure of krypton x must also be computed:

$$x = p_f/p_o \ . \tag{I.8}$$

The saturation pressure of krypton is determined from the vapor pressure relation given by Freeman and Halsey [43] :

$$\log_{10} p_o = 6.9861 - 491.9/T \tag{I.9}$$

where $\underline{p_o}$ is in mm Hg. and $\underline{T}$ is the absolute temperature of the krypton. Liquid nitrogen boiling point is determined from the Farkas and Melville [44] expression for nitrogen saturation pressure $\underline{P}$:

$$\log_{10} P = 7.5778 - 0.00476\ T - 334.64/T \qquad (I.10)$$

in the temperature range 64K to 84K. Nitrogen saturation pressure is taken to be the average Fort Collins, Colorado, barometric pressure 635 mm Hg. [45] These expressions are combined to give the krypton saturation pressure $\underline{p_o}$, referenced to the supercooled liquid, directly as a function of the Fort Collins atmospheric pressure:

$$\log_{10} p_o = 6.9861 - 4.683/\{(7.5778-\log_{10}P) - \sqrt{1.2063-\log_{10}P}\ \} \qquad (I.11)$$

The average value of the krypton saturation pressure is found to be $\underline{p_o}$ = 3.14 mm Hg ± 1.5% which leads to a variance:

$$s^2(p_o) - .0022\ \text{mm}^2. \qquad (I.12)$$

Using equation 7.1, the variance of $\underline{x}$ can also be estimated:

$$s^2(x) = x^2 \left(\frac{s^2(p_f)}{p_f^2} + \frac{s^2(p_o)}{p_o^2} \right). \qquad (I.13)$$

From the total amount adsorbed $\underline{n_a}$ and the equilibrium relative pressure $\underline{x}$, the B.E.T. function $\underline{y}$ is given as:

$$y = x/\{n_a(1-x)\} \qquad (I.14)$$

and the variance of $\underline{y}$ is found to be:

$$s^2(y) = y^2 \left(\frac{s^2(n_a)}{n_a^2} + \frac{1}{(1-x)^2} \frac{s^2(x)}{x^2} \right). \qquad (I.15)$$

In order to use the B.E.T. method of determining the surface area, the variables $\underline{x}$ and $\underline{y}$ must be linearly related. The best fit straight line is found by the method of least squares; the intercept $\underline{a}$ and slope $\underline{b}$ are given by:

$$a = \frac{\Sigma x^2 \Sigma y - \Sigma x \Sigma xy}{N\Sigma x^2 - \Sigma x \Sigma x} \qquad (I.16)$$

$$b = \frac{N\Sigma xy - \Sigma x \Sigma y}{N\Sigma x^2 - \Sigma x \Sigma x} \quad . \qquad (I.17)$$

The sums formed to evaluate I.16 and I.17 have variances that are attributable to the variances in $\underline{x}$ and $\underline{y}$, thus:

$$s^2(\Sigma x) = \sum s^2(x) \qquad s^2(\Sigma x^2) = \sum 4x^2 s^2(x)$$

$$s^2(\Sigma y) = \sum s^2(y) \qquad s^2(\Sigma xy) = \sum [y^2 s^2(x) + x^2 s^2(y)]. \qquad (I.18)$$

That portion of the variance of the slope and intercept due to the variance in the data is found, using equation 7.1, to be:

$$s_d^2(a) = \left(\frac{\Sigma xy \Sigma x \Sigma x + \Sigma x^2 (2\Sigma x \Sigma y - N\Sigma xy)}{(N\Sigma x^2 - \Sigma x \Sigma x)^2} \right)^2 s^2(\Sigma x) + \left(\frac{b\Sigma x}{N\Sigma x^2 - \Sigma x \Sigma x} \right)^2 s^2(\Sigma x^2)$$

$$+ \left(\frac{\Sigma x^2}{N\Sigma x^2 - \Sigma x \Sigma x} \right)^2 s^2(\Sigma y) + \left(\frac{\Sigma x}{N\Sigma x^2 - \Sigma x \Sigma x} \right)^2 s^2(\Sigma xy) \qquad (I.19)$$

and

$$s^2_d(b) = \left(\frac{\Sigma x(2N\Sigma xy - \Sigma x\Sigma y) - N\Sigma x^2\Sigma y}{(N\Sigma x^2 - \Sigma x\Sigma x)^2}\right)^2 s^2(\Sigma x) + \left(\frac{Nb}{N\Sigma x^2 - \Sigma x\Sigma x}\right)^2 s^2(\Sigma x^2)$$

$$+ \left(\frac{\Sigma x}{N\Sigma x^2 - \Sigma x\Sigma x}\right)^2 s^2(\Sigma y) + \left(\frac{N}{N\Sigma x^2 - \Sigma x\Sigma x}\right)^2 s^2(\Sigma xy) \ . \qquad (I.20)$$

A variance in a and b also arises from the scatter of the mean data points such that the variance in y unexplained by the linear regression is:

$$s^2(\hat{y}) = \frac{\Sigma y^2 - \Sigma y\Sigma y/N - b(\Sigma xy - \Sigma x\Sigma y/N)}{N-2} \ . \qquad (I.21)$$

The variance of the intercept due to the regression is:

$$s^2_r(a) = \left(\frac{\Sigma x^2}{N\Sigma x^2 - \Sigma x\Sigma x}\right) s^2(\hat{y}) \qquad (I.22)$$

and the variance of the slope due to the regression is:

$$s^2_r(b) = \left(\frac{N}{N\Sigma x^2 - \Sigma x\Sigma x}\right) s^2(\hat{y}) \ . \qquad (I.23)$$

The total variance of the intercept and slope is given by the sum of equations I.19 and I.22, and I.20 and I.23, respectively.

In the B.E.T. method, the specific surface area A is inversely proportional to the sum of the intercept and slope of the y versus x plot:

$$A = A\sigma/(a+b) \qquad (I.24)$$

where A is Avogadro's number and σ is the surface area occupied by a krypton molecule which Corrin and Storm [7] give as $\sigma = 18.2\ A^2$ at liquid nitrogen temperature; the variance $s^2(\sigma)$ is estimated to be $0.01\ A^4$.

The variance of $\underline{A}$ is given by:

$$s^2(A) = A^2 \left(\frac{s^2(\sigma)}{\sigma^2} + \frac{s^2(a) + s^2(b)}{(a + b)^2} \right) . \qquad (I.25)$$

The results of the krypton isotherm measurements are presented in Fig. I-1. Figure I-2 gives the B.E.T. plot of the isotherm data with the vertical bars through each data point giving the standard deviation. Runs 1 and 2 are for isotherms measured before the water adsorption measurements were made, while run 3 was made after those measurements were completed.

According to this analysis of the krypton adsorption data, the specific surface area of the pure silver iodide powder used in this work is 0.49 m^2/gm with a standard deviation of 5%. No change in the surface area during the course of the water adsorption measurements could be detected.

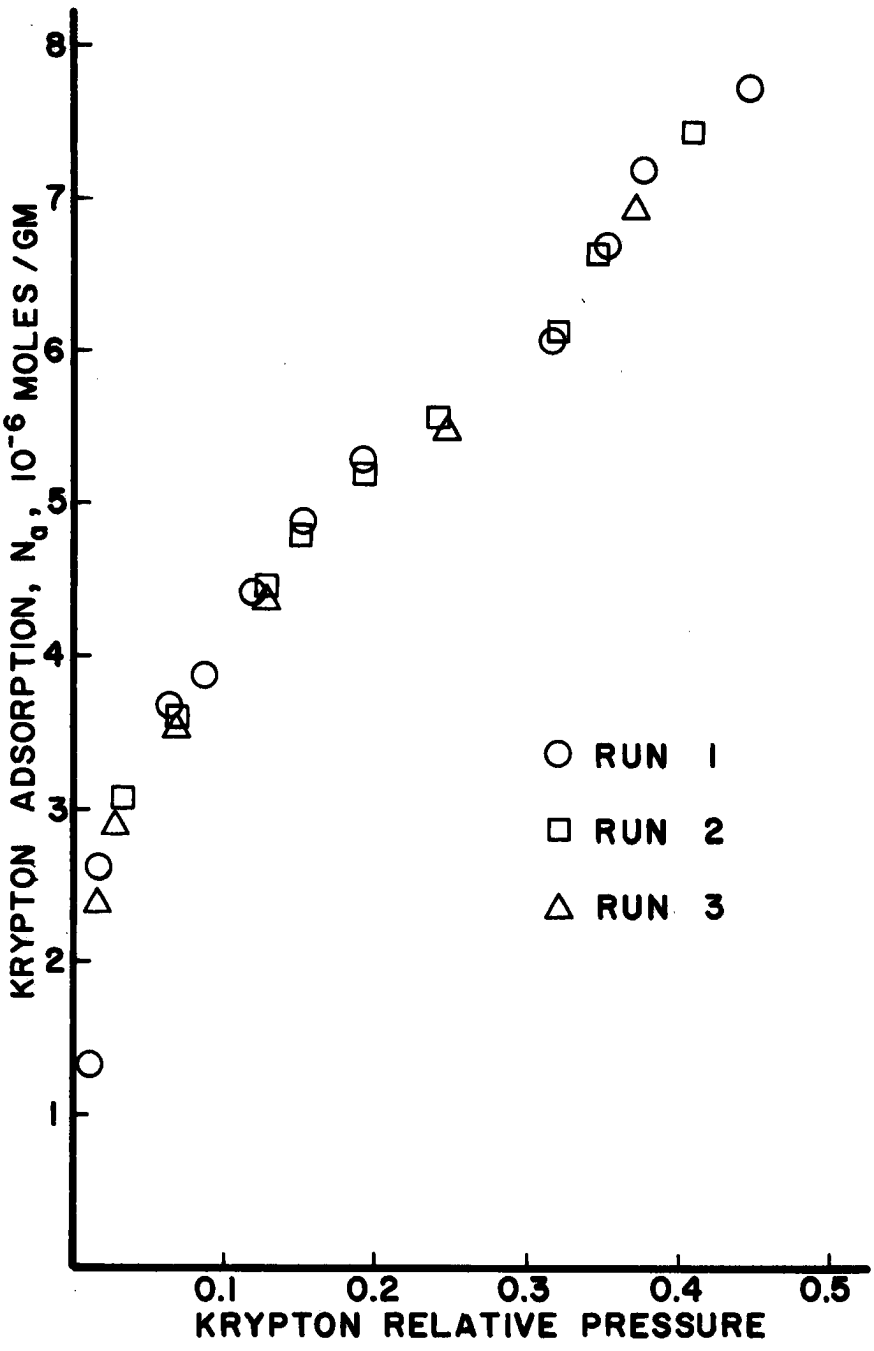

Figure I-1: Krypton adsorption isotherms on pure silver iodide at liquid nitrogen boiling point temperature.

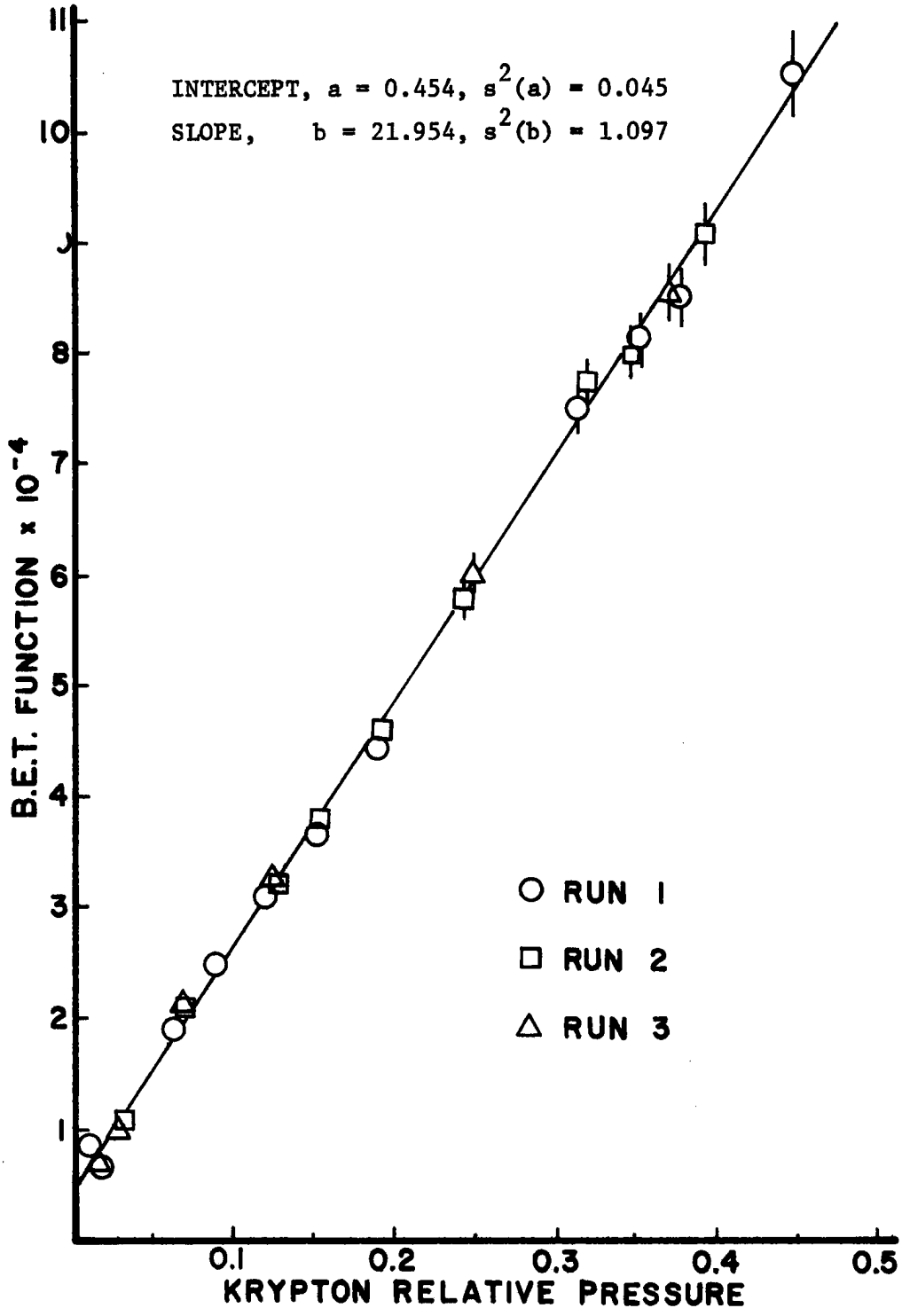

Figure I-2: B.E.T. plot of krypton adsorption data on pure silver iodide to obtain the surface area of the powder, 0.49m^2/gm. No change in the B.E.T. plot over the time period of the adsorption measurements is seen.

APPENDIX II

TABLES

Table I: Adsorption data for the -3.00C isotherms.

Water saturation pressure = 3.677 mm Hg

Ice saturation pressure = 3.572 mm Hg

Blank

Zero Offset = -.050 .003 Calibration Ratio = .99978 .00014

T_{ice}	p_{ice}	x_w	x_i	w_a
-12.99	1.491	.405	.417	.058 .004
-6.79	2.584	.703	.724	.125 .003
-5.33	2.931	.797	.821	.208 .004
-3.90	3.310	.900	.927	.296 .004
-2.76	3.643	.991	1.020	1.603 .005

Run #1: Sample weight = .90210 gm

Zero Offset = 0.000 .039 Calibration Ratio = 1.00000 .00099

T_{ice}	p_{ice}	x_w	x_i	b	w_a	Γ
-13.75	1.392	.378	.390	.050	.066 .045	.083 .056
-11.75	1.668	.454	.467	.061	.459 .045	.578 .063
-9.56	2.028	.552	.568	.089	.451 .045	.568 .062
-7.01	2.536	.690	.710	.129	.531 .045	.668 .065
-4.78	3.072	.835	.860	.230	.580 .045	.730 .066

Table I; Run 1, continued.

T_{ice}	p_{ice}	x_w	x_i	b	w_a	Γ
-4.09	3.258	.886	.912	.284	.886 .045	1.115 .078
-3.80	3.339	.908	.935	.312	.818 .045	1.030 .075
-3.50	3.424	.931	.959	.374	1.016 .046	1.279 .084
-3.28	3.489	.949	.977	.425	1.755 .047	2.209 .122
-3.11	3.539	.962	.991	.495	2.685 .047	3.380 .173
-2.96	3.584	.975	1.003	.590	5.230 .049	6.584 .322
-2.80	3.632	.988	1.017	1.350	18.790 .053	23.654 1.138
-2.71	3.660	.995	1.025	2.150	32.220 .053	40.561 1.950
-2.59	3.697	1.005	1.035	4.000	42.160 .077	53.075 2.551

Run #2: Sample weight = .77880 gm

Zero Offset = -.165
.039

Calibration Ratio = 1.00000
.00099

T_{ice}	p_{ice}	x_w	x_i	b	w_a	Γ
-8.31	2.264	.616	.634	.096	.540 .046	.787 .077
-5.80	2.815	.766	.788	.170	.479 .044	.698 .072
-5.03	3.007	.818	.842	.212	.630 .044	.919 .078
-4.35	3.186	.866	.892	.260	.869 .045	1.267 .089
-3.89	3.313	.901	.928	.361	.959 .045	1.398 .094

Table I; Run 2, continued.

T_{ice}	p_{ice}	x_w	x_i	b	w_a	Γ
-3.49	3.427	.932	.960	.369	1.168	1.703
					.044	.104
-3.16	3.524	.958	.987	.465	2.090	3.048
					.049	.163
-2.86	3.613	.982	1.011	.700	8.898	12.975
					.050	.628
-2.73	3.653	.993	1.023	1.950	20.697	30.180
					.053	1.452
-2.67	3.672	.999	1.028	3.000	23.508	34.279
					.058	1.649
-3.25	3.498	.951	.979	.437	4.950	7.218
					.047	.353

w_a, the net amount adsorbed, and b, the blank, are given in millivolts. To convert to milligrams, multiply by 0.10. The standard deviation is given directly below the value of w_a.

Γ, the surface excess, is given in nanomoles/cm^2. The standard deviation is given directly below the value of Γ.

Table II: Adsorption data for the -10.00C isotherm.

Water saturation pressure = 2.150 mm Hg

Ice saturation pressure = 1.951 mm Hg

Blank

Zero Offset = -.052 .008 Calibration Ratio = .99996 .00023

T_{ice}	p_{ice}	x_w	x_i	w_a
-12.47	1.563	.727	.801	.132 .010
-10.69	1.834	.853	.940	.178 .008
-10.08	1.937	.901	.993	.254 .009
-9.50	2.039	.948	1.045	.388 .008

Run #1: Sample weight = .89670 gm

Zero Offset = 4.998 .072 Calibration Ratio = .99924 .00161

T_{ice}	p_{ice}	x_w	x_i	b	w_a	Γ
-13.34	1.445	.672	.741	.118	.642 .084	.814 .114
-11.41	1.720	.800	.882	.150	.749 .079	.949 .110
-9.92	1.965	.914	1.007	.305	.934 .076	1.183 .112
-9.64	2.008	.935	1.031		Nucleation	

Run #2: Sample weight = .89670 gm (same sample as in Run 1)

Zero Offset = 4.660 .036 Calibration Ratio = .99924 .00125

Table II; Run 2, continued.

T_{ice}	p_{ice}	x_w	x_i	b	w_a	Γ
-12.98	1.493	.695	.766	.121	.442	.559
					.053	.072
-10.69	1.834	.853	.940	.180	.805	1.020
					.047	.077
-9.79	1.988	.925	1.019	.300	1.268	1.606
					.046	.096
-9.63	2.007	.934	1.030		Nucleation	

Run #3: Sample weight = .90418 gm

Zero Offset = .438 Calibration Ratio = .99882
.030 .00066

T_{ice}	p_{ice}	x_w	x_i	b	w_a	Γ
-13.25	1.456	.677	.746	.120	.555	.697
					.042	.062
-12.19	1.604	.746	.822	.131	.755	.948
					.040	.068
-11.00	1.784	.830	.914	.165	1.011	1.269
					.041	.079
-10.20	1.917	.892	.983	.228	1.117	1.403
					.038	.083
-9.85	1.977	.920	1.014	.285	1.430	1.796
					.040	.100
-9.70	2.003	.932	1.027		Nucleation	

w_a, the net amount adsorbed, and b, the blank, are given in millivolts. To convert to milligrams, multiply by 0.10. The standard deviation is given directly below the value of w_a.

Γ, the surface excess, is given in nanomoles/cm^2. The standard deviation is given directly below the value of Γ.

Table III: Adsorption data for the -6.50C isotherm.

Water saturation pressure = 2.823 mm Hg

Ice saturation pressure = 2.650 mm Hg

Run #1; Sample weight = .65414 gm

Zero Offset = 1.278 .010 Calibration Ratio = 1.00156 .00029

T_{ice}	p_{ice}	x_w	x_i	b	w_a	Γ
-12.98	1.492	.529	.563	.075	.489 .020	.849 .054
-8.30	2.267	.803	.855	.173	.637 .031	1.106 .076
-6.98	2.542	.900	.959	.278	.926 .030	1.607 .093
-6.60	2.628	.931	.992	.344	1.206 .030	2.094 .113
-6.25	2.708	.959	1.022	.465	2.132 .027	3.701 .184
-6.15	2.732	.968	1.031		Nucleation	

Run #2: Sample weight = .84866 gm

Zero Offset = -.354 .019 Calibration Ratio = 1.00000 .00047

T_{ice}	p_{ice}	x_w	x_i	b	w_a	Γ
-10.84	1.810	.641	.683	.108	.235 .027	.314 .039
-7.00	2.538	.899	.958	.275	1.035 .038	1.385 .084
-6.39	2.675	.948	1.009	.408	1.990 .033	2.663 .135
-8.14	2.298	.814	.867	.180	.568 .034	.760 .059

Same footnotes apply to Table V as to Tables III and IV. Blank values were estimated from the -3.00C and -10.00C blank isotherms.

Table IV: Empirical isotherm parameters for mean isotherms and one standard deviation envelope isotherms.

Isotherm		x_{min}	Γ_{min}	x_{max}	Γ_{max}	a	b	n
-3.00C #1	Upper	.454	-	.931	1.476	-.609	-.378	1.65
	Mean	.454	-	.931	1.386	-.712	-.396	1.53
	Lower	.454	-	.931	1.297	-.846	-.419	1.39
-3.00C #2	Upper	.931	1.476	.990	32.08	-3.777	-1.575	-.37
	Mean	.931	1.386	.990	24.53	-3.857	-1.534	-.35
	Lower	.931	1.297	.990	29.55	-3.943	-1.593	-.37
-3.00C #3	Upper	.990	32.08	.9999	-	3.001	-.107	8.34
	Mean	.990	24.53	.9999	-	2.954	-.107	8.34
	Lower	.990	29.55	.9999	-	2.905	-.107	8.34
-6.50C #1	Upper	.529	-	.883	1.340	-.858	-.552	.81
	Mean	.529	-	.882	1.250	-.953	-.567	.76
	Lower	.529	-	.880	1.160	-1.059	-.586	.71
-6.50C #2	Upper	.883	1.340	.968	-	-1.660	-.936	.07
	Mean	.882	1.250	.968	-	-1.740	-.946	.06
	Lower	.880	1.160	.968	-	-1.825	-.958	.04
-10.00C #1	Upper	.672	-	.930	-	-.671	-.474	1.11
	Mean	.672	-	.930	-	-.804	-.502	.99
	Lower	.672	-	.930	-	-.955	-.538	.86

Γ in nanomoles/cm^2.

x is relative pressure with respect to water.

Table V: Isostere and isosteric heat of adsorption data.

	-3.00C	-6.50C	-10.00C	Isosteric heats, Kcal/mole		
Γ	ln p	ln p	ln p	q_{12}	q_{st}	q_{23}
0.6	.714	.579	.207	5.50	10.25	14.83
0.7	.903	.688	.354	8.79	11.08	13.30
0.8	1.017	.762	.450	10.46	11.45	12.40
0.9	1.090	.813	.516	11.33	11.59	11.84
1.0	1.140	.851	.563	11.80	11.64	11.48
1.1	1.175	.880	.598	12.04	11.63	11.24
1.2	1.200	.903	.625	12.15	11.60	11.07
1.3	1.218	.917	.645	12.32	11.56	10.82
1.4	1.231	.926	.662	12.48	11.49	10.53
1.5	1.234	.934	.675	12.28	11.28	10.31
1.6	1.237	.941	.686	12.11	11.12	10.15
1.7	1.240	.947	.695	11.97	10.98	10.03
1.8	1.242	.952	.703	11.84	10.88	9.94
2.0	1.246	.961		11.73		
2.2	1.249	.969		11.47		
2.4	1.252	.975		11.34		
2.6	1.254	.980		11.23		
2.8	1.256	.984		11.14		
3.0	1.258	.988		11.06		
3.2	1.260	.991		11.00		
3.4	1.262	.994		10.95		
3.6	1.263	.997		10.90		
3.8	1.265	.999		10.86		
4.0	1.266	1.001		10.83		

q_{12} from -3.00C and -6.50C isostere data.

q_{23} from -6.50C and -10.00C isostere data.

Γ in nanomoles/cm^2.

Table VI: Gibbs equation integration data, from smoothed isotherms; Π(erg/cm^2) and σ(cm^2/nanomole).

-3.00C			-6.50C			-10.00C		
x_w	Π	σ	x_w	Π	σ	x_w	Π	σ
.453	-14.65	1.875	.528	-11.01	2.082	.672	-6.65	1.448
.550	-12.20	1.677	.600	-9.07	1.772	.750	-4.42	1.198
.650	-9.82	1.473	.700	-6.95	1.445	.820	-2.63	.991
.750	-7.46	1.255	.800	-4.63	1.108	.880	-0.90	.794
.860	-4.71	.971	.840	-3.58	.963	.929	0.80	.602
.930	-2.65	.727	.900	-1.74	.677			
.940	-2.28	.577	.930	-0.47	.476			
.960	-1.15	.299	.950	0.69	.342			
.980	1.52	.098	.964	1.83	.249			
.985	2.99	.062						
.990	5.51	.032						
.992	6.96	.031						
.996	9.96	.029						
.999	12.49	.025						

Table VII: Adsorption parameters at the onset of nucleation, including for comparison, -3.00C at which nucleation does not occur; $x_{w,i}$ relative pressure, Γ(nanomoles/cm^2), $\Pi_{\Delta x_i}$(erg/cm^2), q_{st}(Kcal/mole).

Parameter	-3.00C	-6.50C	-10.00C
x_w	1.000	.967	.930
x_i	1.030	1.030	1.025
Γ	51.40	4.486	1.703
$\Pi_{\Delta x_i}$	12.49	1.83	.84
q_{st}		10.83	10.88